

ESTIMATING STORATIVITY AND TRANSMISSIVITY RATIO OF
MULTI-LAYER RESERVOIR AND DUAL-PERMEABILITY
FRACTURED SYSTEMS

ARTHUR LAKES LIBRARY
COLORADO SCHOOL OF MINES
GOLDEN, CO 80401

by

Nab Mahdi Al-Ajmi

ProQuest Number: 10794683

All rights reserved

INFORMATION TO ALL USERS

The quality of this reproduction is dependent upon the quality of the copy submitted.

In the unlikely event that the author did not send a complete manuscript and there are missing pages, these will be noted. Also, if material had to be removed, a note will indicate the deletion.



ProQuest 10794683

Published by ProQuest LLC (2018). Copyright of the Dissertation is held by the Author.

All rights reserved.

This work is protected against unauthorized copying under Title 17, United States Code
Microform Edition © ProQuest LLC.

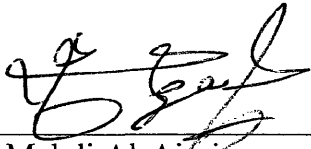
ProQuest LLC.
789 East Eisenhower Parkway
P.O. Box 1346
Ann Arbor, MI 48106 – 1346

A thesis submitted to the Faculty and Board of Trustees of the Colorado School of Mines in partial fulfillment of the requirements for the degree of Master of Science (Petroleum Engineering).

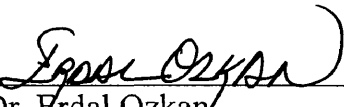
Golden, Colorado

Date: Nov. 13, 2002

Signed: _____

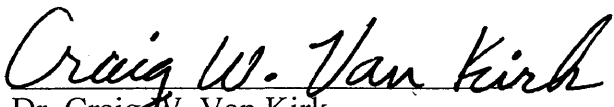

Nab Mahdi Al-Ajmi

Approved: _____


Dr. Erdal Ozkan
Thesis Advisor

Golden, Colorado

Date: Nov. 13, 2002


Dr. Craig W. Van Kirk
Professor and Head,
Department of Petroleum Engineering

ABSTRACT

This thesis presents a method to estimate the storativity ratio of a multi-layer system with cross flow. The method is based on a new analytical formula that expresses the storativity ratio as a function of transmissivity ratio, vertical separation between the two straight lines on pressure versus log-time plot, and skin factor. Therefore, if the layer flow rates are available from production log and the estimates of average system storativity and permeability can be obtained from pressure transient analysis, then the individual layer properties, such as storativity and flow capacity, may be determined by using the method proposed in this work.

The evolution of this thesis involved numerical and analytical modeling studies. The numerical model developed in this study simulates single-phase, transient flow in a radial system. The numerical model is capable of handling multiple layers with vertical-to-horizontal permeability contrast in individual layers as well as between layers, the effects of wellbore storage and skin, and the contribution of gravity. The numerical model was initially utilized in an attempt to develop an empirical correlation for the storativity ratio of multi-layer systems with cross flow. Because this attempt was fruitless, an analytical study was undertaken to derive an expression for the storativity ratio. During this analytical phase of the study, the numerical model served as a tool to compare the analytical results and generate data for the example applications.

In conclusion, the major contribution of this study is a new method to estimate the storativity ratio of layered reservoirs with cross flow. To highlight the importance of the proposed method, the error involved in the estimation of the storativity ratio of a dual-permeability system by using the assumption of dual-porosity is documented. Finally, to demonstrate the use of the method proposed in this work, two simulated examples are presented.

TABLE OF CONTENTS

ABSTRACT.....	iii
TABLE OF CONTENTS	iv
LIST OF FIGURES	vii
LIST OF TABLES	x
ACKNOWLEDGEMENTS	xi

CHAPTER 1

INTRODUCTION.....	1
1.1 Background	3
1.2 Objectives	7
1.3 Organization.....	7
1.4 Literature Review.....	8

CHAPTER 2

NUMERICAL MODEL	10
2.1 Finite Difference Equations	11
2.2 Gravity Effect.....	15
2.3 Harmonic Averaging of Permeability.....	18
2.4 Skin Effect	19
2.4.1 Thin Skin.....	19
2.4.2 Finite Skin.....	20
2.5 Non-Darcy Flow	21
2.6 Construction of the Spatial Grid	23
2.7 Construction of the Time-Step Sequence	24
2.8 The System of Simulator Equations in Matrix Form.....	26
2.9 Gaussian Elimination Method.....	30
2.10 Flow Chart	33

2.11 Comparison between Numerical and Analytical Models	35
---	----

CHAPTER 3

PRESSURE TRANSIENT RESPONSES OF LAYERED RESERVOIRS WITH CROSS FLOW.....	38
3.1 Base Case.....	38
3.2 Sensitivity Study.....	41
3.3 Empirical Correlation.....	44
3.4 Application and Discussion of Results	45

CHAPTER 4

ANALYTICAL STUDY OF LAYERED RESERVOIR RESPONSES.....	49
4.1 Early-Time Behavior	49
4.2 Late-Time Behavior.....	55
4.3 The Vertical Separation between the Parallel Lines (δp)	56
4.4 Solution for ω with $s = 0$	60
4.5 Solution for ω with $s \neq 0$	63
4.6 Effect of Wellbore Storage	66
4.7 Range of Application of the Analytical Solution.....	68
4.8 Solution for κ	73

CHAPTER 5

APPLICATIONS	75
5.1 Example 1	75
Solution of Part A	76
1) Estimation by using Eq. 4.36.....	81
2) Estimation by using Eq. 4.40.....	82
3) Estimation by the Dual-Porosity Equation given by Eq. 3.1	83

4) Bourdet's Dual-Porosity Method.....	83
Solution of Part B.....	85
5.2 Example 2	86
Solution of Part A	88
Solution of Part B.....	92
CHAPTER 6	
SUMMARY AND CONCLUSIONS	93
REFERENCES.....	94
LIST OF SYMBOLS	97
APPENDIX A-NUMERICAL MODEL (FORTRAN 90) FOR RADIAL TRANSIENT FLOW	100
APPENDIX B-THE ANALYTICAL SOLUTION FOR THE STORATIVITY RATIO DUAL-POROSITY SYSTEM	127
B.1 Analytical Solution for Homogeneous System	127
B.2 Analytical Solution for Commingled System	129
APPENDIX C-PRESSURE VERSUS TIME DATA FOR EXAMPLE APPLICATIONS	133
Table C-1: The pressure data of Example 1.....	133
Table C-2: The pressure data of Example 2.....	134
APPENDIX D-COMPUTER PROGRAM FOR THE NEWTON RAPHSON METHOD	135
D.1 Newton Raphson Method for Storativity Ratio (FORTRAN 90).....	135
D.2 Newton Raphson Method for Transmissivity Ratio (FORTRAN 90).....	138

LIST OF FIGURES

Fig. 1. 1 The semi-log plot of the transient pressure responses of dual-porosity and dual-permeability systems.....	6
Fig. 2. 1 The effect of ignoring gravity for single-phase flow in horizontal formations..	17
Fig. 2. 2 Schematic of the spatial grid system used in the finite difference equations	23
Fig. 2. 3 Comparison of the simulated dimensionless pressures with the analytical results for a homogeneous reservoir.....	35
Fig. 2. 4 Grid refinement for numerical modeling of commingled reservoir.	36
Fig. 2. 5 The comparison of the results for course and fine grids with the analytical solution for commingled system.	37
Fig. 3. 1 Effect of test duration on the existence of straight lines on pressure versus log-time plot.	40
Fig. 3. 2 The log-log plot of layered reservoir responses	43
Fig. 3. 3 The correlation of the shrinkage factor.....	45
Fig. 3. 4 Error plot for the storativity ratio correlation given by Eq. 3.3.....	47
Fig. 3. 5 Shrinkage factor as a function of κ and ω	48
Fig. 4. 1 The correspondence of the early-time responses of commingled and the cross flow systems.....	50

Fig. 4. 2 The equivalence of the homogeneous and cross flow systems.	56
Fig. 4. 3 Semi-log plot of layered reservoir responses for small values of ω	57
Fig. 4. 4 Layered reservoir responses and the approximate solutions at early and late times.	59
Fig. 4. 5 The estimation of ω as function of RHS from Eq. 4.29	62
Fig. 4. 6 Error plot for the estimates of ω from Eq. 4.32 for the data in Table 3.6	63
Fig. 4. 7 Error plot for Eq. 4.40 with $s = 10$ and the data in Table 4.1.	66
Fig. 4. 8 The effect of wellbore storage on the early time flow regime.	67
Fig. 4. 9 The start of the intermediate time flow regime as a function of k_{z2}	68
Fig. 4. 10 Estimation of ω from Eq. 4.29 within the practical ranges of parameters.	70
Fig. 4. 11 The error plot for Eq. 4.40 for the data in Table 3.6.	71
Fig. 4. 12 The coefficient a in Eq. 4.40 as a function of the skin factor for different values of κ	72
Fig. 4. 13 The coefficient b in Eq. 4.40 as a function of the skin factor for different values of κ	72
Fig. 4. 14 The κ values calculated from Eq. 4.44 as a function of the RHS of Eq. 4.44 for $s = 0$	74

Fig. 5. 1 Schematic of the reservoir system considered in Example 1.	75
Fig. 5. 2 The semi-log plot for Example 5.1	77
Fig. 5. 3 The diagnostic plot for Example 1	79
Fig. 5. 4 Homogeneous system type curve.	79
Fig. 5. 5 Simulated flow rates for Example .1	80
Fig. 5. 6 The plot of $(t \, dp/dt)_{\min}$ as a function of ω for Bourdet's method.	85
Fig. 5. 7 The schematic of the reservoir for Example 2.....	87
Fig. 5. 8 The semi-log plot for the buildup test of Example 2.....	88
Fig. 5. 9 The diagnostic plot for the buildup test of Example 2	89
Fig. 5. 10 Simulated production logging results for Example 2.	91
Fig. 5. 11 The influx of each layer for Example 2.....	91

LIST OF TABLES

Table 3. 1 Well and fluid data for the base case.	39
Table 3. 2 Reservoir properties for the base case	39
Table 3. 3 The values of k_2 and λ as a function of κ for the sensitivity analysis	42
Table 3. 4 Slope of the semi-log straight lines and δp as a function of κ	43
Table 3. 5 The ratio, $\delta p/m$, as a function of κ	44
Table 3. 6 The obtained values of δp and m as a function of ω and κ	46
Table 3. 7 Error involved in the estimation of ω by using Eq. 3.3.	46
Table 4. 1 Simulated data for draw down tests with a uniform skin of 10.	65
Table 4. 2 The upper limits of ω based on the practical minimum of δp_D	69
Table 5. 1 Well and reservoir data for Example 1.	76
Table 5. 2 Well and reservoir data for Example 2	87

ACKNOWLEDGEMENTS

I Thank Dr. Erdal Ozkan, my thesis advisor, for his guidance and assistance in preparing this report. I am grateful for the time he spent with me and giving me the opportunity to learn from him.

I offer thanks to Dr. Hossien Kazemi for giving me his guidance to construct the numerical model. This study would not have been possible without your contributions.

I ask Dr. Turhan Yildiz to accept my appreciation for serving as a member of my thesis committee and for his comments in preparing this report.

I dedicate this work to my wife for her encouragement, understanding and support that I could ever have to achieve this goal.

CHAPTER 1

INTRODUCTION

Pressure transient analysis is a powerful tool to estimate reservoir properties. The reservoir properties estimated by pressure transient analysis are needed to characterize reservoirs and predict well performances. Although the physical properties of hydrocarbon bearing formations may change as a function of location, pressure transient analysis provides single values for these properties which are believed to represent the averages over the volume of the reservoir investigated during the test.

When the production performance of the system may be adequately modeled by using the average properties, as in the case of primary recovery from a reservoir of continuously changing permeability, the well-test estimated properties may be of direct utility. In some other cases, especially where the heterogeneity manifests itself in the form of jump discontinuities at the boundaries of otherwise homogeneous zones, the individual zone properties may be required to characterize the fluid transfer among various zones. The characteristics of fluid transfer between the zones, in turn, dictate the depletion characteristics of the overall system. Multi-layer systems with cross flow are good examples of reservoirs that fall into this category.

For layered systems with cross flow, the capability of pressure transient analysis to provide the average system properties may not be sufficient for reservoir description unless the average properties lead to the estimation of the individual layer properties. It can be shown that to obtain the individual layer properties from the average properties, two parameters are required. These are the storativity ratio, defined as the ratio of the storativity of the layer with high flow capacity to the total system storativity, and the transmissivity ratio, which is the ratio of the maximum layer flow rate to the total system rate.

The transmissivity ratio may be obtained from production logs. The storativity ratio on the other hand needs to be determined from the pressure transient data or by independent means. The objective of this thesis is to develop a method that may be used to estimate the storativity ratio of a layered reservoir from pressure transient data.

It is a common trend to utilize the similarities between the pressure transient characteristics of dual-permeability and dual-porosity systems in the estimation of the properties of layered systems. A layered reservoir with cross flow may be represented by a dual-permeability model in which separate zones (layers) are in direct communication with the wellbore and with each other. Therefore, the results and discussions presented in this study for layered reservoirs with cross flow are applicable to dual-permeability fractured systems. A dual-porosity system, on the other hands, consists of two separate media, one of which only stores and supplies the fluids to the other medium which then transmits fluids to the wellbore.

For dual-porosity systems, such as naturally fractured systems and carbonate reservoirs, the estimation of the storativity ratio from well-test data has been well documented in the literature.^{1,2} Specifically, the storativity ratio may be uniquely determined from the displacement between the two parallel straight lines on the pressure versus log-time plot. For dual-permeability systems, as in the case of layered reservoirs with cross flow, however, the displacement between the two parallel semi-log straight lines is not only a function of the storativity ratio but also a function of the transmissivity ratio. Therefore, the objective of this study is to obtain a practical relation for the storativity ratio of layered systems with cross flow in terms of the displacement between the two semi-log straight lines and the transmissivity ratio. Below, a brief background of the research presented in this study is discussed, followed by the objectives and organization of the thesis.

1.1 Background

In the literature, dual-porosity and dual-permeability system definitions are usually associated with naturally fractured and layered systems, respectively. In principle, dual-porosity systems constitute a subset (a limiting case) of the dual-permeability systems and, as such, possesses many characteristics that resemble those of dual-permeability systems. In other words, dual-porosity systems may be considered as a relatively simpler form of the dual-permeability systems and the analysis techniques developed for dual-porosity-systems may serve as a first approximation in the development of the analysis techniques for dual-permeability systems. Because this approach has also been used in this study to develop a technique to determine the storativity ratio of layered reservoirs with cross flow, it should be useful to provide the formal definitions of the dual-porosity and dual-permeability models.

A dual-porosity system is a heterogeneous reservoir where the fluid is stored in two different media with significant contrast in their storage capacity. The flow to the wellbore is attributed mainly to the high permeability medium (fissure) whereas the vertical transmissibility of the other medium (matrix) is much more significant than the radial transmissibility; that is, the fluid flows from the matrix medium to the fissure and then to the wellbore. In other words, the direct communication of the matrix with the wellbore is negligible and the depletion of the matrix is through communication with the high-permeability fissure system. Usually, the storage capacity of the fissure is very small compared with that of the matrix.

A dual-permeability system is a heterogeneous reservoir where the fluid is produced from two different zones with significant contrast in their radial permeability-thickness product as well as their storage capacity. In contrast to the dual-porosity systems, both zones are in direct communication with the wellbore and contribute to the total system flow rate proportionally to their flow capacities. Similar to the dual-porosity systems, the higher permeability zone usually has smaller storage capacity compared to the lower permeability zone.

Warren and Root¹ showed that the transient pressure responses of wells in dual-porosity systems are controlled by two parameters:

Interporosity flow coefficient:

$$\lambda = \sigma r_w^2 \frac{k_m}{k_f}. \quad (1.1)$$

The interporosity flow coefficient is a measure of the efficiency of fluid flow from the matrix to the fissure. The term σ is the shape factor, which is a function of the size and shape of the matrix blocks, k_m is the permeability of the matrix system, and k_f is the permeability of the fissure (fracture) system.

Storativity ratio:

$$\omega = \frac{(\phi c_t h)_f}{(\phi c_t h)_f + (\phi c_t h)_m}, \quad (1.2)$$

where the subscripts f and m stand for the fissure-and matrix-system properties, respectively. Therefore, the storativity ratio, ω , defined in Eq. 1.2 is the ratio of the storativity of the fissure system to the total storativity of the system (fissure and matrix).

The corresponding definitions of λ and ω for a layered-reservoir with cross flow (a dual-permeability system) are given by

$$\lambda = \sigma r_w^2 \frac{k_{v2}}{k_1 h_1 + k_2 h_2} \quad (1.3)$$

$$h$$

and

$$\omega = \frac{(\phi c_i h)_1}{(\phi c_i h)_1 + (\phi c_i h)_2}. \quad (1.4)$$

In Eqs. 1.3 and 1.4, the subscripts 1 and 2 indicate the layers of higher and lower horizontal permeabilities, k_1 and k_2 , respectively, k_{v2} is the vertical permeability of Layer 2, and h_i denotes the thickness of Layer i . Note that this formulation assumes two layers only, but as will be discussed later, if there are more than two layers, they can be grouped in two layers of high and low permeability. Note that the definition of λ given in Eq. 1.3 is slightly different from the definition given by Bourdet³. Bourdet's definition uses k_2 instead of k_{v2} in the nominator of Eq. 1.3. Because this definition yields $\lambda = 0$ when the horizontal permeability of Layer 2, $k_2 = 0$, (that is, Layer 2 does not communicate with the wellbore and the system reduces to dual porosity), we prefer the definition given in Eq. 1.3.

It must be also noted that because both media (layers) produce to the wellbore in the dual-permeability model, their horizontal flow capacities govern the performance of the reservoir. The effect of the individual layer flow capacities is represented by the transmissivity ratio defined by

$$\kappa = \frac{(kh)_1}{(kh)_1 + (kh)_2}. \quad (1.5)$$

For dual-porosity systems, the flow capacity of Layer 2 in the horizontal direction is negligible so that $\kappa \approx 1$. It is also known⁴ that during transient flow (prior to the effect of boundaries), the flow rates of the layers are proportional to their flow capacities; that is,

$$\frac{q_i}{q_1 + q_2} = \frac{(kh)_i}{(kh)_1 + (kh)_2}. \quad (1.6)$$

Therefore, for transient flow, the transmissivity ratio given in Eq. 1.5 may also be expressed in terms of layer flow rates as follows:

$$\kappa = \frac{q_1}{q_1 + q_2} . \quad (1.7)$$

Fig 1.1 shows the transient pressure responses of dual-porosity and dual-permeability systems under the same conditions. Both systems display the same characteristics; specifically, two parallel lines can be drawn at early- and late-times on the semi-log plot of the pressure responses. For the dual-porosity system, the vertical separation between the parallel lines is a measure of ω . On the other hand, for the dual-permeability system, the vertical separation is governed by both ω and κ . We will confirm this observation in this study and use to obtain an expression for ω .

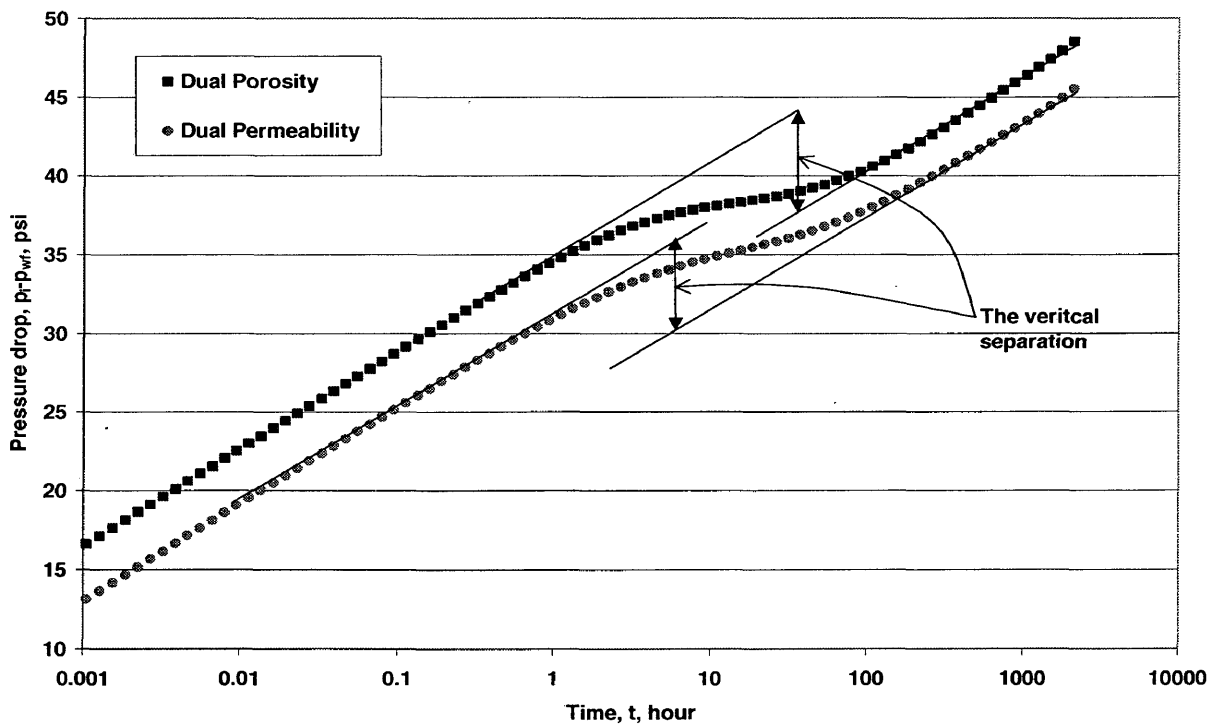


Fig. 1.1 *The semi-log plot of the transient pressure responses of dual-porosity and dual-permeability systems.*

1.2 Objectives

The broad objective of this work is to study and understand the pressure responses of a well producing at a constant rate from a layered reservoir with cross flow. The specific objectives are the following:

1. Evaluate the characteristics of pressure transient responses in multi-layered reservoirs with cross flow.
2. Develop a methodology and tools to estimate the properties of layered systems with cross flow (dual-permeability systems) from pressure transient data.
3. Demonstrate the use of the proposed analysis technique on simulated tests.

1.3 Organization

The chapters of this research are presented in the chronological order of the steps taken to accomplish the objectives of this study.

Chapter 1 is an introduction in which the problem is defined and the objectives of this study are stated. Chapter 2 presents the methodology to construct the numerical model, which is used in this study to simulate transient flow in dual-porosity and dual-permeability systems. Chapter 3 summarizes the attempt to develop an empirical correlation for the storativity ratio by using the simulator-generated data. The results of this chapter lead to the analytical study discussed in Chapter 4 that yielded an expression to calculate the storativity ratio. Chapter 5 demonstrates the applications of the analytical expression derived in Chapter 4. Finally, Chapter 6 presents the summary and conclusions that are inferred from this study.

1.4 Literature Review

J. S. Olarewaju and W. J. Lee⁴ conducted a history-match study for a gas well in a layered formation with cross flow called Travis Peak formation in east Texas. They claimed that history matching the production of a layered reservoir with cross flow to that of a homogeneous system could yield reasonably good results. They, however, concluded that when the reservoir's geology indicates a layered system, the use of the adequate reservoir properties would always yield higher accuracy.

Kazemi⁶ emphasizes that a realistic estimate of the fracture porosity and fracture spacing is very important in improved oil recovery by gravity drainage. Also, for the determination of an estimate of non-Darcy skin, one needs both the magnitude of the fracture spacing and fracture width. Realistic estimates of this information may be obtained from the knowledge of effective permeability, storativity ratio, and transmissivity ratio.

The properties of the individual layers have been reported as a crucial piece of information in Ref. 7 for pressure maintenance projects; such as CO₂ flooding. In addition, one of the concerns that must be taken into account is the order of the vertical sequences of the layers in accordance with their permeability contrast. This issue, however, is out of the scope of this study.

Another study indicating the importance of the determination of layer properties has been presented by Saul Vela et al.⁸ This study concluded that to evaluate Polymer Flooding in a layered reservoir with cross flow, layer permeabilities must be known because polymer shear degradation, resistance factor, and retention are all permeability dependent.

As a final example of the relevant literature, Watson and Lee⁹ reported a history-matching algorithm for layered systems. The applicability of the algorithm was demonstrated by history matching of the actual production data with an analytical dual-porosity model.

CHAPTER 2

NUMERICAL MODEL

As noted before, a numerical model has been developed in this study to simulate single-phase, transient flow in a radial system.⁶ The numerical model is capable of simulating flow in multiple layers with different vertical and horizontal permeabilities, and considering the effects of wellbore storage, skin and gravity. This chapter presents the details of the development of the numerical simulator and the numerical code is given in Appendix A in FORTRAN 90 language.

Section 2.1 of this chapter presents the details of the finite-difference equations for the multi-layer, radial reservoir model. Here, the gravitational effects are assumed to be negligible. The incorporation of the gravitational effects is discussed in Section 2.2.

Section 2.3 covers the harmonic averaging of permeability for fluid transfer between grid faces. The skin and non-Darcy flow effects are discussed in Sections 2.4 and 2.5, respectively.

Section 2.6 presents the methodology to construct the radial grid system and Section 2.7 discusses the selection of time steps. The matrix-vector form of the finite-difference equations is given in Section 2.8 and the matrix solver is discussed in Section 2.9. Finally, the flow chart of the computer program is given in Section 2.10 and some guidelines to be considered when simulating heterogeneous systems are discussed in Section 2.11.

2.1 Finite Difference Equations

The general, basic differential equation that governs the flow of a single-phase in a porous medium is given by

$$\frac{1}{r} \frac{\partial}{\partial r} \left(r \frac{k_r}{\mu} \frac{\partial p}{\partial r} \right) + \frac{\partial}{\partial z} \left(r \frac{k_z}{\mu} \frac{\partial p}{\partial z} \right) = \hat{\phi} c_t \frac{\partial p}{\partial t}. \quad (2.1)$$

where, $\hat{\phi}$ is the local porosity of each layer; that is different from the global porosity which is equal to the local porosity – thickness ratio product, e.g. $\phi_{gj} = \hat{\phi}_j h_j / h_{total}$ for layer j.

Application of finite difference to Eq. 2.1 yields

$$\Delta_r T_r \Delta_r p + \Delta_z T_z \Delta_z p + (q_k B_k)_{Total} = \frac{V_R}{\Delta t / 24} (\hat{\phi} c_t) \Delta_t p, \quad (2.2)$$

where

$$\Delta_r T_r \Delta_r p = T_{r,i+1/2,k} (p_{i+1,k}^{n+1} - p_{i,k}^{n+1}) - T_{r,i-1/2,k} (p_{i,k}^{n+1} - p_{i-1,k}^{n+1}), \quad (2.3)$$

$$\Delta_z T_z \Delta_z p = T_{z,i,k+1/2} (p_{i,k+1}^{n+1} - p_{i,k}^{n+1}) - T_{z,i,k-1/2} (p_{i,k}^{n+1} - p_{i,k-1}^{n+1}), \quad (2.4)$$

and

$$\Delta_t p = (p_{i,k}^{n+1} - p_{i,k}^n). \quad (2.5)$$

Substituting Eqs. 2.3, 2.4, and 2.5 into Eq. 2.2 gives,

$$\begin{aligned} & T_{r,i+1/2,k} (p_{i+1,k}^{n+1} - p_{i,k}^{n+1}) - T_{r,i-1/2,k} (p_{i,k}^{n+1} - p_{i-1,k}^{n+1}) + T_{z,i,k+1/2} (p_{i,k+1}^{n+1} - p_{i,k}^{n+1}) \\ & - T_{z,i,k-1/2} (p_{i,k}^{n+1} - p_{i,k-1}^{n+1}) + (q_{1,k} B_{1,k})_{Total} = \frac{V_R}{\Delta t / 24} (\hat{\phi} c_t) (p_{i,k}^{n+1} - p_{i,k}^n) \end{aligned}$$

(2.6)

where the flow rate, q , is in cubic feet,

$$T_{r,i\pm 1/2,k} = 0.006328 \left(\frac{k_r}{\mu B} \right) \frac{2\pi r_{i\pm 1/2} \Delta z_k}{\Delta r_{i\pm 1/2}}, \quad (2.7)$$

and

$$T_{z,i,k\pm 1/2} = 0.006328 \left(\frac{k_r}{\mu B} \right) \frac{\pi (r_{i+1/2}^2 - r_{i-1/2}^2)}{\Delta z_{k\pm 1/2}}. \quad (2.8)$$

The volume of each grid is defined by

$$V_{Ri,k} = \pi (r_{i+1/2}^2 - r_{i-1/2}^2) \Delta z_k. \quad (2.9)$$

The total flow rate incorporating the wellbore storage effect and layer contribution is given by

$$(q_{1,k} B_{1,k})_{Total} = q_{1,1} B_{1,1} + q_{1,2} B_{1,2} + \dots + q_{1,n} B_{1,n} + \frac{C_{wb}}{\Delta t / 24} (p_{0,1}^{n+1} - p_{0,1}^n), \quad (2.10)$$

where

$$q_1 B_1 = -WI_1 [p_{1,1}^{n+1} - p_{0,1}^{n+1}]. \quad (2.11)$$

Consequently,

$$q_{1,k} B_{1,k} = -WI_{1,k} [p_{1,k}^{n+1} - p_{0,k}^{n+1}], \quad (2.12)$$

where, WI is the wellbore index defined by

$$WI_{1,K} = \frac{0.006328(2\pi)k_{r1,K} \Delta z_k}{\mu \left(\frac{\Delta r_{1/2}}{r_{1/2}} \right)}. \quad (2.13)$$

The terms, $\Delta r_{1/2}$ and $r_{1/2}$ in Eq. 2.13 are defined in detail in Section 4.6.

Recasting Eq. 2.10 into a general form yields

$$(q_{1,k} B_{1,k})_{Total} = \sum -WI_{1,k} [p_{1,k}^{n+1} - p_{0,k}^{n+1}] + \frac{C_{wb}}{\Delta t / 24} (p_{0,1}^{n+1} - p_{0,1}^n). \quad (2.14)$$

Rearranging Eq. 2.14 based on unknown and known pressures yields

$$\begin{aligned} & -WI_{1,1} p_{1,1}^{n+1} - WI_{1,1} p_{0,1}^{n+1} - WI_{1,2} p_{1,2}^{n+1} - WI_{1,2} p_{0,2}^{n+1} - \dots - WI_{1,k} p_{1,k}^{n+1} - WI_{1,k} p_{0,k}^{n+1} \\ & + \frac{C_{wb}}{\Delta t / 24} p_{0,1}^{n+1} = (q_{1,k} B_{1,k})_{Total} + \frac{C_{wb}}{\Delta t / 24} p_{0,1}^n. \end{aligned} \quad (2.15)$$

Now, for the nodes that represent pressures of the reservoir grid, the rearrangement of Eq. 2.6 yields,

$$\begin{aligned} & T_{r,i+1/2,k} p_{i+1,k}^{n+1} - T_{r,i+1/2,k} p_{i,k}^{n+1} - T_{r,i-1/2,k} p_{i,k}^{n+1} - T_{r,i-1/2,k} p_{i-1,k}^{n+1} + T_{z,i,k+1/2} p_{i,k+1}^{n+1} - T_{z,i,k+1/2} p_{i,k}^{n+1} \\ & - T_{z,i,k-1/2} p_{i,k}^{n+1} - T_{z,i,k-1/2} p_{i,k-1}^{n+1} = \frac{V_R}{\Delta t / 24} (\hat{\phi} c_t) p_{i,k}^{n+1} - \frac{V_R}{\Delta t / 24} (\hat{\phi} c_t) p_{i,k}^n \end{aligned} \quad (2.16)$$

or,

$$\begin{aligned} & T_{r,i+1/2,k} p_{i+1,k}^{n+1} - T_{r,i-1/2,k} p_{i-1,k}^{n+1} + T_{z,i,k+1/2} p_{i,k+1}^{n+1} - T_{z,i,k-1/2} p_{i,k-1}^{n+1} \\ & - \left[T_{r,i+1/2,k} p_{i,k}^{n+1} + T_{r,i-1/2,k} p_{i,k}^{n+1} + T_{z,i,k+1/2} p_{i,k}^{n+1} + T_{z,i,k-1/2} p_{i,k}^{n+1} + \frac{V_R}{\Delta t / 24} (\hat{\phi} c_t) \right] p_{i,k}^{n+1} \\ & = - \frac{V_R}{\Delta t / 24} (\hat{\phi} c_t) p_{i,k}^n \end{aligned}$$

Using abbreviations for the long terms in the parentheses of Eq. 2.17, the following (2.17) is obtained:

$$F_{i,k} p_{i+1,k}^{n+1} + D_{i,k} p_{i-1,k}^{n+1} + G_{i,k} p_{i,k+1}^{n+1} + C_{i,k} p_{i,k-1}^{n+1} + E_{i,k} p_{i,k}^{n+1} = R_{i,k}. \quad (2.18)$$

Eq. 2.18 represent the nodes of a layer grid inside the reservoir where,

$$F_{i,k} = T_{r,i+1/2,k} = 0.006328 \left(\frac{k_r}{\mu B} \right) \frac{2\pi r_{i+1/2} \Delta z_k}{\Delta r_{i+1/2}}, \quad (2.19)$$

$$D_{i,k} = T_{r,i-1/2,k} = 0.006328 \left(\frac{k_r}{\mu B} \right) \frac{2\pi r_{i-1/2} \Delta z_k}{\Delta r_{i-1/2}}, \quad (2.20)$$

$$G_{i,k} = T_{z,i,k+1/2} = 0.006328 \left(\frac{k_r}{\mu B} \right) \frac{\pi (r_{i+1/2}^2 - r_{i-1/2}^2)}{\Delta z_{k+1/2}}, \quad (2.21)$$

$$C_{i,k} = T_{z,i,k-1/2} = 0.006328 \left(\frac{k_r}{\mu B} \right) \frac{\pi (r_{i+1/2}^2 - r_{i-1/2}^2)}{\Delta z_{k-1/2}}, \quad (2.22)$$

$$e_{i,k} = -\frac{\left(\hat{\phi} c_i \right)}{\Delta t / 24} \left[\pi (r_{i+1/2}^2 - r_{i-1/2}^2) \Delta z_k \right], \quad (2.23)$$

$$R_{i,k} = e_{i,k} p_{i,1}^n, \quad (2.24)$$

and

$$E_{i,k} = -[C_{i,k} + D_{i,k} + F_{i,k} + G_{i,k} + e_{i,k}]. \quad (2.25)$$

2.2 Gravity Effect

The gravity effect is neglected in the previous derivations. Thus, the assumption of equal bottom hole pressures in the vertical direction, inside the wellbore and the reservoir, is implicitly embedded. The effect of gravity is important for multi-phase flow and should be incorporated into the numerical solution. For single-phase flow, the effect of gravity needs to be modeled only if the gravity effects are known to be significant. Therefore, the effect of gravity and fluid density has been added to the numerical model as an option by the following:

For the general case (gravity is not neglected), the governing general differential equation is given by

$$\frac{1}{r} \frac{\partial}{\partial r} \left[r \frac{k_r}{\mu} \left(\frac{\partial p}{\partial r} - \gamma \frac{\partial D}{\partial r} \right) \right] + \frac{\partial}{\partial z} \left[r \frac{k_z}{\mu} \left(\frac{\partial p}{\partial z} - \gamma \frac{\partial D}{\partial z} \right) \right] = \hat{\phi} c_t \frac{\partial p}{\partial t}, \quad (2.26)$$

where γ is the specific gravity of the fluid. The differentials, $\frac{\partial D}{\partial r}$ and $\frac{\partial D}{\partial z}$ are the change in depth in the r and z directions, respectively. Because we assume that the producing strata lay horizontally, $\frac{\partial D}{\partial r} = 0$ and $\frac{\partial D}{\partial z} = -1$. Therefore, the finite difference of Eq. 2.26 yields

$$\Delta_r T_r \Delta_r p + \Delta_z T_z (\Delta_z p - \gamma \Delta_z D) + (q_k B_k)_{Total} = \frac{V_R}{\Delta t / 24} (\hat{\phi} c_t) \Delta_t p, \quad (2.27)$$

or, more explicitly

$$\begin{aligned}
& T_{r,i+1/2,k} (p_{i+1,k}^{n+1} - p_{i,k}^{n+1}) - T_{r,i-1/2,k} (p_{i,k}^{n+1} - p_{i-1,k}^{n+1}) \\
& + [T_{z,i,k+1/2} (p_{i,k+1}^{n+1} - p_{i,k}^{n+1}) - T_{z,i,k-1/2} (p_{i,k}^{n+1} - p_{i,k-1}^{n+1})] \\
& + [T_{z,i,k+1/2} (D_{i,k+1}^n - D_{i,k}^n) - T_{z,i,k-1/2} (D_{i,k}^n - D_{i,k-1}^n)] \cdot \\
& + (q_{1,k} B_{1,k})_{Total} = \frac{V_R}{\Delta t / 24} (\hat{\phi} c_i) (p_{i,k}^{n+1} - p_{i,k}^n)
\end{aligned} \tag{2.28}$$

The derivation of the pressure coefficients follows the same lines as mentioned in Section 2.1 and only affects the right-hand side term and the equations of layer flow-rates. Therefore, the right-hand side term of Eq. 2.18 becomes

$$R_{i,k} = T_{z,i,k-1/2} (D_{i,k}^n - D_{i,k-1}^n) - T_{z,i,k+1/2} (D_{i,k+1}^n - D_{i,k}^n) + e_{i,k} p_{i,k}^n, \tag{2.29}$$

which, by using Eqs. 2.21 and 2.22, can be written as

$$R_{i,k} = C_{i,k} (D_{i,k}^n - D_{i,k-1}^n) - G_{i,k} (D_{i,k+1}^n - D_{i,k}^n) + e_{i,k} p_{i,k}^n. \tag{2.30}$$

On the other hand, due to the hydrostatic differences between $p_{0,1}$ of the top node of the wellbore and $p_{0,k}$ of the lower nodes, the flow rate equations of the bottom layers become

$$q_2 B_2 = -W I_2 [p_{1,2}^{n+1} - p_{0,1}^{n+1} - \gamma_f (D_2 - D_1)], \tag{2.31}$$

and

$$q_k B_k = -W I_k [p_{1,k}^{n+1} - p_{0,1}^{n+1} - \gamma_f (D_k - D_1)]. \tag{2.32}$$

When the density or specific gravity terms are set to zero, the above equations reduce to the forms neglecting gravity effect given in Section 2.1.

Figure 2.1 highlights the effect of neglecting gravity for single-phase flow simulation. The comparison shown in Fig. 2.1 considers two cases. One of the cases includes gravity

by assigning 12 lbf/cu-ft for the density while the other case ignores it. The difference in the pressure and derivative profiles is less than 1 psia and Fig. 2.1 displays a very good match between the two cases. This result verifies that for single-phase flow in horizontal formations considered in this study, the effect of gravity can be neglected.

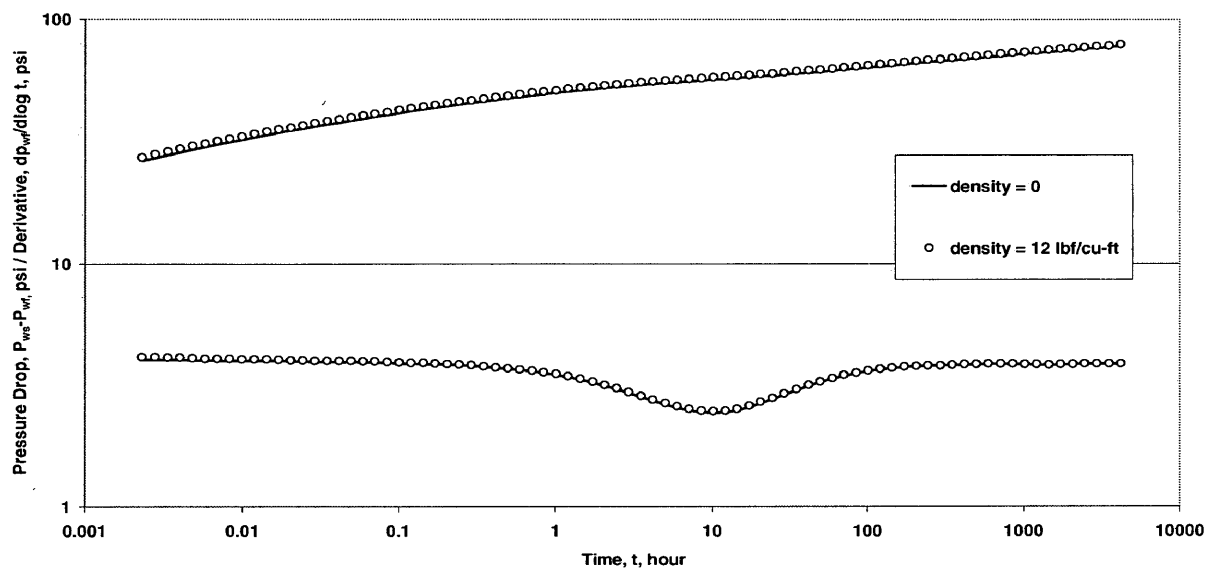


Fig. 2. 1 The effect of ignoring gravity for single-phase flow in horizontal formations.

2.3 Harmonic Averaging of Permeability

The intercommunication or cross flow between layers may be simulated by using an average permeability for the transmissibility terms at the layer interfaces. It has been demonstrated by Hollabauch and Slotboom⁹ that harmonic average gives the best approximation for the measured vertical permeability of the cores from heterogeneous reservoir.

The equation for the harmonic average of permeability is given by

$$k_{harmonic} = \frac{\sum_{j=1}^n h_j}{\sum_{j=1}^n \frac{h_j}{k_j}} \quad (2.33)$$

This expression is introduced in the numerical model as follow

$$\left(k_{z_{k+\frac{1}{2}}} \right)_{harmonic} = \frac{2 \Delta z_{k+\frac{1}{2}}}{\frac{\Delta z_k}{k_{z_k}} + \frac{\Delta z_{k+1}}{k_{z_{k+1}}}}, \quad (2.34)$$

for vertical permeabilities, and

$$\left(k_{r_{i+\frac{1}{2}}} \right)_{harmonic} = \frac{k_{r_i} k_{r_{i+1}} (r_{i+1} - r_i)}{k_{r_i} \left(r_{i+1} - r_{i+\frac{1}{2}} \right) + k_{r_{i+1}} \left(r_{i+\frac{1}{2}} - r_i \right)} \quad (2.35)$$

for the radial (or horizontal) permeabilities.

2.4 Skin Effect

The permeability of the formation near the wellbore is often reduced by the infiltration of drilling and workover fluids. This damaged region can be treated by acid stimulation or hydraulic fracturing.

Formation damage creates extra pressure drop and hence reduces the potential productivity of the well. Pressure transient tests may be used to determine if the well is damaged or stimulated. The skin factor, s , for ideal conditions is zero and $s > 0$ indicate damage while $s < 0$ result from stimulation.

The skin can be modeled by either infinitesimally thin skin or thick (finite volume) skin. These are discussed below:

2.4.1 Thin Skin

Although the skin zone has a finite volume, its effect may be approximated by an infinitesimally thin skin covering the wall of the wellbore. In the numerical model, the skin factor is included in the first grids of the layers that are surrounding the wellbore. For these first grids, the wellbore indices, WI_k , must be subtracted from their pressure coefficients as follows:

$$E_{1k} = E_{ik} - WI_{1,k} \quad (2.36)$$

To incorporate the effect of the skin factor, the wellbore index is defined as

$$WI_{1,K} = \frac{0.006328(2\pi)k_{r1,K} \Delta z_k}{\mu \left[\frac{\Delta r_{1/2}}{r_{1/2}} + s_k \right]} \quad (2.37)$$

where, $\Delta r_{1/2}$ and $r_{1/2}$ are defined in detail in Section 4.6.

2.4.2 Finite Skin

Robert and Ramey¹¹ have shown that for negligible wellbore storage, the skin radius of $10r_w$ could distort the characteristics of the early-time pressure data significantly. Specifically, for negligible wellbore storage, the effect of composite or altered permeability may be observed as two straight lines on well-test data. One of these straight lines stands for the altered permeability zone and the other has the slope of 1.151 which represents the formation or reservoir flow capacity. Therefore, if the skin radius is comparable to $10r_w$, then the assumption of infinitesimally thin skin may not be appropriate.

A finite-volume skin zone may be modeled by altering the permeability of the grid blocks surrounding the wellbore. This model is similar to a composite reservoir system where the permeability in the vicinity of the wellbore could be higher or lower than the reservoir permeability for stimulated and damaged skin, respectively. The damaged zone permeability and its radius is estimated from Hawkins' equation¹² given by

$$s = \left(\frac{k}{k_s} - 1 \right) \ln \left(\frac{r_s}{r_w} \right), \quad (2.38)$$

where,

- s Infinitesimally thin skin, dimensionless
- k Formation permeability, md
- k_s Altered permeability, md
- r_s Damaged skin radius, ft
- r_w Wellbore radius, ft

When this option is selected in the simulation, the skin factor used in the wellbore index given by Eq. 2.37 is set to zero.

2.5 Non-Darcy Flow

The Darcy's law is valid for low flow velocity. Hence, Darcy's law is not applicable for gas wells producing at high flow rates. Also, it has been found that the reservoir flow equations based on Darcy's law overpredicts the performance of high-volume wells in naturally fractured reservoirs as much as 50 percent.¹³ This is because of the fact that Darcy's law considers the viscous effects but neglects the inertial effects. When the flow rates become high, inertial effects become significant compared to the viscous effects and Darcy's law may not represent the flux of fluid flow in porous media accurately. In this study, the effect non-Darcy flow on the estimation of layer properties has not been investigated. However, to build a numerical code for more general applicability than the scopes of this thesis, non-Darcy flow has been included as an option in the numerical simulator. Below, the incorporation of non-Darcy flow into the numerical simulator is discussed briefly.

When non-Darcy flow is important, Forchheimer's Equation is used to model fluid flow. Forchheimer's equation is given by

$$\Delta p_w = F_A q + F_B q^n, \quad (2.39)$$

where, F_A and F_B are the coefficient for the reservoir system and n is the flow rate exponent. These three unknowns may be estimated from well test data.¹³

Taking non-Darcy flow into account in the numerical model requires correlating the inertial effects with the reservoir and fluid properties. Therefore, in this study, a modified permeability called non-Darcy permeability suggested by Kazemi⁶ has been used for the grid blocks that are affected by high flow rates. The non-Darcy permeability is less than the original permeability and a function of both the fluid velocity in the porous medium and the reservoir/grid permeability. Thus, the non-Darcy permeability is given by

$$k_{nondarcy} = \frac{\bar{k}_{grid}}{1 + \left(1.8295 \times 10^{-16} \beta' \rho \frac{\bar{k}_{grid}}{\mu} |V_r|_{grid} \right)} \quad (2.40)$$

where \bar{k}_{grid} is given by Eq. 2.35 and β' is defined by ¹⁴

$$\beta' = 6.15 \times 10^{10} (\bar{k}_{grid})^{-1.55} \quad (2.41)$$

and, V_r is the fluid velocity in the grid block given by the following expression in ft/day:

$$V_r = \frac{-0.006328 \bar{k}_{grid} (p_{i-1} - p_i)}{\Delta r_{i+1/2} \mu (1 + \alpha)}. \quad (2.42)$$

Here α is defined by

$$\alpha = 1.8295 \times 10^{-16} \beta' \rho \frac{\bar{k}_{grid}}{\mu} |V_r|_{grid} \quad (2.43)$$

which is exactly the term in the parenthesis of Eq. 2.40. Hence, Eq. 2.40 can be rewritten as

$$k_{nondarcy} = \frac{\bar{k}_{grid}}{1 + \alpha} \quad (2.44)$$

Since V_r and α are dependent on each other; that is V_r is a function of α and α is a function of V_r , an iteration process is needed to estimate α . Usually, one iteration is sufficient to obtain α by first substituting $\alpha = 0$ into Eq. 2.42 and then, using the resulting value of V_r in Eq. 2.43.

2.6 Construction of the Spatial Grid

Different pressure nodes and indices have different radii involved in their calculations. The following are the definitions of these radii. Figure 1.2 shows a schematic of the grid system.

The parameter Δu is used to allocate distances for each grid radius between r_w and r_e and is defined by

$$\Delta u = \ln(r_e/r_w) / I_{max}. \quad (2.45)$$

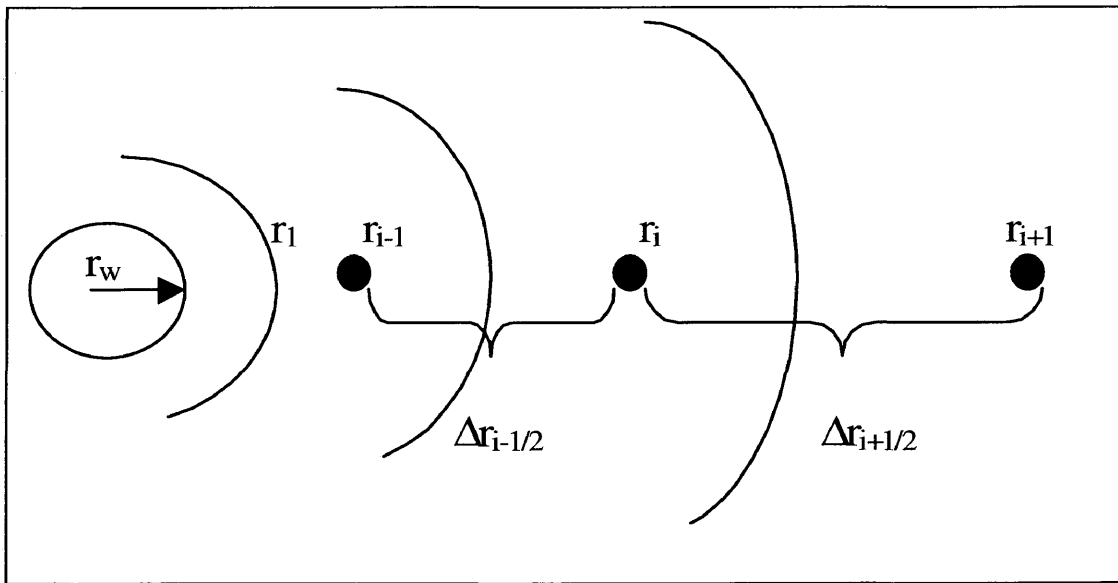


Fig. 2. 2 Schematic of the spatial grid system used in the finite difference equations

The definition of the radius for the middle grid (r_i) and the backward and forward grids (r_{i-1} and r_{i+1}) are given respectively by

$$r_i = r_1 e^{(i-1)\Delta u}, \quad (2.46)$$

$$r_{i-1} = r_w e^{(i-1) \Delta u}, \quad (2.47)$$

and

$$r_{i+1} = r_w e^{i \Delta u}, \quad (2.48)$$

where,

$$r_1 = r_w e^{\Delta u/2}. \quad (2.50)$$

The definitions of $\Delta r_{i-1/2}$ and $\Delta r_{i+1/2}$ are given by

$$\Delta r_{i-1/2} = r_i - r_{i-1} \quad (2.51)$$

and

$$\Delta r_{i+1/2} = r_{i+1} - r_i. \quad (2.52)$$

On the other hand, the height of the grids in the z direction are constructed in Cartesian fashion; that is, Δz_k is the thickness of each layer or sub-layer and $\Delta z_{k+1/2}$ is given by

$$\Delta z_{k+1/2} = \frac{\Delta z_k + \Delta z_{k+1}}{2}. \quad (2.53)$$

2.7 Construction of the Time-Step Sequence

For unsteady state condition, the bottom hole pressure of a well changes abruptly in the beginning and then the changes over time becomes less and less until the boundary effect

is felt. Therefore, this behavior of pressure change with time requires the time steps used in the simulator be smaller in the beginning and increase as the pressure change decreases during late times. To have time steps increase in logarithmic fashion, the following equation is used:

$$\tau = \frac{\ln\left(\frac{t_{\max}}{c}\right)}{n_{\max}} \quad (2.54)$$

The term τ is a coefficient for having time steps increase in logarithmic fashion, t_{\max} is the duration of the test period, c is the increment constant, and n_{\max} is the number of time steps to be used for calculating pressures. The expression given in Eq. 2.54 is required to specify and fit the maximum time into the range of the given number of time steps.

After τ is determined, the second step is to calculate the cumulative time for each time step (n) by the following expression:

$$t_{cum} = c e^{(n \tau)} \quad (2.55)$$

The incremental time (Δt) required for computing the pressure may be obtained from Eq. 2.55 as follows:

$$\Delta t = t_{Cum}^{n+1} - t_{Cum}^n, \quad (2.56)$$

or by using Eq. 2.55 in Eq. 2.56,

$$\Delta t = c \left[e^{((n+1) \tau)} - e^{(n \tau)} \right]. \quad (2.57)$$

An anomaly is observed in the early-time build-up pressures simulated by using the logarithmic time increments as described above. It is also reflected by fluctuation in the

$$E_{11} = E_{11} - WI_1, \quad (2.59)$$

$$E_{12} = E_{12} - WI_2, \quad (2.60)$$

$$E_{13} = E_{13} - WI_3, \quad (2.61)$$

and

$$E_{14} = E_{14} - WI_4. \quad (2.62)$$

However, reducing the previous matrix from (16 x 16) to (13 x 13) will make the running time of the code more efficient. This reduction can be achieved by the elimination method, as follow

$$\begin{array}{c}
 1 \quad 2 \quad 3 \quad 4 \quad 5 \quad 6 \quad 7 \quad 8 \quad 9 \quad 10 \quad 11 \quad 12 \quad 13 \\
 \left[\begin{array}{cccccccccccc}
 E_{11} & F_{11} & & G_{11} & & & & & & & & & WI_1 \\
 D_{21} & E_{21} & F_{21} & & G_{21} & & & & & & & & \\
 & D_{31} & E_{31} & & & G_{31} & & & & & & & \\
 C_{12} & & & E_{12} & F_{12} & & G_{12} & & & & & WI_2 & 0 \\
 & C_{22} & & D_{22} & E_{22} & F_{22} & & G_{22} & & & & & \\
 & & C_{32} & D_{32} & E_{32} & & & G_{32} & & & & & \\
 & & & C_{13} & & & E_{13} & F_{13} & & G_{13} & & WI_3 & 0 \\
 & & & & C_{23} & & D_{23} & E_{23} & F_{23} & & G_{23} & & \\
 & & & & & C_{33} & D_{33} & E_{33} & & & G_{33} & & \\
 & & & & & & C_{14} & & & E_{14} & F_{14} & & WI_4 & 0 \\
 & & & & & & & C_{24} & & D_{24} & E_{24} & F_{24} & & \\
 & & & & & & & & C_{34} & & D_{34} & E_{34} & & \\
 -WI_1 & & & -WI_2 & & & -WI_3 & & & -WI_4 & & & \sum WI + c & 0 & 0 & 0 \\
 & & & & & & & & & & & & & 1 & -1 & \\
 & & & & & & & & & & & & & & 1 & -1 \\
 & & & & & & & & & & & & & & & 1 & -1
 \end{array} \right]
 \begin{bmatrix}
 P_{11}^{n+1} \\
 P_{21}^{n+1} \\
 P_{31}^{n+1} \\
 P_{12}^{n+1} \\
 P_{22}^{n+1} \\
 P_{23}^{n+1} \\
 P_{13}^{n+1} \\
 P_{23}^{n+1} \\
 P_{33}^{n+1} \\
 P_{14}^{n+1} \\
 P_{24}^{n+1} \\
 P_{34}^{n+1} \\
 P_{01}^{n+1} \\
 P_{02}^{n+1} \\
 P_{03}^{n+1} \\
 P_{04}^{n+1}
 \end{bmatrix}
 =
 \begin{bmatrix}
 R_{11}^n \\
 R_{21}^n \\
 R_{31}^n \\
 R_{12}^n - l_1 \\
 R_{22}^n \\
 R_{23}^n \\
 R_{13}^n - l_2 \\
 R_{23}^n \\
 R_{33}^n \\
 R_{14}^n - l_3 \\
 R_{24}^n \\
 R_{34}^n \\
 (qB)_{total} + c P_{01}^n - f \\
 -\gamma_f (d_2 - d_1) \\
 -\gamma_f (d_3 - d_2) \\
 -\gamma_f (d_4 - d_3)
 \end{bmatrix}
 \end{array}$$

where,

$$l_1 = WI_2 \gamma (d_2 - d_1), \quad (2.63)$$

$$l_2 = WI_3 \gamma [(d_3 - d_2) + (d_2 - d_1)], \quad (2.64)$$

$$l_3 = WI_4 \gamma [(d_4 - d_3) + (d_3 - d_2) + (d_2 - d_1)], \quad (2.65)$$

and

$$f = \gamma \{ [WI_4 + WI_3 + WI_2](d_2 - d_1) + [WI_4 + WI_3](d_3 - d_2) + WI_4(d_4 - d_3) \}. \quad (2.66)$$

The reduction of the original matrix to (13 x 13) has been implemented in the code given in Appendix A. The running time may be further improved by reducing the matrix size from (13 x 13) to (12 x 12). The following steps should be taken to accomplish the matrix reduction:

1. Multiply Row 13 by $-WI_4 / \left(\sum WI + \hat{c} \right)$ and add to Row 10
2. Multiply Row 13 by $-WI_3 / \left(\sum WI + \hat{c} \right)$ and add to Row 7
3. Multiply Row 13 by $-WI_2 / \left(\sum WI + \hat{c} \right)$ and add to Row 4
4. Multiply Row 13 by $-WI_1 / \left(\sum WI + \hat{c} \right)$ and add to Row 1

Therefore, when proceeding with the above steps, the matrix will be reduced to the form shown below:

$$\begin{array}{cccccccccccc}
& 1 & 2 & 3 & 4 & 5 & 6 & 7 & 8 & 9 & 10 & 11 & 12 \\
1 & \left[\begin{array}{cccccccccccc}
E_{11} & F_{11} & G_{1+x_1} & & & & x_2 & & & & x_3 & & 0 \\
D_{21} & E_{21} & F_{21} & & G_{21} & & & & & & & & \\
& D_{31} & E_{31} & & & G_{31} & & & & & & & \\
C_{12+x_1} & & & E_{12} & F_{12} & G_{12+y_1} & & & & & y_2 & & 0 & 0 \\
& C_{22} & & D_{22} & E_{22} & F_{22} & & G_{22} & & & & & \\
& & C_{32} & & D_{32} & E_{32} & & & G_{32} & & & & \\
x_2 & & & G_{13+y_1} & & & E_{13} & F_{13} & G_{13+z_1} & & & & 0 & 0 \\
& & & & C_{23} & & D_{23} & E_{23} & F_{23} & & G_{23} & & & \\
& & & & & C_{33} & & D_{33} & E_{33} & & & G_{33} & & \\
x_3 & & & y_2 & & & C_{14+z_1} & & & E_{14} & F_{14} & & 0 & 0 \\
& & & & & & & C_{24} & & D_{24} & E_{24} & F_{24} & & \\
& & & & & & & & C_{34} & & D_{34} & E_{34} & & \\
-WI_1 & & & -WI_2 & & & -WI_3 & & & -WI_4 & & & WI_1+c & 0 & 0 & 0 & 0
\end{array} \right]
\begin{array}{c}
P_{11}^{r+h} \\
P_{21}^{r+h} \\
P_{31}^{r+h} \\
P_{12}^{r+h} \\
P_{22}^{r+h} \\
P_{32}^{r+h} \\
P_{13}^{r+h} \\
P_{23}^{r+h} \\
P_{33}^{r+h} \\
P_{14}^{r+h} \\
P_{24}^{r+h} \\
P_{34}^{r+h} \\
P_{01}^{r+h}
\end{array}
=
\begin{array}{c}
R_{11}^r + v_1 \\
R_{21}^r \\
R_{31}^r \\
R_{12}^r - l_1 + v_2 \\
R_{22}^r \\
R_{32}^r \\
R_{13}^r - l_2 + v_2 \\
R_{23}^r \\
R_{33}^r \\
R_{14}^r - l_3 + v_3 \\
R_{24}^r \\
R_{34}^r \\
qB + cP_{01}^r - f
\end{array}
\end{array}$$

where,

$$x_1 = WI_1 WI_2 / \left(\sum WI + \hat{c} \right), \quad (2.67)$$

$$x_2 = WI_1 WI_3 / \left(\sum WI + \hat{c} \right), \quad (2.68)$$

$$x_3 = WI_1 WI_4 / \left(\sum WI + \hat{c} \right), \quad (2.69)$$

$$y_1 = WI_2 WI_3 / \left(\sum WI + \hat{c} \right), \quad (2.70)$$

$$y_2 = WI_2 WI_4 / \left(\sum WI + \hat{c} \right), \quad (2.71)$$

$$z_1 = WI_4 / \left(\sum WI + \hat{c} \right), \quad (2.72)$$

$$E_{11} = E_{11} - WI_1 + WI_1^2 / \left(\sum WI + \hat{c} \right), \quad (2.73)$$

$$E_{12} = E_{12} - WI_2 + WI_2^2 / \left(\sum WI + \hat{c} \right), \quad (2.74)$$

$$E_{13} = E_{13} - WI_3 + WI_3^2 / \left(\sum WI + \hat{c} \right), \quad (2.75)$$

$$E_{14} = E_{14} - WI_4 + WI_4^2 / \left(\sum WI + \hat{c} \right), \quad (2.76)$$

$$v_1 = -WI_1 / \left(\sum WI + \hat{c} \right) \left[5.6146(qB)_{total} + \hat{c} p_{01}^n - f \right], \quad (2.77)$$

$$v_2 = -WI_2 / \left(\sum WI + \hat{c} \right) \left[5.6146(qB)_{total} + \hat{c} p_{01}^n - f \right], \quad (2.78)$$

$$v_3 = -WI_3 / \left(\sum WI + \hat{c} \right) \left[5.6146(qB)_{total} + \hat{c} p_{01}^n - f \right], \quad (2.79)$$

and

$$v_4 = -WI_4 / \left(\sum WI + \hat{c} \right) \left[5.6146(qB)_{total} + \hat{c} p_{01}^n - f \right]. \quad (2.80)$$

Then, solving for p_{01}^{n+1} from row 13 yields

$$p_{01}^{n+1} = \left[5.6146(qB)_{total} + \hat{c} p_{01}^n - f \right] + \left[WI_1 p_{11}^{n+1} + WI_2 p_{12}^{n+1} + WI_3 p_{13}^{n+1} + WI_4 p_{14}^{n+1} \right] / \left(\sum WI + \hat{c} \right). \quad (2.81)$$

2.9 Gaussian Elimination Method

The matrix solver used for the numerical model is the Gaussian Elimination method. This method is the basis for most direct solving methods of linear system. The principles or the algebraic bases of Gaussian elimination method are as follows

For a given linear system

$$[A] \{X\} = \{B\}, \quad (2.82)$$

where $[A]$ is a matrix or array of the known coefficients, $\{X\}$ is a vector of unknown parameters such as the pressure of reservoir grids in well testing, and $\{B\}$ is a vector of the known values. The principle of Gaussian method is to decompose the coefficient matrix $[A]$ into lower $[L]$ and upper $[U]$ triangle matrices. The product of lower and upper triangle arrays or matrices should give the original matrix $[A]$. The following is an explanation of the method. If

$$[L] [U] = [A], \quad (2.83)$$

then, Eq. 2.82 becomes

$$[L] [U] \{X\} = \{B\}. \quad (2.84)$$

An intermediate solution is given by

$$\{Y\} = [U] \{X\}. \quad (2.85)$$

Thus Eq. 2.84 becomes

$$[L] \{Y\} = \{B\}. \quad (2.86)$$

If we can determine $[L]$, then the new unknown parameters $\{Y\}$ can be obtained easily by forward substitution. In this process, the solution starts from the first unknown of $\{Y\}$, y_1 , and continues down to solve the rest of the unknowns y_i terms. After determining $\{Y\}$, $\{X\}$ can be obtained by back substitution of y_i in Eq. 2.85.

The key element of the algorithm is the decomposition of [A] matrix into [L] and [U]. This decomposition can be accomplished by using the elements of [L] defined by

$$l_{i,j} = a_{i,j}/a_{i=j}. \quad (2.87)$$

This can be illustrated as shown below:

$$[L] = \begin{bmatrix} 1 & 0 & 0 \\ l_{2,1} & 1 & 0 \\ l_{3,1} & l_{3,2} & 1 \end{bmatrix} = \begin{bmatrix} 1 & 0 & 0 \\ a_{2,1}/a_{1,1} & 1 & 0 \\ a_{3,1}/a_{1,1} & a_{3,1}/a_{2,2} & 1 \end{bmatrix} \quad (2.88)$$

Here $a_{i,j}$ are the elements of the matrix [A] divided by a pivot element which is $a_{i,j}$ for $i = j$.

The pivot element must be nonzero, otherwise, the linear system is said to be a singular system and does not have a unique solution. The algorithm used for Gaussian Elimination method proceeds by solving the matrix with partial pivoting.

In partial pivoting, the rows in the matrix of interest are rearranged in such way that a pivot number has to be the largest absolute value. This is because of the fact that if a pivot element is the largest absolute value then the round off error in the computation will be minimized.

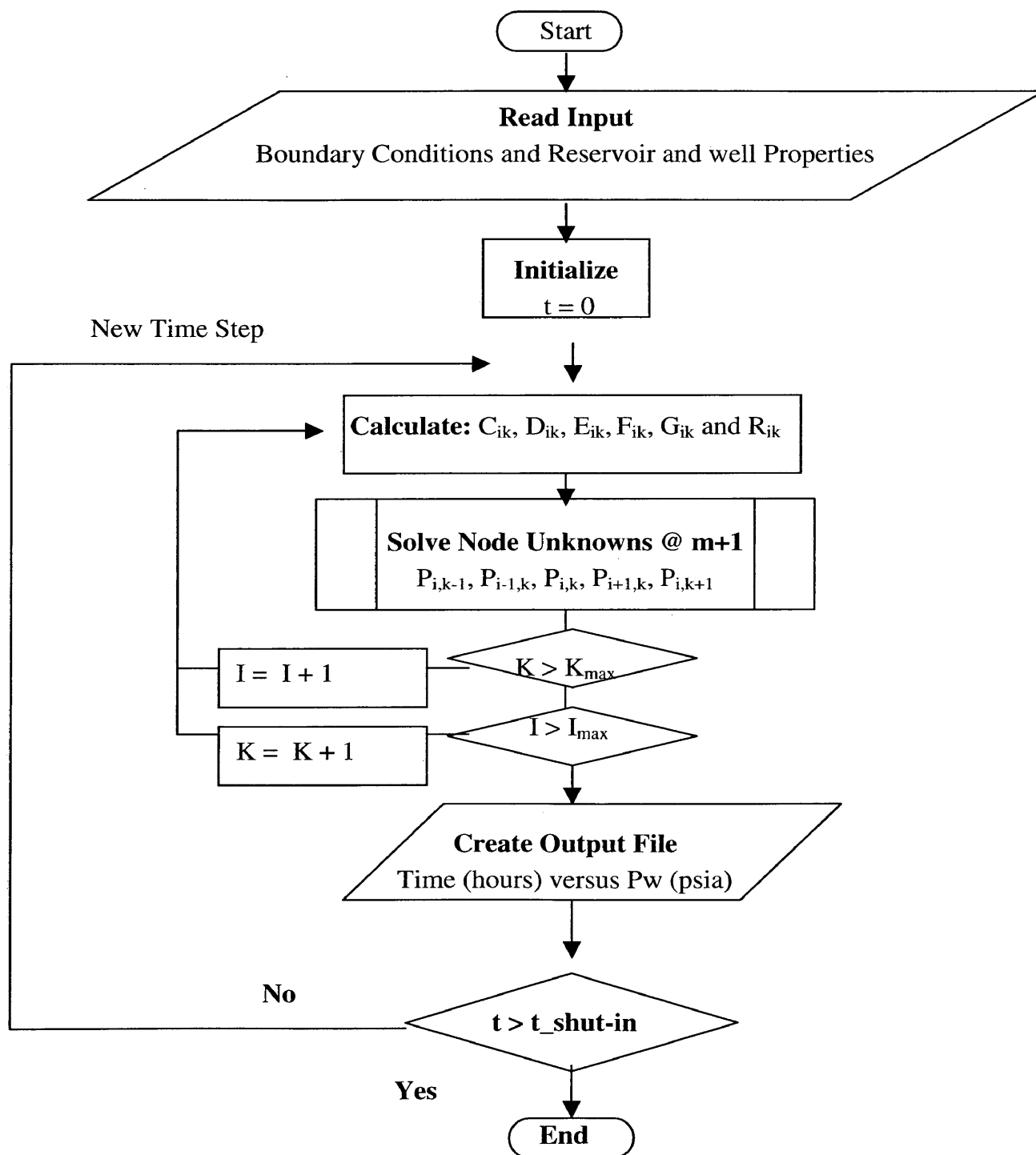
Second the product of $[L]^{-1} [A]$ must give [U]. It is easily demonstrated that $[L]^{-1}$ is simply [L] with the sign of the none-diagonal elements reversed. Thus,

$$[L]^{-1} = \begin{bmatrix} 1 & 0 & 0 \\ -l_{2,1} & 1 & 0 \\ -l_{3,1} & -l_{3,2} & 1 \end{bmatrix} = \begin{bmatrix} 1 & 0 & 0 \\ -a_{2,1}/a_{1,1} & 1 & 0 \\ -a_{3,1}/a_{1,1} & -a_{3,1}/a_{2,2} & 1 \end{bmatrix} \quad (2.89)$$

Therefore, using [L] in Eq. 2.86 to get {Y} and then substituting {Y} in Eq.2.85 will give the x unknowns, which, in our case, are the pressures of the wellbore and reservoir grids.

2.10 Flow Chart

Here a flow chart for the numerical simulation is presented.



2.11 Comparison between Numerical and Analytical Models

Figure 2.2 shows a comparison of the results obtained from the numerical model by with those from the analytical model which will be discussed later for a homogeneous reservoir.

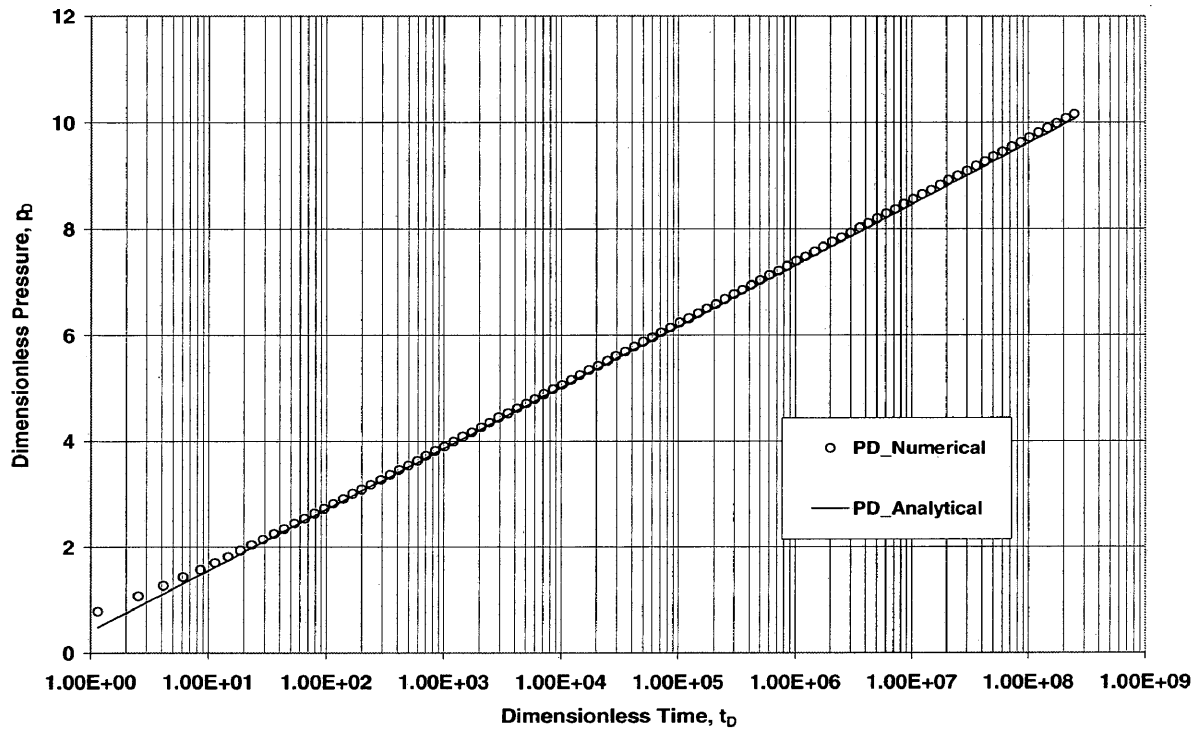


Fig. 2. 3 Comparison of the simulated dimensionless pressures with the analytical results for a homogeneous reservoir.

Simulation of heterogeneous systems requires additional considerations about grid refinement. For example, the simulated pressures for a multi-layered reservoir with cross flow would match with the analytical model if the term σ of Eq. 1.3 is calculated by

$$\sigma = \frac{2}{(h_1 + h_2) h_2} \quad (2.90)$$

For commingled reservoirs where the layers communicate only via wellbore, the numerical model matches the analytical solution by grid refinement for each layer. The grid refinement has to be in the vertical direction as illustrated in Fig. 2.4.

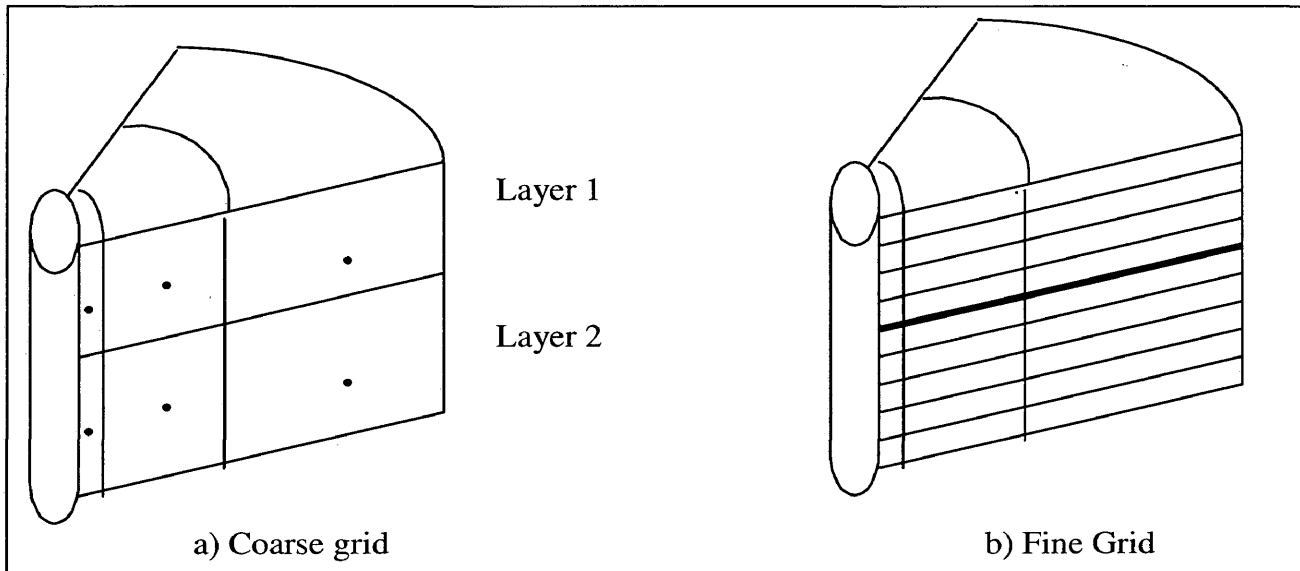


Fig. 2. 4 Grid refinement for numerical modeling of commingled reservoir.

Figure 2.5 highlights the differences between using course and fine grids by comparing the results with the analytical solution. As demonstrated in Fig. 2.5, grid refinement improves the match with the analytical solution.

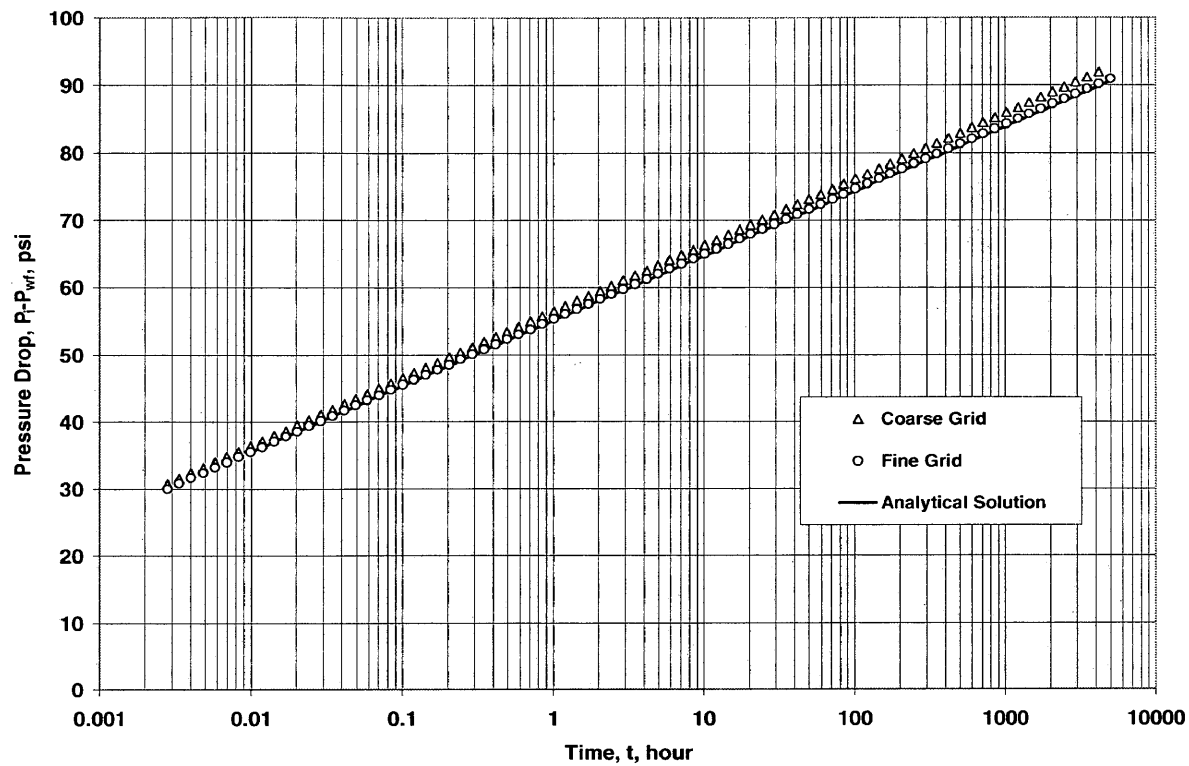


Fig. 2. 5 The comparison of the results for course and fine grids with the analytical solution for commingled system.

CHAPTER 3

PRESSURE TRANSIENT RESPONSES OF LAYERED RESERVOIRS WITH CROSS FLOW

This chapter discusses the characteristics of pressure transient responses of layered reservoirs with cross flow. Comparisons with the responses of dual-porosity systems are also presented. The numerical results are used to obtain a practical correlation to estimate the storativity ratio, ω , for dual-permeability systems and the validity of the correlation for general use is discussed.

Section 3.1 defines the base case as a dual-porosity system ($\kappa = 1$) and presents the rock and fluid data for the base case. Section 3.2 discusses the sensitivity of layered (dual-permeability) reservoir simulations to the transmissivity ratio, κ . The results of the sensitivity analysis are used in Section 3.3 to obtain an empirical correlation for the storativity ratio, ω . Section 3.4 discusses the ranges of accuracy of the correlation for ω and comments on the general validity of the correlation.

3.1 Base Case

It is useful to define a base case consisting of a dual-porosity system to discuss and compare the characteristics of pressure transient responses of layered reservoirs. The base case considers a fully penetrating vertical well at the center of a radial, layered reservoir system. Tables 3.1 and 3.2 present the well and reservoir data for the base case.

The reservoir contains a dry gas at a uniform initial pressure of 5000 psi. The viscosity of the reservoir fluid is 0.02 cp and the total compressibility of the system is 2×10^{-4} psi⁻¹. It is assumed that the pressure does not drop below 3000 psi during the times of interest so that the reservoir fluid may be treated like a liquid. The well produces at a constant rate

of 22 Mscf/D, which is equivalent to 4000 stb/D liquid production. For simplicity, wellbore storage and skin effects are neglected. The wellbore radius is 0.3 ft and the formation volume factor of 1 rbbl/stb.

Table 3. 1 Well and fluid data for the base case.

Constant flow rate	4000 STB/D
Wellbore radius	0.3 ft
Wellbore storage	Neglected
Skin effect	Neglected
Fluid viscosity	0.02 cp
Formation volume factor	1 rbbl/ stb

Table 3. 2 Reservoir properties for the base case

	Layer 1	Layer 2
Initial pressure, psi	5000	5000
Pay thickness, ft	30	270
Total compressibility, psi^{-1}	0.0002	0.0002
Porosity, fraction	0.06	0.06
Radial permeability, md	41	0
Vertical permeability, md	1	1

Bourdet ³ claimed that complex systems with several layers may be simulated by two layers that represent the averages of the high-and low-permeability layers. Therefore, in this study, the attention has been restricted to two-layer systems only. No fault, gas cap, or water drive is present in the system. Fluid expansion is assumed to be the only drive mechanism. The reservoir system is horizontal and each layer is homogeneous.

Both layers have the same porosity of 0.02. The thickness of the first layer is 30 ft and the second layer is 270 ft. Therefore, the storativity ratio for the base case is 0.1. The radial

permeability of layer 1 is 41 md whereas the radial permeability of layer 2 is 0. The vertical permeability is the same for both layers and is 1md. Therefore, this case may also represent a dual-porosity system in which Layer 1 is the fissure or the streak formation with high permeability and Layer 2 is the reservoir matrix with high storage capacity.

Two allow for a long period of infinite acting, a large reservoir of $r_e = 10000$ ft has been assumed. Two test durations for $t_p = 100$ and 1000 hours have been modeled. As shown in Fig. 3.1, both tests are long enough to capture the fundamental characteristics of layered reservoir responses at early and late times. However, the longer test duration will be used in the following discussions to ensure that the correct semi-log straight can be drawn at late times.

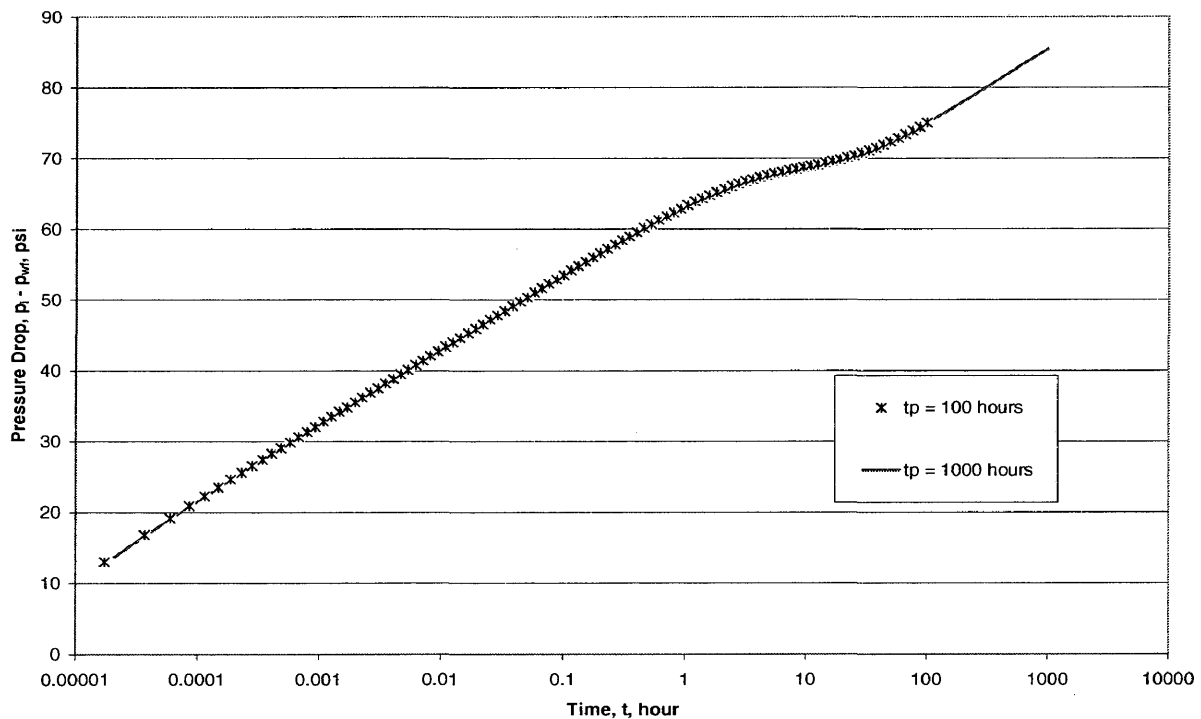


Fig. 3. 1 Effect of test duration on the existence of straight lines on pressure versus log-time plot.

3.2 Sensitivity Study

As mentioned in the previous sections, the base case represents the dual-porosity system in which the matrix medium (layer 2) indirectly communicates with wellbore through high permeable formation (layer 1). This case is relatively simple to analyze by pressure transient testing only. However, if the matrix medium has significant radial permeability and communicates directly with the wellbore (dual-permeability system), then well test analysis may not be sufficient to estimate the layer properties. In such systems, the pressure transient analysis should be supplemented by the knowledge on the storativity ratio, ω , and/or transmissivity ratio κ .

Draw down and buildup responses of dual-permeability and dual-porosity systems display similar characteristics. On a semi-log plot of pressure versus time data, two parallel straight lines characterize two major flow regimes at early and late times (see Fig. 1.1). For the dual-porosity model, the vertical separation between these two parallel lines, δp , is a function of the storativity ratio, ω , and may be used to calculate ω by the following relation¹

$$\omega = e^{-2.303 \frac{\delta p}{m}}, \quad (3.1)$$

where m is the slope of the parallel straight lines (see Appendix B for the derivation)

For dual-permeability systems, a sensitivity analysis is required to determine the parameters influencing the separation between the semi-log straight lines, δp . From the discussion of the physical representation of the dual-permeability systems, it can be expected that δp is a function of the parameters ω , κ . To test the dependency of δp on κ , several cases of layered reservoirs with cross flow have been simulated. The input data for these simulations are the same as the base case except the permeability of the second layer is $k_2 \geq 0$ and the transmissivity ratio has a range of $0.6 \leq \kappa \leq 1$. The values of k_2

and λ for each case can be calculated from the values of k_1 , h_1 , and h_2 by using the definitions of λ and κ given by Eqs. 1.3 and 1.5. Table 3.3 shows the values of k_2 and λ as a function of κ .

Table 3. 3 The values of k_2 and λ as a function of κ for the sensitivity analysis

κ	$k_2, \text{ md}$	λ
1	0	5.42E-07
0.99	0.046016	5.37E-07
0.97	0.140893	5.26E-07
0.95	0.239766	5.15E-07
0.9	0.506173	4.88E-07
0.8	1.138889	4.34E-07
0.7	1.952381	3.79E-07
0.6	3.037037	3.25E-07
0.5	4.555556	2.71E-07

Figure 3.2 shows the diagnostic plots of the pressure and derivative responses for the cases described above. As shown in Fig. 3.2, when κ converges to one, the pressure responses approach those of the dual-porosity system (the base case). The responses approach those of a homogenous reservoir when $\kappa \rightarrow 0.5$. All the other dual-permeability responses for $0.5 < \kappa < 1$ lay in between the dual-porosity and homogeneous system responses. Note that the flat portions of the pressure derivatives shown in Fig. 3.2 correspond to the slopes of the early- and late-time semi-log straight lines. The slopes (m) and the displacements between the semi-log straight lines (δp) are shown in Table 3.4 for each case in Fig. 3.2. (The values of δp have been obtained by making a semi-log plot of the data shown in Fig. 3.2 for each case.) The information derived from Fig. 3.2 and documented in Table 3.4 is used in the next section to obtain an empirical correlation for the storativity ratio, ω , as a function κ .

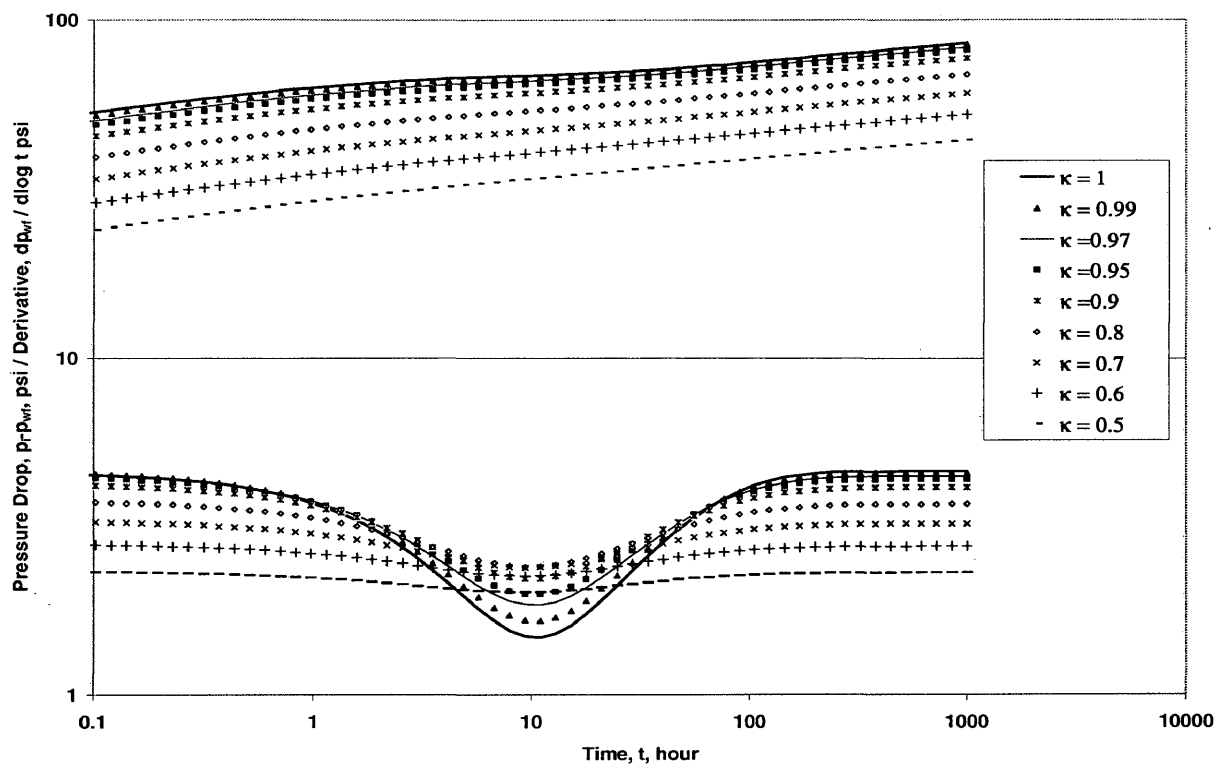


Fig. 3. 2 The log-log plot of layered reservoir responses

Table 3. 4 Slope of the semi-log straight lines and δP as a function of κ

κ	Slope (m)	δP
1	10.57561	9.5
0.99	10.46985	9
0.97	10.25834	8
0.95	10.04683	7.8
0.9	9.518049	6
0.8	8.460488	3.5
0.7	7.402927	2.2
0.6	6.345366	1.5
0.5	5.287805	-

3.3 Empirical Correlation

The results shown in Fig. 3.2 and Table 3.4 indicate that the slope, m , and displacement, δp , change with κ . To obtain a correlation, the ratio, $\delta p/m$, may be assumed as a unique function of κ as shown in Table 3.5.

Table 3.5 The ratio, $\delta p/m$, as a function of κ

κ	$\delta p/m$
1	0.898293
0.99	0.859611
0.97	0.779853
0.95	0.776364
0.9	0.630381
0.8	0.413688
0.7	0.29718
0.6	0.236393

It is clear from Table 3.5 that $\delta p/m$ is smaller for dual-permeability systems ($0.5 < \kappa < 1$) compared to dual-porosity systems ($\kappa = 1$). The objective of this section is to obtain a shrinkage factor that would match the $\delta p/m$ of the dual-permeability system to the corresponding value of the dual-porosity system and incorporate the shrinkage factor into Eq. 3.1.

Normalizing the second column of Table 3.5 with δp_{\max} (the value of δp for the dual-porosity system) and plotting the results against the corresponding κ values yields the trend shown in Fig. 3.3. The best fit through the data yields the following shrinkage factor:

$$SF = 0.025042 e^{3.687198 \kappa} \quad (3.2)$$

Incorporating Eq. 3.2 into Eq. 3.1, yields

$$\omega = e^{-2.303 \frac{\delta p}{m SF}} \quad (3.3)$$

However, as shown in Fig. 3.3, this correlation does not capture all the data points and, hence, an error is expected when using this correlation to calculate the storativity ratio. The magnitude of the error and the validity of the correlation in Eq. 3.3 is discussed in the next section.

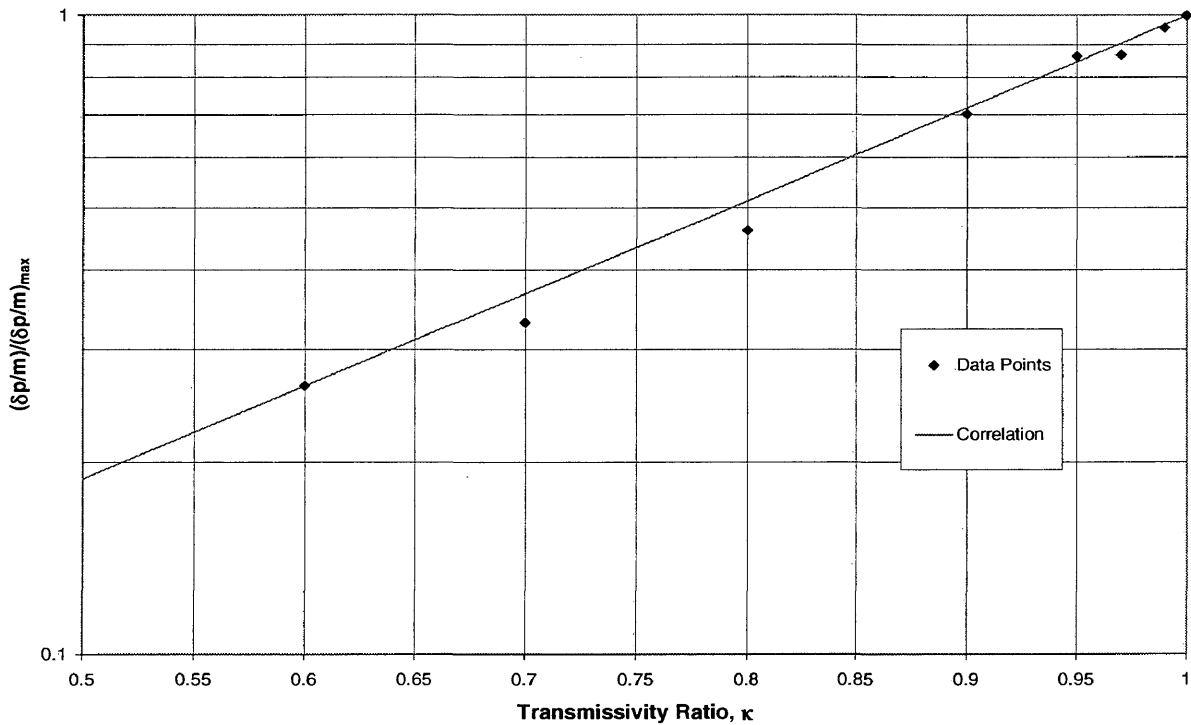


Fig. 3. 3 The correlation of the shrinkage factor.

3.4 Application and Discussion of Results

The empirical correlation derived in the previous section was obtained from a sensitivity study of the base case. The base case, however, has a fixed storativity ratio of $\omega = 0.1$. Here we investigate the effect of ω on the shrinkage factor correlation given by Eq. 3.2.

Table 3.6 shows δp as a function of κ and ω and Table 3.7 documents the error involved in the use of the correlation given by Eq. 3.3.

Table 3. 6 The obtained values of δp and m as a function of ω and κ

ω	κ	m	δp
0.02	0.6	6.345366	3
0.02	0.8	8.460488	6.5
0.02	0.97	10.25834	14
0.05	0.6	6.345366	2
0.05	0.8	8.460488	5
0.05	0.97	10.25834	10
0.1	0.6	6.345366	1.5
0.1	0.8	8.460488	3.5
0.1	0.97	10.25834	8
0.2	0.6	6.345366	1
0.2	0.8	8.460488	2
0.2	0.97	10.25834	5.8
0.3	0.8	8.460488	1.5
0.3	0.97	10.25834	4
0.4	0.8	8.460488	1
0.4	0.97	10.25834	3

Table 3. 7 Error involved in the estimation of ω by using Eq. 3.3.

Input ω	κ	$\delta p/m$	SF	$\delta p/(m \text{ SF})$	Estimated ω	Error %
0.02	0.6	0.472786	0.228806	2.066315056	0.00857655	57.12
0.02	0.8	0.768277	0.478337	1.606141964	0.024749625	23.75
0.02	0.97	1.364743	0.895283	1.524371362	0.029878168	49.39
0.05	0.6	0.315191	0.228806	1.377543371	0.041899458	16.20
0.05	0.8	0.590982	0.478337	1.235493818	0.058114373	16.23
0.05	0.97	0.974816	0.895283	1.088836687	0.081464259	62.93
0.1	0.6	0.236393	0.228806	1.033157528	0.092609663	7.39
0.1	0.8	0.413688	0.478337	0.864845673	0.136457839	36.46
0.1	0.97	0.779853	0.895283	0.871069349	0.134515921	34.52
0.2	0.6	0.157595	0.228806	0.688771685	0.204693571	2.35
0.2	0.8	0.236393	0.478337	0.494197527	0.32041543	60.21
0.2	0.97	0.565394	0.895283	0.631525278	0.233539812	16.77
0.3	0.6	0.177295	0.478337	0.370648146	0.425877864	41.96
0.3	0.8	0.389927	0.895283	0.435534675	0.366764122	22.25
0.3	0.97	0.118196	0.478337	0.247098764	0.566052498	41.51
0.4	0.6	0.292445	0.895283	0.326651006	0.471292072	17.82

Table 3.7 indicates that the maximum error of using the correlation given in Eq. 3.3 is 60 % and most of the estimated storativity ratios have errors above 20%. Figure 3.4 is a plot of the estimated ω versus the input ω . The result shown on this figure indicates that the empirical correlation has a good estimation only at $\omega = 0.1$, which is the value used in the derivation of the shrinkage factor. Therefore, the empirical correlation given in Eq. 3.3 does not have general applicability.

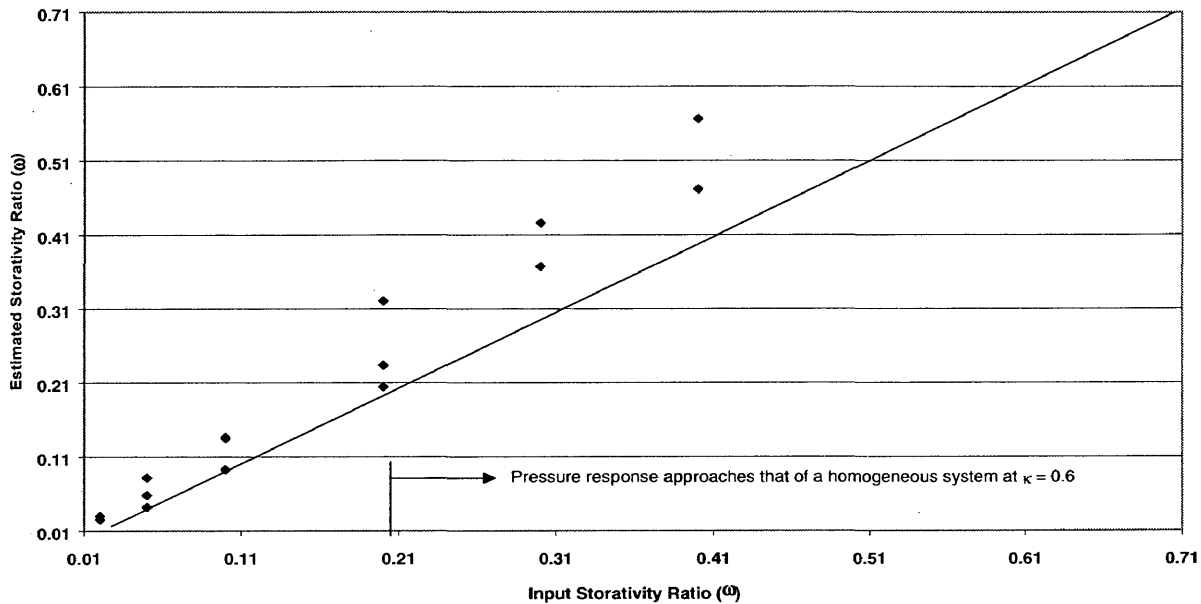


Fig. 3. 4 Error plot for the storativity ratio correlation given by Eq. 3.3.

To finalize our discussion in this section, Fig. 3.5 shows κ as a function of the shrinkage factor at different storativity ratios. The results shown in Fig. 3.5 reaffirm that the shrinkage factor is sensitive to κ and ω and hence the empirical correlation given in Eq. 3.3 is not general. This conclusion has led to the initiation of the analytical study presented in the next chapter.

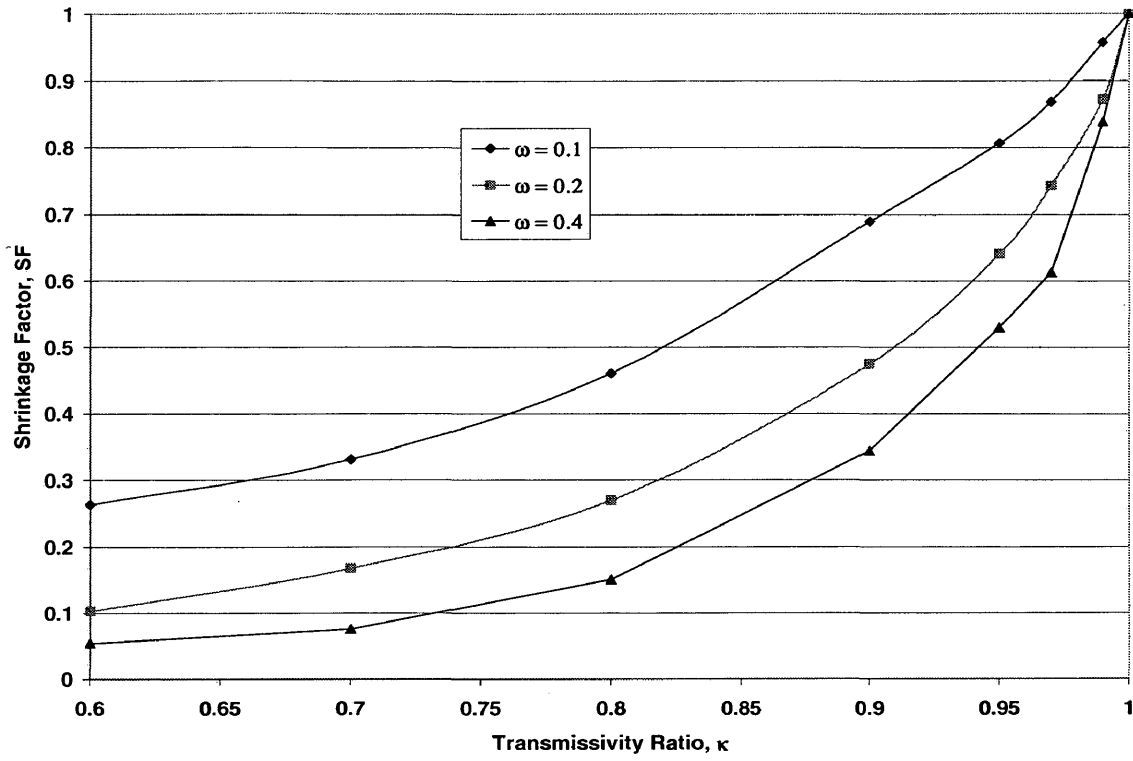


Fig. 3. 5 Shrinkage factor as a function of κ and ω

CHAPTER 4

ANALYTICAL STUDY OF LAYERED RESERVOIR RESPONSES

This chapter discusses the derivation of the analytical solution for storativity and the transmissivity ratios. The first two sections (4.1 & 4.2) highlight the similarities of the layered system responses to those of the commingled and homogeneous systems during early- and late-time flow regimes. Section 4.3 combines the expressions for the early- and late-time pressures of layered reservoirs with cross flow to derive an analytical expression for δp . Sections 4.4 and 4.5 use the analytical solution for δp to obtain an expression to calculate ω for zero and nonzero skin factors, respectively. The applications of the new solutions are also demonstrated in these sections. Section 4.6 discusses the effect of the wellbore storage and Section 4.7 gives the limits and constraints for the approximation of the analytical solution. Finally, Section 4.8 presents an expression to estimate the transmissivity ratio κ .

4.1 Early-Time Behavior

As mentioned before, the objective of this study is to develop a procedure to determine ω defined by Eq. 1.4. This requires an estimate of the vertical separation (δp) between the two parallel straight lines on the semi-log plot of the pressure transient responses. To obtain an analytical expression for δp , the solutions for the early- and late-time semi-log straight lines must be known. The expressions for the semi-log straight lines correspond to the early- and late-time approximations of the general pressure solution. In this section, an early-time approximation is derived. The late-time approximation is obtained in the next section.

To derive a short-time approximation, we first note the equivalence of a layered system with cross flow to a commingled system during the early-time flow regime³ (see Fig. 4.1). The reason of the equivalence between the layered system with cross flow and the corresponding commingled system at early times is dominance of the high-permeability layer until considerable pressure differential is attained in the low-permeability layer to start horizontal and vertical flow. Therefore, until the low-permeability layer starts feeding the wellbore and cross flow begins between the layers, the commingled and cross flow systems display the same pressure responses. Once cross flow starts, then a transitional flow regime begins. The vertical permeability of the layers has a major role to either delay or expedite the transitional flow regime. Based on these physical observations, the commingled system solution can also be used to express the pressure responses of cross flow systems at early times.

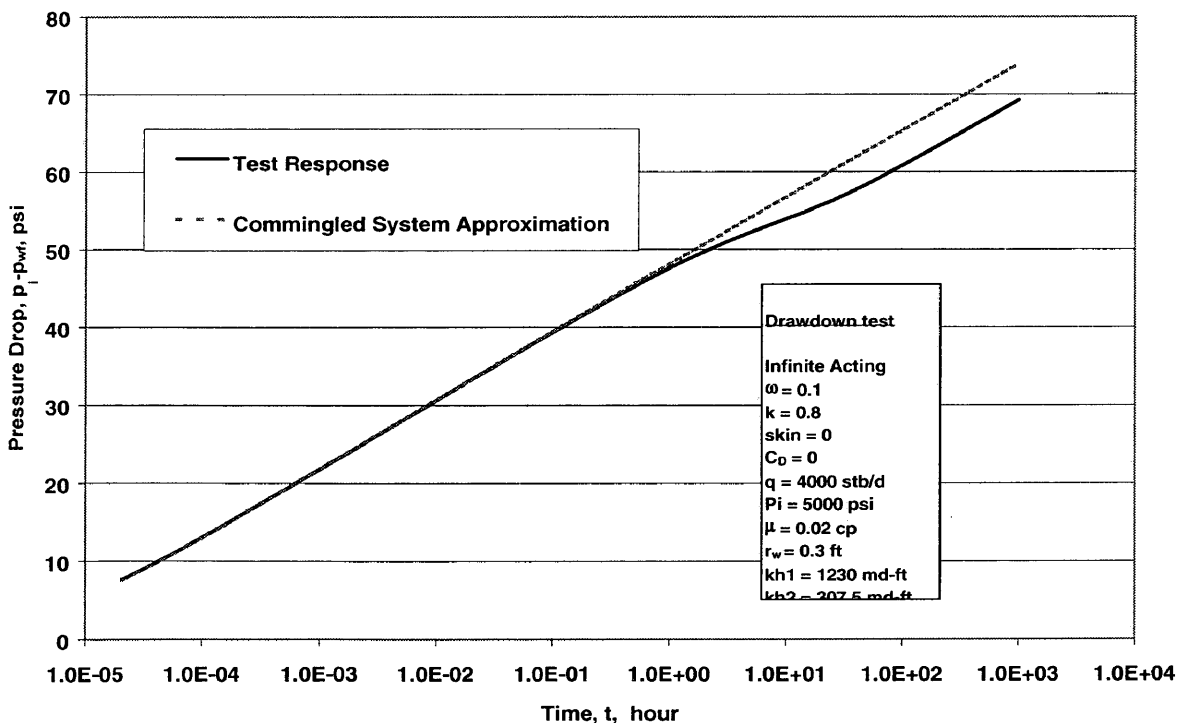


Fig. 4. 1 The correspondence of the early-time responses of commingled and the cross flow systems.

Wijesinghe and Culham¹⁵ have presented the following formulation for naturally fractured reservoirs with significant matrix permeability that might also be used for commingled reservoirs at early times:

$$\begin{cases} \kappa \nabla^2 p_{1D} = \omega \frac{\partial p_{1D}}{\partial t_D} - \tilde{\lambda} (p_{2D} - p_{1D}) \\ (1 - \kappa) \nabla^2 p_{1D} = (1 - \omega) \frac{\partial p_{1D}}{\partial t_D} + \tilde{\lambda} (p_{2D} - p_{1D}) \end{cases}, \quad (4.1)$$

where

$$\tilde{\lambda} = \alpha r_w^2 \frac{k_2 h_2}{k_1 h_1 + k_2 h_2}. \quad (4.2)$$

The subscripts 1 and 2 stand for the high-and low-permeability layers, respectively and the dimensionless pressure and time are defined by

$$p_{Dj} = \frac{k_j h_j}{141.2 q B \mu} (p_i - p_{wj}) \quad (4.3)$$

and

$$t_D = \frac{2.637 \times 10^{-4} \bar{k} t}{\phi c_i \mu r_w^2}. \quad (4.4)$$

where, $k_j h_j$ denotes for the flow capacity of layer j. \bar{k} is the average permeability of the total system.

The problem formulation in Eq. 4.1 assumes pseudosteady fluid transfer from the low-permeability layer to the high-permeability layer.

The solution of Eq. 4.1 for $t \rightarrow 0$ is given in the Laplace domain by ³

$$\bar{p}_{wD} = \frac{1}{z \left[z C_D + \frac{1-\kappa}{s_2 + K_1^o \left(\sqrt{\frac{1-\omega}{1-\kappa}} z \right)} + \frac{\kappa}{s_1 + K_1^o \left(\sqrt{\frac{\omega}{\kappa}} z \right)} \right]}, \quad (4.5)$$

where, s_1 and s_2 are the skin factors of the high-and low-permeability layers, respectively, and $K_1^o(x) = x^{-1} K_o(x)/K_1(x)$. The term C_D denotes the dimensionless wellbore storage coefficient defined by

$$C_D = \frac{5.615 C_{wb}}{2\pi(\phi c_i) h r_w^2} \quad (4.6)$$

with C_{wb} denoting the wellbore storage coefficient.

An approximate inversion of Eq. 4.5 to the real time domain may be obtained as follows. For relatively late times the Laplace transform parameter $z \rightarrow 0$. Because $\lim_{x \rightarrow 0} x K_1(x) = 1$, Eq. (4.5) becomes

$$\bar{p}_{wD} = \frac{1}{z \left[z C_D + \frac{1-\kappa}{s_2 + K_o \left(\sqrt{\frac{1-\omega}{1-\kappa}} z \right)} + \frac{\kappa}{s_1 + K_o \left(\sqrt{\frac{\omega}{\kappa}} z \right)} \right]}. \quad (4.7)$$

Neglecting the wellbore storage effect ($C_D = 0$) and rewriting Eq. 4.7 yields

$$\bar{p}_{wD} = \frac{\left[s_2 + K_o \left(\sqrt{\frac{1-\omega}{1-\kappa}} z \right) \right] \left[s_1 + K_o \left(\sqrt{\frac{\omega}{\kappa}} z \right) \right]}{z \left[(1-\kappa) \left[s_1 + K_o \left(\sqrt{\frac{\omega}{\kappa}} z \right) \right] + (\kappa) \left[s_2 + K_o \left(\sqrt{\frac{1-\omega}{1-\kappa}} z \right) \right] \right]}. \quad (4.8)$$

Substituting the small-argument approximation of $K_0(x) = -\ln(e^\gamma \sqrt{x}/2)$ into Eq. 4.8, gives

$$\bar{p}_{wD} = \frac{\left[s_2 - \ln \left(\frac{e^\gamma}{2} \sqrt{\frac{1-\omega}{1-\kappa}} z \right) \right] \left[s_1 - \ln \left(\frac{e^\gamma}{2} \sqrt{\frac{\omega}{\kappa}} z \right) \right]}{z \left[(1-\kappa) \left[s_1 - \ln \left(\frac{e^\gamma}{2} \sqrt{\frac{\omega}{\kappa}} z \right) \right] + (\kappa) \left[s_2 - \ln \left(\frac{e^\gamma}{2} \sqrt{\frac{1-\omega}{1-\kappa}} z \right) \right] \right]}. \quad (4.9)$$

where $\gamma = 0.5772\dots$ Using Schapery Approximation¹⁶ with Najurieta's Modification¹⁷ to achieve an approximate inversion of Eq. 4.9 yields

$$p_{wD} = \frac{\left[s_2 - \ln \left(\sqrt{\frac{e^\gamma}{4} \frac{1-\omega}{1-\kappa} \frac{1}{t_D}} \right) \right] \left[s_1 - \ln \left(\sqrt{\frac{e^\gamma}{4} \frac{\omega}{\kappa} \frac{1}{t_D}} \right) \right]}{\left[(1-\kappa) \left[s_1 - \ln \left(\sqrt{\frac{e^\gamma}{4} \frac{\omega}{\kappa} \frac{1}{t_D}} \right) \right] + (\kappa) \left[s_2 - \ln \left(\sqrt{\frac{e^\gamma}{4} \frac{1-\omega}{1-\kappa} \frac{1}{t_D}} \right) \right] \right]}. \quad (4.10)$$

The expression given in Eq. 4.10 may be simplified by the following lines. Let

$$p_{wD} = \frac{N}{D} \quad (4.11)$$

where, N and D denote the nominator and denominator of Eq. 4.10, respectively. Then, N and D can be written, respectively, as

$$\begin{aligned}
N &= 0.25[\ln t_D]^2 + 0.5 \left[s_1 + s_2 + \ln \left(\sqrt{\frac{4}{e^\gamma} \frac{1-\kappa}{1-\omega}} \right) + \ln \left(\sqrt{\frac{4}{e^\gamma} \frac{\kappa}{\omega}} \right) \right] \ln t_D \\
&+ s_1 s_2 + s_2 \ln \left(\sqrt{\frac{4}{e^\gamma} \frac{\kappa}{\omega}} \right) + s_1 \ln \left(\sqrt{\frac{4}{e^\gamma} \frac{1-\kappa}{1-\omega}} \right) + \ln \left(\sqrt{\frac{4}{e^\gamma} \frac{\kappa}{\omega}} \right) \ln \left(\sqrt{\frac{4}{e^\gamma} \frac{1-\kappa}{1-\omega}} \right),
\end{aligned} \tag{4.12}$$

and

$$D = 0.5 \ln t_D + (1-\kappa) s_1 + \kappa s_2 + (1-\kappa) \ln \left(\sqrt{\frac{4}{e^\gamma} \frac{\kappa}{\omega}} \right) + \kappa \ln \left(\sqrt{\frac{4}{e^\gamma} \frac{1-\kappa}{1-\omega}} \right). \tag{4.13}$$

Hence, substituting Eqs. 4.12 and 4.13 for N and D into Eq. 4.11 yields

$$\begin{aligned}
p_{wD} &= \left\{ 0.25[\ln t_D]^2 + 0.5 \left[s_1 + s_2 + \ln \left(\sqrt{\beta} \frac{1-\kappa}{1-\omega} \right) + \ln \left(\sqrt{\beta} \frac{\kappa}{\omega} \right) \right] \ln t_D \right. \\
&+ s_1 s_2 + s_2 \ln \left(\sqrt{\beta} \frac{\kappa}{\omega} \right) + s_1 \ln \left(\sqrt{\beta} \frac{1-\kappa}{1-\omega} \right) + \ln \left(\sqrt{\beta} \frac{1-\kappa}{1-\omega} \right) \ln \left(\sqrt{\beta} \frac{\kappa}{\omega} \right) \left. \right\}, \\
&/ \left[0.5 \ln t_D + (1-\kappa) s_1 + \kappa s_2 + (1-\kappa) \ln \left(\sqrt{\beta} \frac{\kappa}{\omega} \right) + \kappa \ln \left(\sqrt{\beta} \frac{1-\kappa}{1-\omega} \right) \right],
\end{aligned} \tag{4.14}$$

where, $\beta = 4/e^\gamma$

Eq. 4.14 can be rewritten as

$$p_{wD} = \frac{0.25 (\ln t_D)^2 + 0.5 a \ln t_D + b}{0.5 \ln t_D + d}, \tag{4.15}$$

where,

$$a = s_1 + s_2 + \ln\left(\sqrt{\beta \frac{1-\kappa}{1-\omega}}\right) + \ln\left(\sqrt{\beta \frac{\kappa}{\omega}}\right), \quad (4.16)$$

$$b = s_1 s_2 + s_2 \ln\left(\sqrt{\beta \frac{\kappa}{\omega}}\right) + s_1 \ln\left(\sqrt{\beta \frac{1-\kappa}{1-\omega}}\right) + \ln\left(\sqrt{\beta \frac{1-\kappa}{1-\omega}}\right) \ln\left(\sqrt{\beta \frac{\kappa}{\omega}}\right), \quad (4.17)$$

and

$$d = (1-\kappa) s_1 + \kappa s_2 + (1-\kappa) \ln\left(\sqrt{\beta \frac{\kappa}{\omega}}\right) + -k \ln\left(\sqrt{\beta \frac{1-\kappa}{1-\omega}}\right). \quad (4.18)$$

4.2 Late-Time Behavior

The pressure responses of the late flow period of dual-permeability/porosity systems typically agree with the responses of homogeneous reservoirs.¹⁸⁻²⁰ The layered system acts at late times as a homogeneous system which has an equivalent flow capacity equal to total flow capacity of the layers. This equivalence of the late-time responses of the two systems is shown in Fig. 4.2. Therefore, the late-time approximation of the homogeneous reservoir solution given below may also be used for layered systems with cross flow (see Appendix B for the derivation):

$$p_{wD} = 0.5 \ln t_D + \ln(\sqrt{\beta}) + s_a, \quad (4.19)$$

where s_a is the apparent skin factor. This equation represents the second semi-log straight line that occurs in the late-time region of the pressure versus time plot.

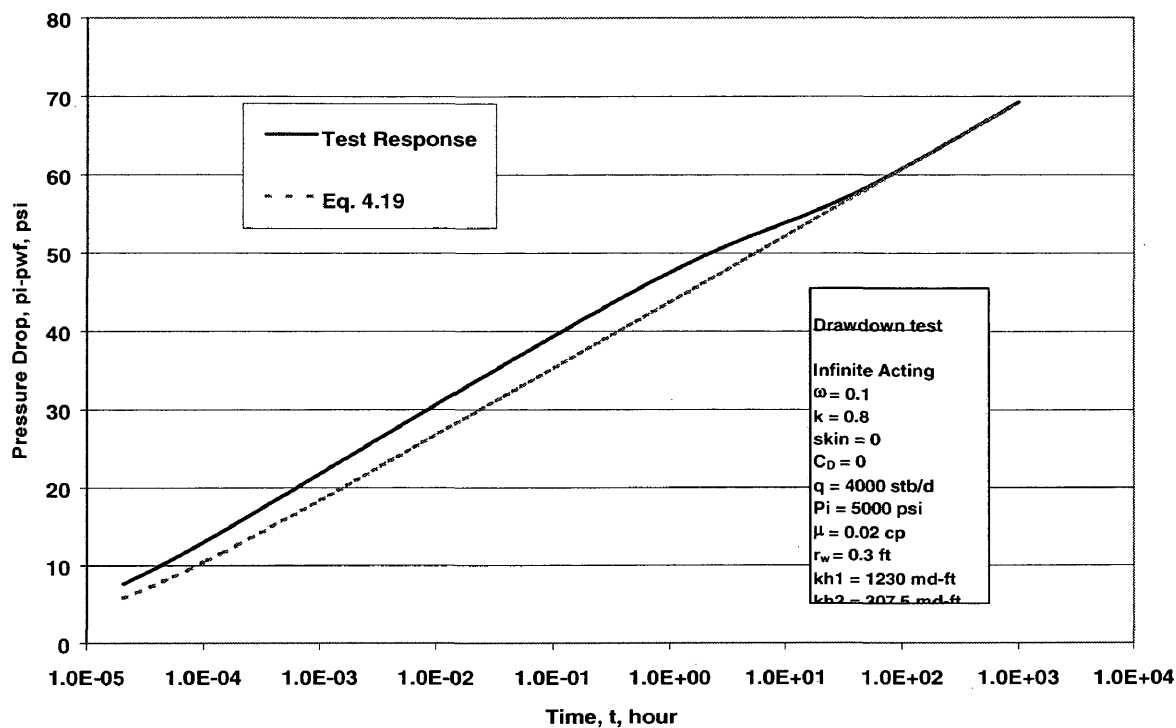


Fig. 4. 2 The equivalence of the homogeneous and cross flow systems.

4.3 The Vertical Separation between the Parallel Lines (δp)

As mentioned above, the separation between the late-and early-time semi-log straight lines, δp , can be determined from the early-and late-time approximations of the pressure solution. Therefore, if we let $(p_D)_l$ and $(p_D)_e$ denote the late-and early-time approximations given by Eqs. 4.19 and 4.15, respectively, an expression for δp_D is given by

$$\begin{aligned} \delta p_D &= (p_D)_e - (p_D)_l \\ &= \frac{0.25 (\ln t_D)^2 + 0.5 a \ln t_D + b}{0.5 \ln t_D + d} - \left[0.5 \ln t_D + \ln(\sqrt{\beta}) + s_a \right] \end{aligned} \quad (4.20)$$

However, δp_D given by Eq. 4.20 is time dependent because $(p_D)_e$ given by Eq. 4.15 does not represent a semi-log relation if $\omega < 0.02$. This reflects the fact that the layered reservoir responses do not display a semi-log straight line at early-times if $\omega < 0.02$ as shown in Fig. 4.3.

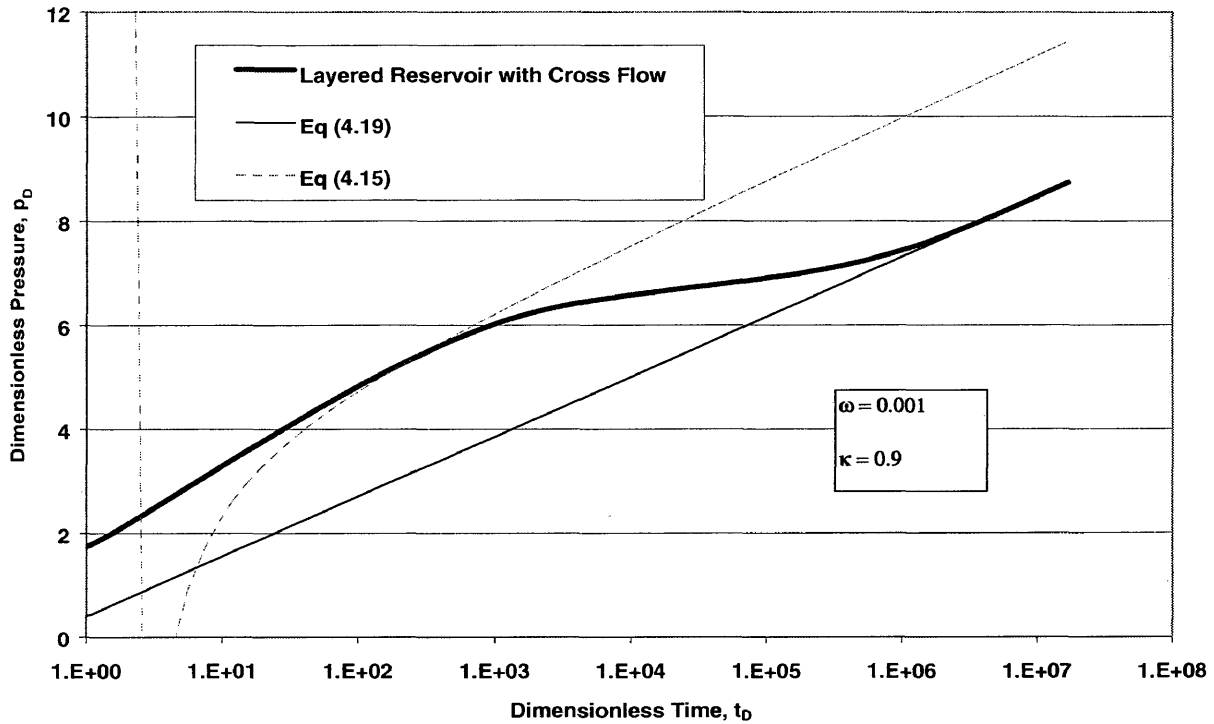


Fig. 4. 3 Semi-log plot of layered reservoir responses for small values of ω

To eliminate this dependency of δp_D on time, the early-time approximation may be written as

$$(p_D)_e = 0.5 \ln t_D + c, \quad (4.21)$$

where

$$c = \frac{0.25 (\ln t_D)^2 + 0.5 a \ln t_D + b}{0.5 \ln t_D + d} - 0.5 \ln t_D. \quad (4.22)$$

If we let $\alpha' = \ln t_D$, then

$$c = \frac{0.5 \alpha' (a - d) + b}{0.5 \alpha' + d}. \quad (4.23)$$

Numerical experiments with more than 20 cases covering a large range of reservoir and fluid properties have indicated that Eq. 4.21 yields the correct straight line relation to be used to calculate δp_D if $\alpha' = 5$. Thus, the equation of the first straight line is given by

$$(p_D)_{1^{st} \text{ line}} = 0.5 \ln t_D + \frac{2.5 (a - d) + b}{2.5 + d}. \quad (4.24)$$

It must be emphasized that Eq. 4.24 does not represent an approximation for Eq. 4.15. The purpose of defining the semi-log straight-line relation given by Eq. 4.24 is to obtain an expression for δp_D . Figure 4.4 displays the layered reservoir responses and the results of various approximations developed above.

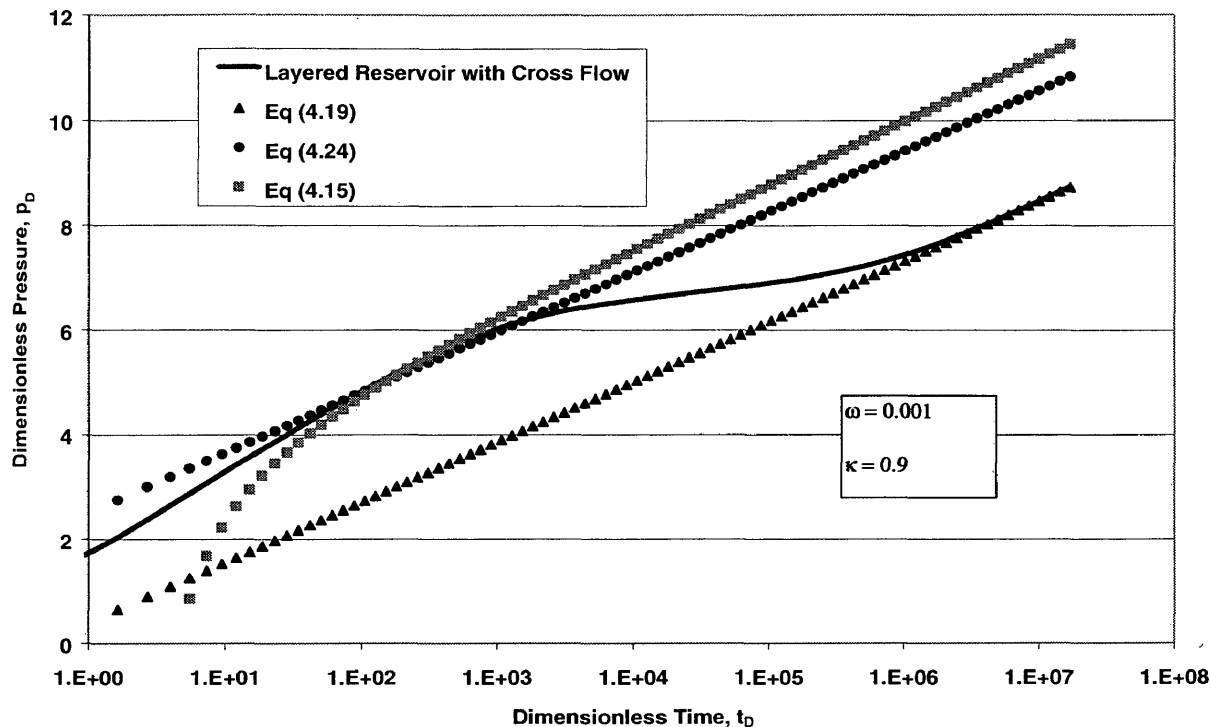


Fig. 4. 4 Layered reservoir responses and the approximate solutions at early and late times.

Using Eq. 4.24 instead of 4.15 in Eq. 4.20 gives

$$\delta p_D = \frac{2.5(a-d)+b}{2.5+d} - \ln(\sqrt{\beta}) - s_a. \quad (4.25)$$

Substituting Eqs. 4.16 to 4.18 into Eq. 4.25 yields

$$\begin{aligned}
\delta p_D = & \left\{ 2.5 \left[s_1 + s_2 + \ln \left(\sqrt{\beta \frac{1-\kappa}{1-\omega}} \right) + \ln \left(\sqrt{\beta \frac{\kappa}{\omega}} \right) - (1-\kappa) s_1 + \kappa s_2 - (1-\kappa) \ln \left(\sqrt{\beta \frac{\kappa}{\omega}} \right) \right. \right. \\
& \left. \left. - \kappa \ln \left(\sqrt{\beta \frac{1-\kappa}{1-\omega}} \right) \right] + s_1 s_2 + s_2 \ln \left(\sqrt{\beta \frac{\kappa}{\omega}} \right) + s_1 \ln \left(\sqrt{\beta \frac{1-\kappa}{1-\omega}} \right) + \ln \left(\sqrt{\beta \frac{1-\kappa}{1-\omega}} \right) \ln \left(\sqrt{\beta \frac{\kappa}{\omega}} \right) \right\} \\
& / \left[2.5 + (1-\kappa) s_1 + \kappa s_2 + (1-\kappa) \ln \left(\sqrt{\beta \frac{\kappa}{\omega}} \right) + -\kappa \ln \left(\sqrt{\beta \frac{1-\kappa}{1-\omega}} \right) \right] - \ln(\sqrt{\beta}) - s_a
\end{aligned} \tag{4.26}$$

4.4 Solution for ω with $s = 0$

Here, an analytical solution for storativity ratio, ω , is derived from Eq. 4.26 as a function of κ and δp_D . The skin factor is neglected for simplicity. Incorporating non-zero skin into the equation for ω is discussed in the next section.

Neglecting skin ($s = 0$), Eq. 4.26 becomes

$$\begin{aligned}
\delta p_D = & \left\{ 2.5 \left[\ln \left(\sqrt{\beta \frac{1-\kappa}{1-\omega}} \right) + \ln \left(\sqrt{\beta \frac{\kappa}{\omega}} \right) - (1-\kappa) \ln \left(\sqrt{\beta \frac{\kappa}{\omega}} \right) - \kappa \ln \left(\sqrt{\beta \frac{1-\kappa}{1-\omega}} \right) \right] \right. \\
& \left. + \ln \left(\sqrt{\beta \frac{1-\kappa}{1-\omega}} \right) \ln \left(\sqrt{\beta \frac{\kappa}{\omega}} \right) \right\} / \left[2.5 + (1-\kappa) \ln \left(\sqrt{\beta \frac{\kappa}{\omega}} \right) + -\kappa \ln \left(\sqrt{\beta \frac{1-\kappa}{1-\omega}} \right) \right] - \ln(\sqrt{\beta})
\end{aligned} \tag{4.27}$$

Solving Eq. 4.27 for ω in terms of κ and δp_D yields

$$\begin{aligned}
& \ln(1-\omega) \ln(\omega) + [2 \kappa \delta p_D + \kappa \ln(\beta) - \ln(\beta \kappa) - 5(1-\kappa)] \ln(1-\omega) \\
& + \{2(1-\kappa) \delta p_D + (1-\kappa) \ln(\beta) - 5 \kappa - \ln[\beta(1-\kappa)]\} \ln(\omega) \\
& + [\ln(\beta \kappa) + 5(1-\kappa) - 2 \delta p_D \kappa - \kappa \ln(\beta)] \ln(1-\kappa) \\
& + [5 \kappa - 2(1-\kappa) \delta p_D - (1-\kappa) \ln(\beta) + \ln(\beta)] \ln(\kappa) = 2 \delta p_D \ln(\beta) + 10 \delta p_D
\end{aligned} \tag{4.28}$$

Taking the exponential of the both sides of Eq. 4.28 gives

$$(1-\omega)^{\ln(\omega)+A'} \omega^{B'} = (1-\kappa)^{A'} \kappa^{B'+\ln(1-\kappa)} e^{E'} \tag{4.29}$$

where,

$$A' = [2 \kappa \delta p_D + \kappa \ln(\beta) - \ln(\beta \kappa) - 5(1-\kappa)], \tag{4.30}$$

$$B' = [2(1-\kappa) \delta p_D + (1-\kappa) \ln(\beta) - 5 \kappa - \ln(\beta(1-\kappa))], \tag{4.31}$$

and

$$E' = 2 \delta p_D \ln(\beta) + 10 \delta p_D. \tag{4.32}$$

Figure 4.5 shows ω versus the right hand side (RHS) of Eq. 4.29 at different κ values and Fig. 4.6 shows the error estimates resulting from the use of Eq. 4.29 for the data in Table 3.6. The results indicate that the solution given in Eq. 4.29 yields satisfactory estimates of ω .

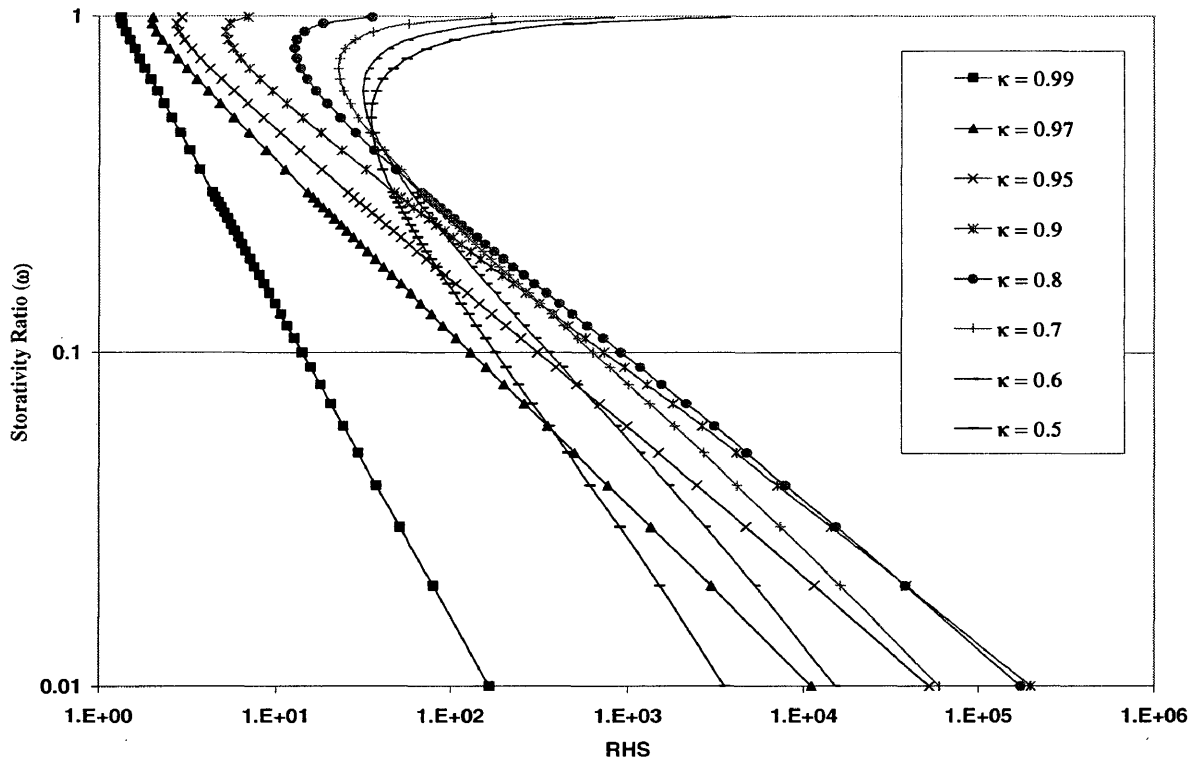


Fig. 4.5 The estimation of ω as function of RHS from Eq. 4.29

It must be noted from Fig. 4.6 that the error is higher for $\omega = 0.2$ and $\kappa = 0.6$, because for this case δp_D becomes too small to obtain graphically from the semi-log plot. It is also important to note that Eq. 4.29 predicts double values for ω for some values of RHS and κ as shown in Fig. 4.5. This apparent flaw of Eq. 4.29 is eliminated when the practical ranges of Eq. 4.29 are considered in Section 4.7.

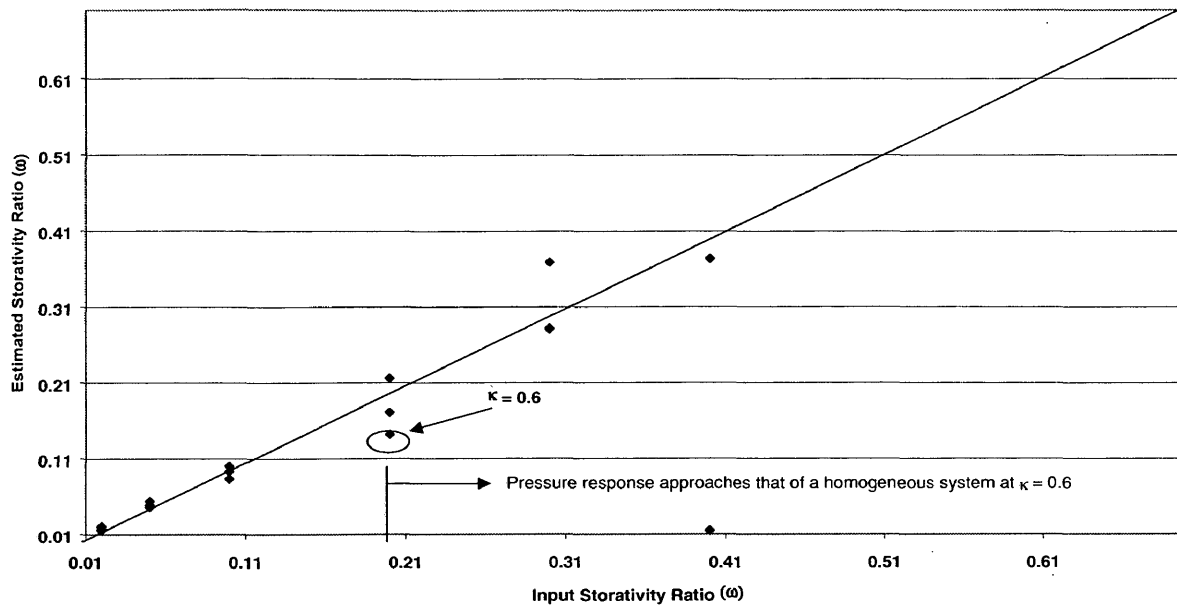


Fig. 4. 6 Error plot for the estimates of ω from Eq. 4.32 for the data in Table 3.6

As stated earlier, Eq. 4.29 ignores the skin factor ($s = 0$), which is an ideal condition. The next section discusses the incorporation of the skin effect into Eq. 4.29.

4.5 Solution for ω with $s \neq 0$

When the apparent skin, s_a , is nonzero, it is possible to consider two cases; uniform skin, $s_1 = s_2$, and none uniform skin, $s_1 \neq s_2$. However, the apparent skin term for the none uniform skin case is a function of different reservoir parameters and is represented by complex correlations such as the one given by Ref. 21. Therefore, only the uniform skin case is considered in this study and

$$s_a = s = s_1 + s_2 \quad (4.33)$$

is used in the following derivations.

With the assumption expressed by Eq. 4.33, Eq. 4.26 becomes

$$\begin{aligned}
\delta p_D = & \left\{ 2.5 \left[s + \ln \left(\sqrt{\beta \frac{1-\kappa}{1-\omega}} \right) + \ln \left(\sqrt{\beta \frac{\kappa}{\omega}} \right) - (1-\kappa) \ln \left(\sqrt{\beta \frac{\kappa}{\omega}} \right) \right. \right. \\
& \left. \left. - \kappa \ln \left(\sqrt{\beta \frac{1-\kappa}{1-\omega}} \right) \right] + s^2 + s \ln \left(\sqrt{\beta \frac{\kappa}{\omega}} \right) + s \ln \left(\sqrt{\beta \frac{1-\kappa}{1-\omega}} \right) + \ln \left(\sqrt{\beta \frac{1-\kappa}{1-\omega}} \right) \ln \left(\sqrt{\beta \frac{\kappa}{\omega}} \right) \right\} \\
& / \left[2.5 + s + (1-\kappa) \ln \left(\sqrt{\beta \frac{\kappa}{\omega}} \right) + \kappa \ln \left(\sqrt{\beta \frac{1-\kappa}{1-\omega}} \right) - \ln(\sqrt{\beta}) - s \right]
\end{aligned} \tag{4.34}$$

Solving Eq. 4.34 for ω in term of κ , δp_D , and s gives

$$\begin{aligned}
& \ln(1-\omega) \ln(\omega) + 2 \left[\kappa \delta p_D + 0.5 \kappa \ln(\beta) - 0.5 \ln(\beta \kappa) - 2.5 (1-\kappa) + \kappa s - s \right] \ln(1-\omega) \\
& + 2 \left[(1-\kappa) \delta p_D + 0.5 (1-\kappa) \ln(\beta) - 2.5 \kappa - 0.5 \ln(\beta(1-\kappa)) - \kappa s \right] \ln(\omega) \\
& + 2 \left[0.5 \ln(\beta \kappa) + 2.5 (1-\kappa) - \delta p_D \kappa - 0.5 \kappa \ln(\beta) \right] \ln(1-\kappa) \\
& + 2 \left[2.5 \kappa - (1-\kappa) \delta p_D - 0.5 (1-\kappa) \ln(\beta) + 0.5 \ln(\beta) \right] \ln(\kappa) \\
& = 2 \delta p_D \ln(\beta) + 10 \delta p_D + 4 \delta p_D s
\end{aligned} \tag{4.35}$$

Taking the exponential of the both sides of Eq. 4.35 gives

$$(1-\omega)^{\ln(\omega)+A'} \omega^{B'} = (1-\kappa)^{A'} k^{B'+\ln(1-\kappa)} e^E \tag{4.36}$$

where,

$$A' = 2 [\kappa \delta p_D + 0.5 \kappa \ln(\beta) - 0.5 \ln(\beta \kappa) - 2.5 (1 - \kappa) + \kappa s - s] \quad (4.37)$$

$$B' = 2 [(1 - \kappa) \delta p_D + 0.5 (1 - \kappa) \ln(\beta) - 2.5 \kappa - 0.5 \ln(\beta(1 - \kappa))] \quad (4.38)$$

and

$$E' = 2 \delta p_D \ln(\beta) + 10 \delta p_D + 4 \delta p_D s. \quad (4.39)$$

Table 4.1 shows the simulated data for a uniform skin factor of 10 and Fig. 4.7 shows the error in the estimates of ω by using Eq. 4.36. The results indicate that Eq. 4.36 is sufficiently accurate for practical estimations of ω for uniform skin factors. However, more work is needed to extend these results to none-uniform skin cases.

Table 4. 1 Simulated data for draw down tests with a uniform skin of $s=10$.

ω	κ	m, psi	δp , psi
0.02	0.6	6.345366	4.5
0.02	0.8	8.460488	9.5
0.02	0.97	10.25834	16
0.05	0.6	6.345366	3
0.05	0.8	8.460488	7
0.05	0.97	10.25834	12
0.1	0.6	6.345366	2
0.1	0.8	8.460488	5
0.1	0.97	10.25834	10
0.2	0.6	6.345366	1.1
0.2	0.8	8.460488	3
0.2	0.97	10.25834	6.5
0.3	0.8	8.460488	2
0.3	0.97	10.25834	5
0.4	0.8	8.460488	1.2
0.4	0.97	10.25834	3.5

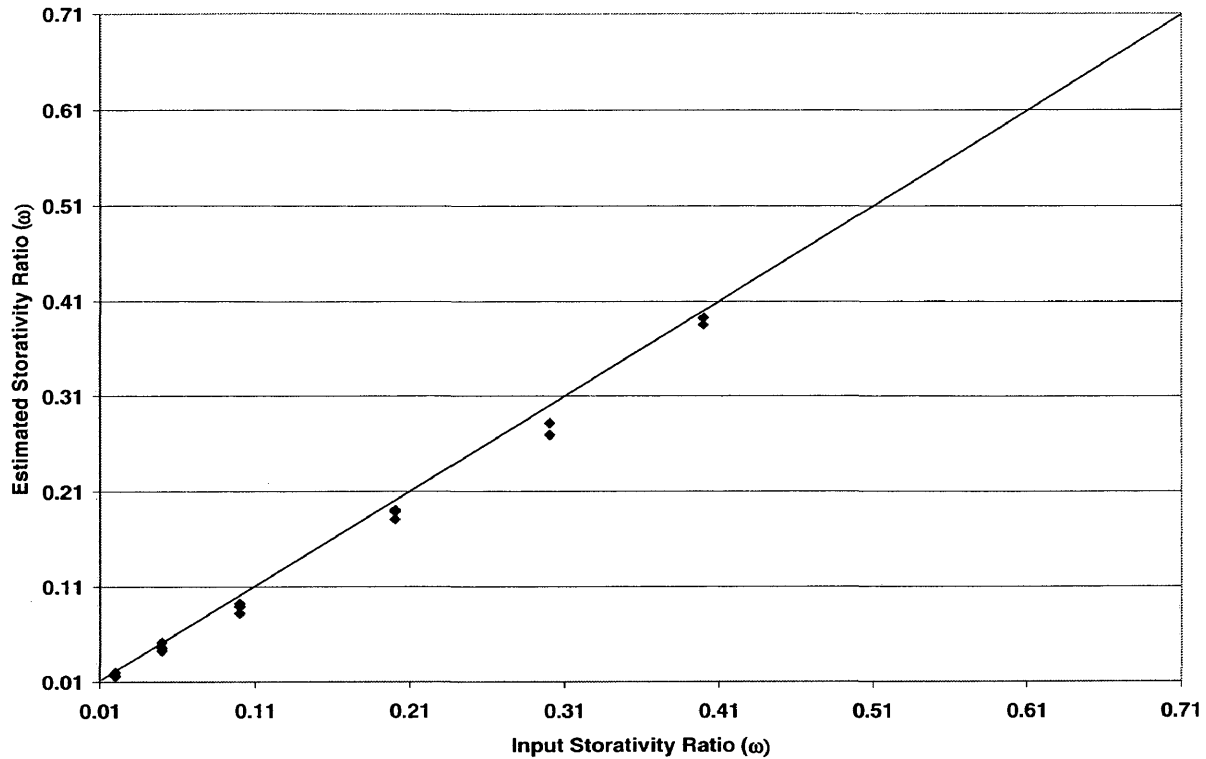


Fig. 4. 7 Error plot for Eq. 4.40 with $s = 10$ (uniform) and the data in Table 4.1.

4.6 Effect of Wellbore Storage

Wellbore storage can mask the early time flow regime and the first straight line on the semi-log plot of the pressure responses may not exist or may be difficult to identify. Figure 4.8 illustrates the effect of wellbore storage on the early-time flow regime of a layered reservoir with cross flow.

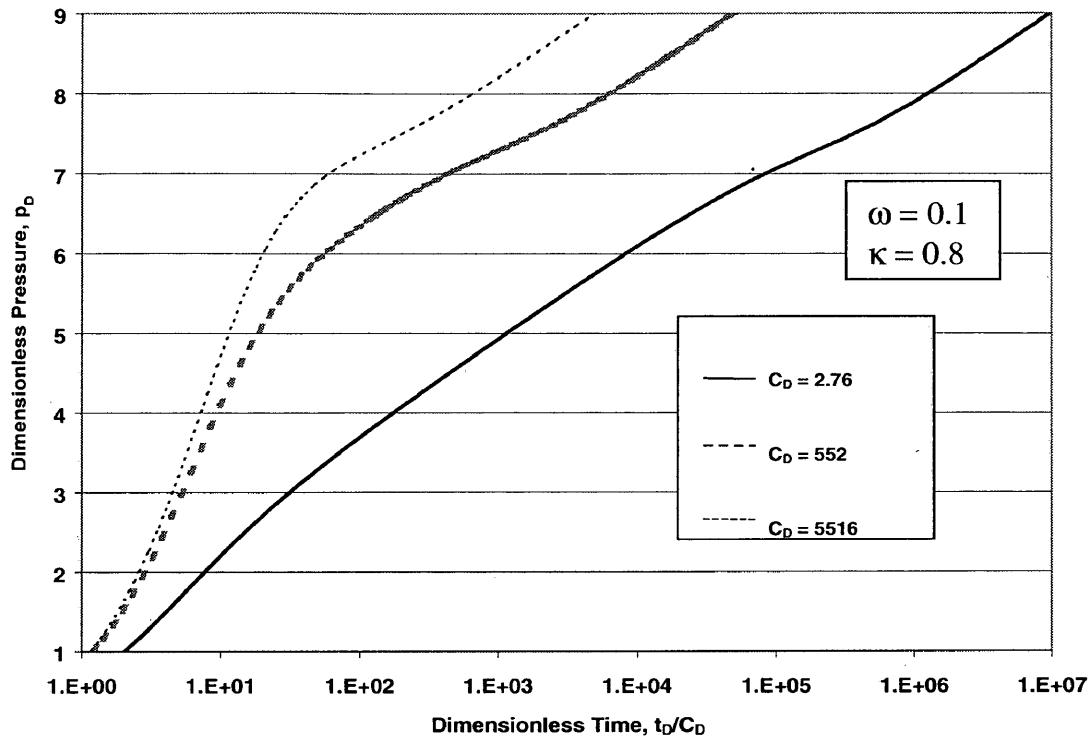


Fig. 4. 8 The effect of wellbore storage on the early time flow regime.

When the vertical permeability of the matrix medium is high, the problem is aggravated because the transient flow regime begins earlier. As a result, the early flow period may not be long enough to detect. In general, small wellbore storage and low vertical permeability increases the probability of the first semi-log straight line to occur. Figure 4.9 highlights this problem.

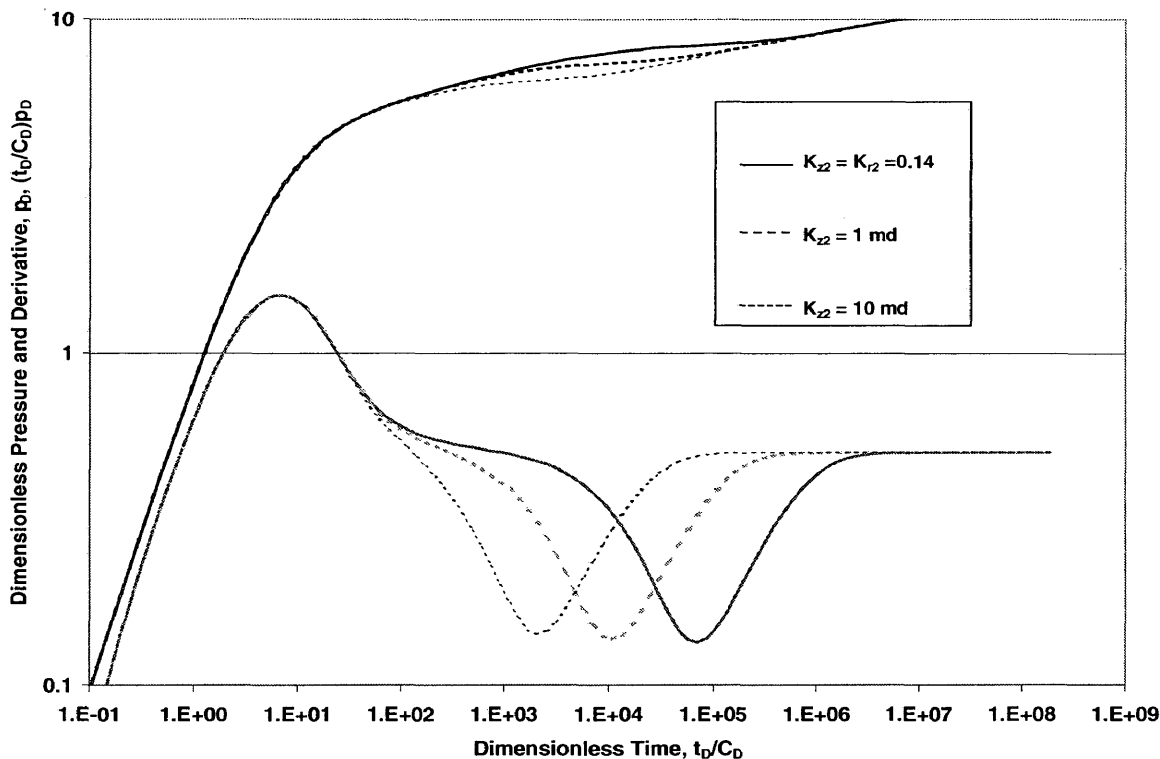


Fig. 4. 9 The start of the intermediate time flow regime as a function of k_{z2} .

4.7 Range of Application of the Analytical Solution

A heterogeneous system is identified as a dual-permeability system if $0.5 < \kappa < 1$.³ For $\kappa < 0.5$, the system is more likely to be homogeneous than dual-permeability. No practical range for ω has been documented in the literature. However, J.S. Olarewju and W.J. Lee²² claim that for $\omega = 0.5$, the characteristics of the intermediate-time flow regime are difficult to detect. In this study, for $\omega = 0.5$ the intermediate-time flow regime has been detected for long tests. However, the intermediate-time flow regime may be detected for short tests if the vertical permeability is relatively high. Vertical permeability does not affect the duration of the intermediate-time flow period but it plays a role on the start of this flow regime. Hence, the intermediate-time flow regime may be more likely to detect for large values of ω if the test is short.

In this study, it was observed that when $\delta p_D < 0.08$, the dual-permeability behavior approaches that of a homogeneous system. In this case, the vertical separation between the two semi-log straight lines at early- and late-times becomes small; that is, δp is difficult to estimate graphically from the semi-log plot. Therefore, $\delta p_D \approx 0.08$ may be taken as the practical minimum of δp_D that can be graphically determined from semi-log plots. Based on these observations, Table 4.2 presents the upper limits of ω that correspond to the practical minimum of $\delta p_D \approx 0.08$ for $0.5 \leq \kappa < 1$. In other words, Table 4.2 indicates the ranges for which the method to estimate ω proposed in this study is applicable. Based on the above discussion, however, it can be assumed that outside the range indicated in Table 4.2, the heterogeneous system may be closely approximated by a homogeneous system.

Table 4.2 *The upper limits of ω based on the practical minimum of δp_D .*

κ	Upper limit of ω
0.99	0.7
0.97	0.7
0.95	0.6
0.9	0.5
0.8	0.4
0.7	0.3
0.6	0.2
0.5	0.1

It should be also noted that the application of the practical ranges in Table 4.2 removes the problem of double ω estimates demonstrated in Fig. 4.5. Considering the practical ranges of Eq. 4.29, the results shown in Fig. 4.5 have been replotted in Fig. 4.10. Unlike Fig. 4.5, Fig. 4.10 yields single-valued estimates of ω .

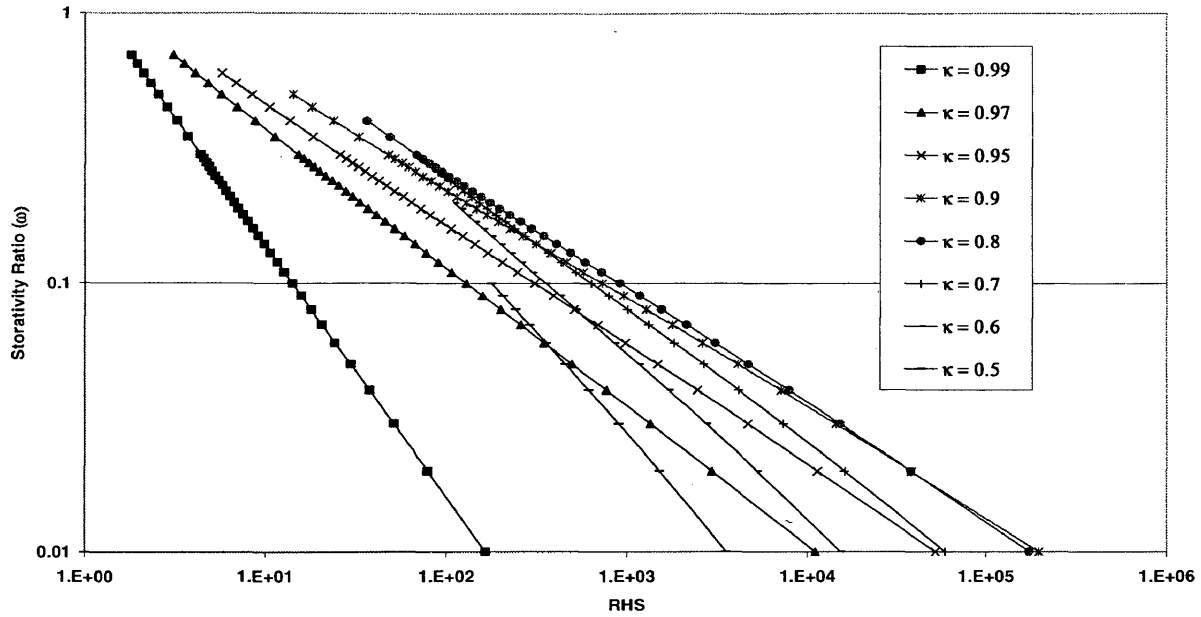


Fig. 4.10 Estimation of ω from Eq. 4.29 within the practical ranges of parameters.

Fig. 4.10 also shows that within the practical ranges of parameters, ω displays a linear relation with the right hand side (RHS) of Eq. 4.29. This relation can be defined by the following approximation:

$$\omega = a' RHS^{b'}, \quad (4.40)$$

where

$$RHS = (1 - \kappa)^{A'} \kappa^{B' + \ln(1 - \kappa)} e^{E'}, \quad (4.41)$$

and the constants, a and b, are defined, respectively, by

$$a' = 1.1759 \kappa^{-3.0932}, \quad (4.42)$$

and

$$b = \begin{cases} -0.57780\kappa^3 - 1.7189\kappa^2 + 4.4076\kappa - 2.5965 & \text{for } 0.5 < \kappa < 0.95 \\ -10.117 \ln \kappa - 0.2678 & \text{for } 0.95 \leq \kappa \leq 0.99 \end{cases} \quad (4.43)$$

Figure 4.11 documents the error resulting from the use of the approximate relation for ω given by Eq. 4.40 for the data in Table 3.6. Although Fig. 4.11 indicates that Eq. 4.40 is a very good approximation, it is only applicable for $s = 0$. For $s \neq 0$, the coefficients, a and b , in Eq. 4.40 are functions of s (see Fig. 4.12 and 4.13) and the relationship between ω and the RHS is not linear. Thus a simple approximation similar to Eq. 4.40 could not be derived for $s \neq 0$ in this study.

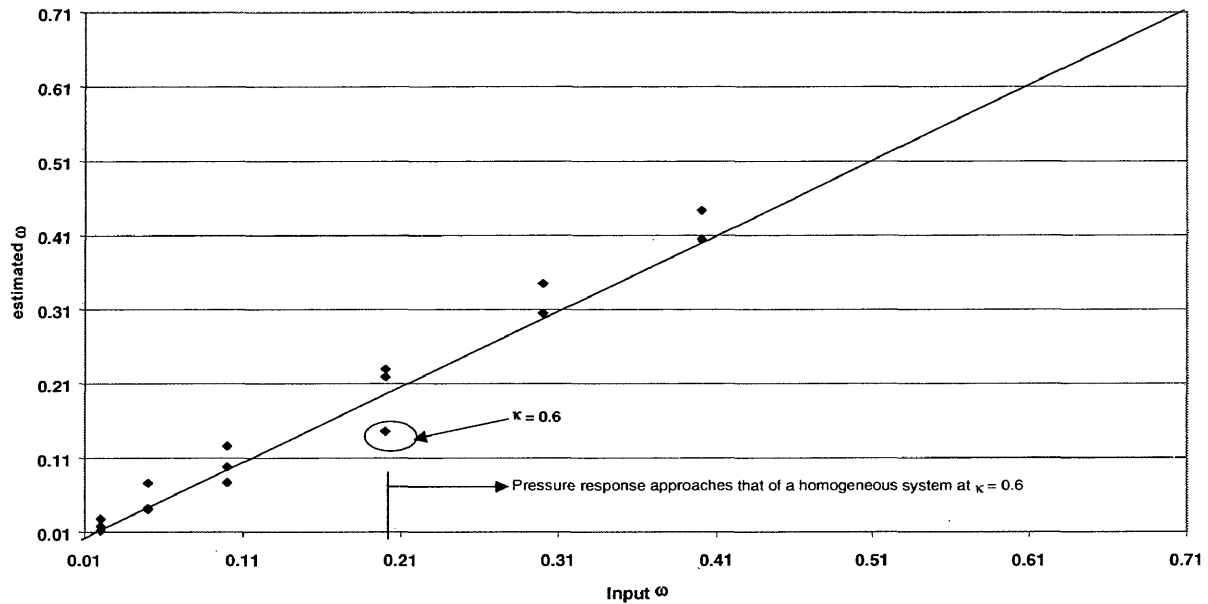


Fig. 4. 11 The error plot for Eq. 4.40 for the data in Table 3.6.

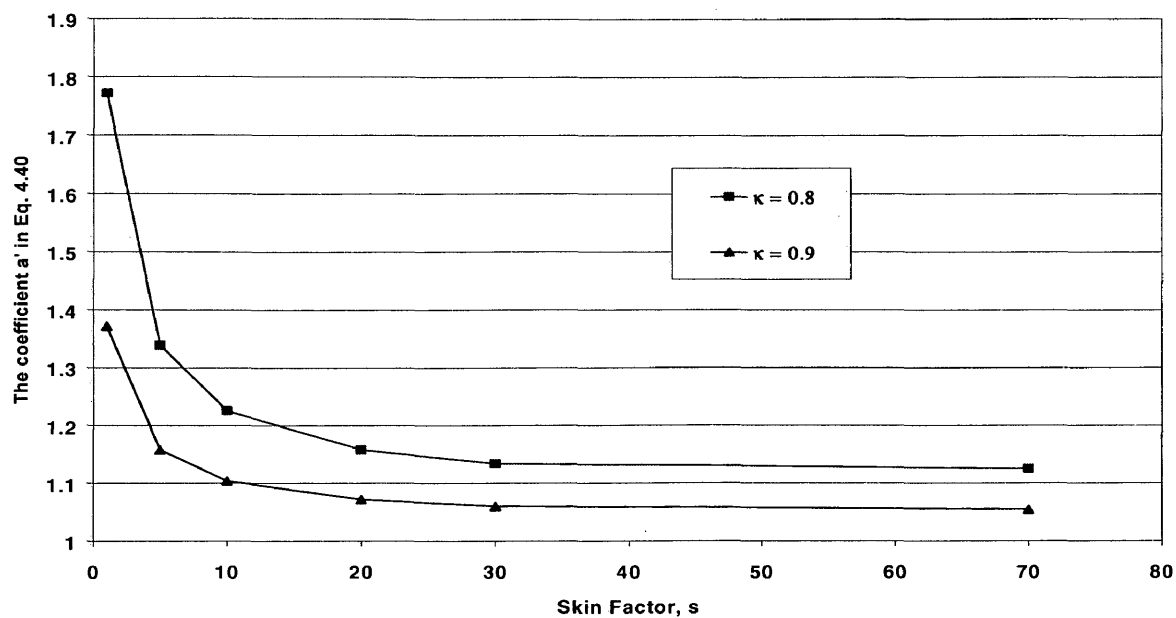


Fig. 4. 12 The coefficient a in Eq. 4.40 as a function of the skin factor for different values of κ

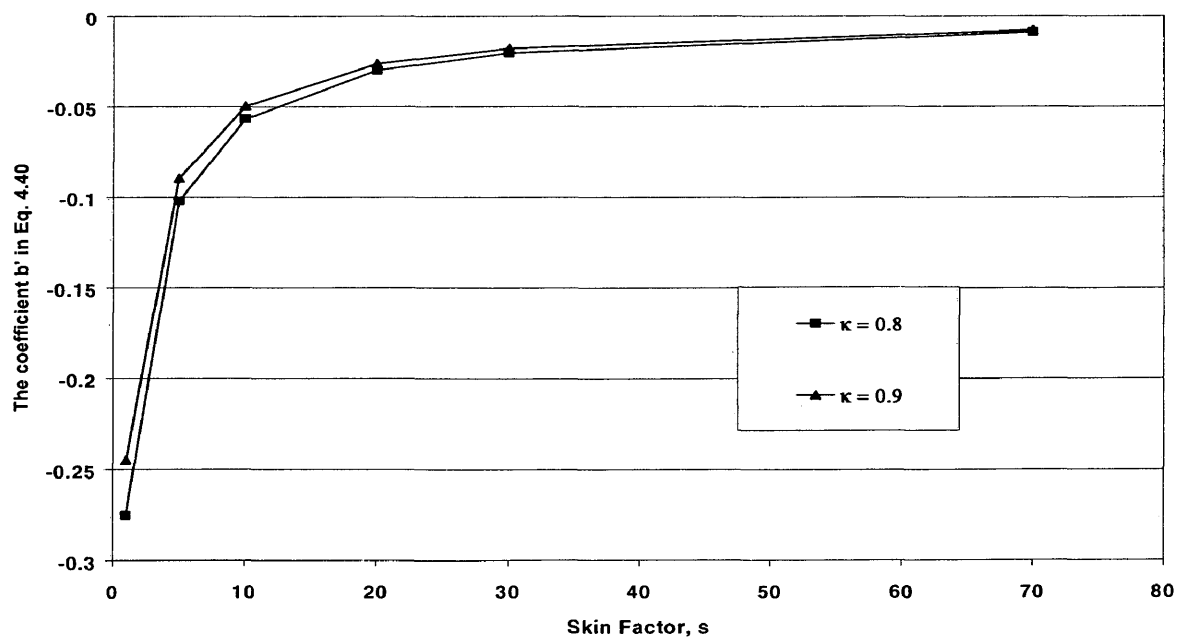


Fig. 4. 13 The coefficient b in Eq. 4.40 as a function of the skin factor for different values of κ

4.8 Solution for κ

Similar to the procedure to obtain an analytical expression for ω , Eq. 4.34 may be used to obtain an expression for κ in terms of ω , δp_D , and s . This yields

$$(1 - \kappa)^{\ln(\kappa) + A'' + B'' \kappa} \kappa^{C'' - B'' \kappa} e^{F'' \kappa} = e^{G''} \quad (4.44)$$

where

$$A'' = 5 - \ln\left(\frac{\omega}{\beta}\right) + 2s \quad (4.45)$$

$$B'' = -5 - 2\delta p_D - \ln(\beta) - 2s \quad (4.46)$$

$$C'' = -\ln(1 - \omega) - 2\delta p_D \quad (4.47)$$

$$F'' = (5 + 2\delta p_D + \ln(\beta) + 2s)(\ln(1 - \omega) - \ln(\omega)) \quad (4.48)$$

and

$$G'' = 10\delta p_D + 5\ln(\beta) + \left[5 + 2s - \ln\left(\frac{\omega}{\beta}\right)\right] \ln\left(\frac{1 - \omega}{\beta}\right) - [2\delta p_D + \ln(\beta)] \ln\left(\frac{\omega}{\beta}\right) + 4\delta p_D s + 2s \ln(\beta) \quad (4.49)$$

Figure 4.14 shows κ versus the right hand side (RHS) of Eq. 4.44 for different ω values and $s = 0$. Unfortunately, the profiles are nonlinear and thus cannot be approximated.

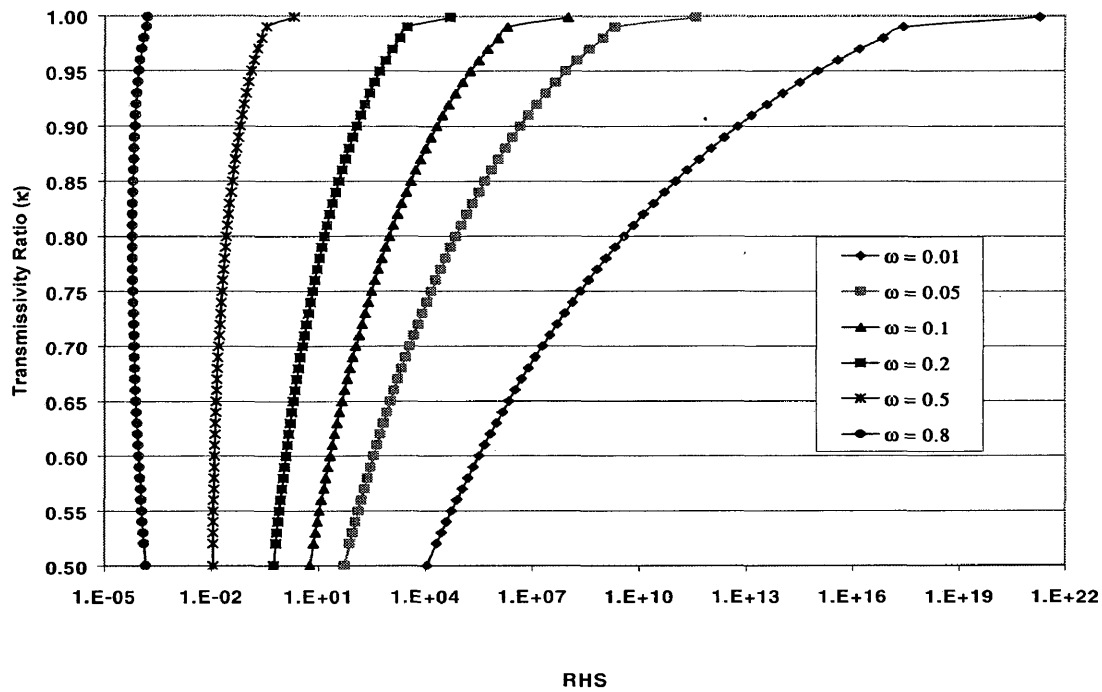


Fig. 4. 14 The κ values calculated from Eq. 4.44 as a function of the RHS of Eq. 4.44 for $s = 0$.

CHAPTER 5

APPLICATIONS

This chapter discusses the applications of Eqs. 4.36 and 4.44 for estimating the storativity and transmissivity ratios, respectively, for dual-permeability systems. Two examples are presented. The first example is a simulated drawdown test performed in a two-layer reservoir with cross flow. Example 2 is a drawdown test followed by a buildup test that is conducted in a four-layer system with cross flow. Both examples show the methodology to estimate the storativity ratio, ω , and or the transmissivity ratio, κ . In Example 1, a comparison of different approaches to estimate ω is also presented.

5.1 Example 1

Figure 5.1 shows a schematic of the system considered in this example. A drawdown test is performed in a two-layer reservoir containing light oil. The pressure data for this example are given in Table C-1 of Appendix C. The duration of the test is seven days (168 hours). Other input data are given in Table 5.1.

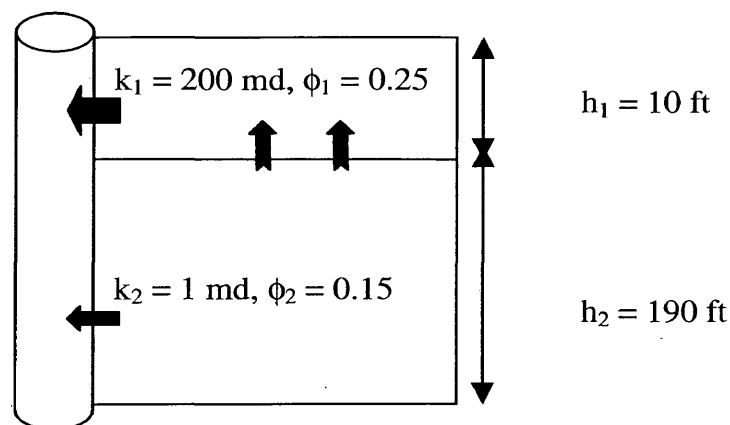


Fig. 5.1 Schematic of the reservoir system considered in Example 1.

Table 5. 1 Well and reservoir data for Example 1.

q	800 stb/D
p _i	2000 psi
μ	1 cp
B	1 rbbl/stb
c _t	0.00003 psi ⁻¹
C _{wb}	0.001 stb/psi
k _{z1} = k _{z2}	10 md
r _w	0.3 ft
r _e	5000 ft

Analyze the pressure data using Eqs. 4.36 and 4.44 to estimate the following:

- a) The storativity ratio ω , ϕ_1 , and ϕ_2 . Compare the results with those obtained by using Eq. 4.40, Eq. 3.1 and Bourdet's method²³ for dual-porosity reservoirs.
- b) The Transmissivity ratio, κ , and the radial permeabilities of the layers, k_1 and k_2 .

Solution of Part A:

In order to use Eq. 4.36, δp_D , s , and κ must be known. Estimation of these parameters is summarized below:

- 1) The pressure responses are plotted on semi-log coordinates (Fig. 5.2) and two parallel straight-lines are drawn on the early-and late-time portions of the data. The slope (m) of the straight lines is 59 psi/cycle and δp is 40 psi.

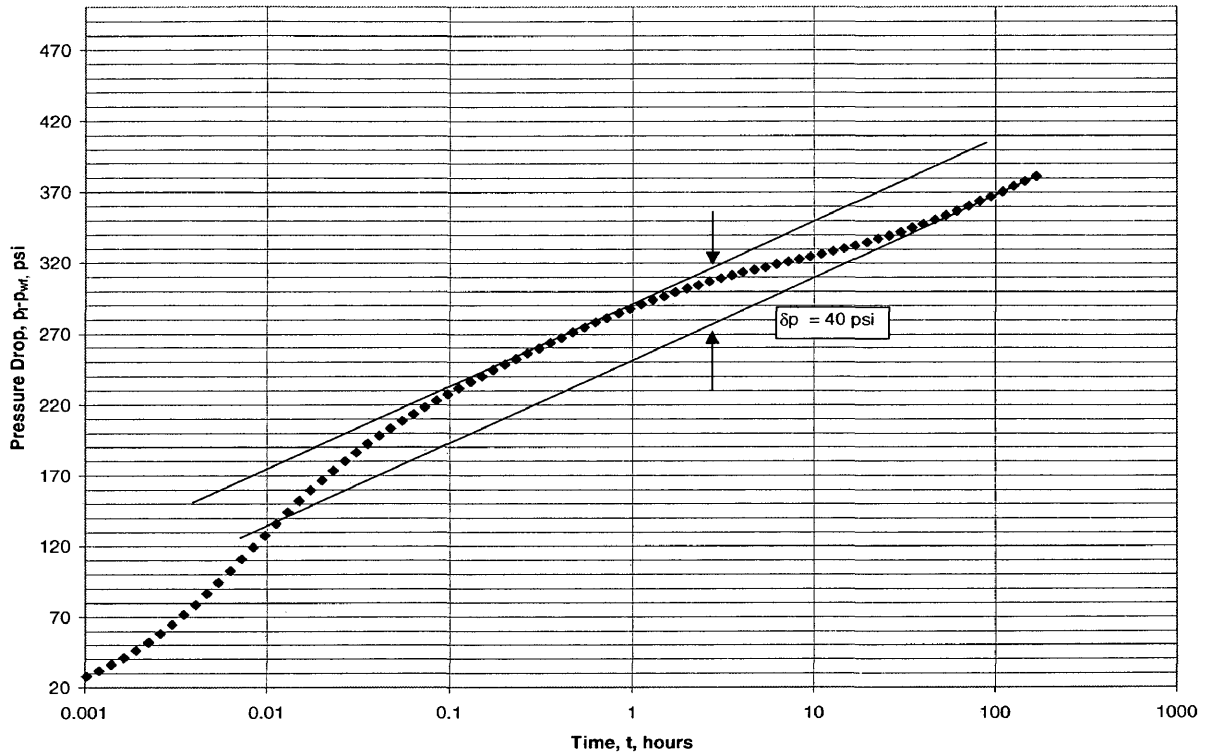


Fig. 5. 2 The semi-log plot for Example 5.1

Consequently,

$$\bar{k}h_{\text{total}} = \frac{162.6 qB\mu}{m} = \frac{162.6 (800 \text{ stb/d})(1 \text{ res bbl/stb})(1 \text{ cp})}{59 \text{ psi/cycle}} = 2205 \text{ md.ft}$$

hence,

$$\bar{k} = \frac{2205 \text{ md.ft}}{h_{\text{total}}} = \frac{2205 \text{ md.ft}}{200 \text{ ft}} = 11.024 \text{ md.}$$

Also,

$$\delta p_D = 1.151 \frac{\delta p}{m} = 1.151 \frac{40 \text{ psi}}{59 \text{ psi/cycle}} = 0.78 .$$

2) Figure 5.3 is the diagnostic plot of the pressure data. Type-curve matching the late-time data in Fig. 5.3 with the homogeneous system type curve shown in Fig. 5.4 yields

$$s = 0$$

$$\begin{aligned} \bar{\phi} c_t &= \frac{0.000264 \bar{k}}{\mu r_w^2} \left(\frac{t}{t_D} \right)_{MP} \\ &= \frac{0.000264 (11.024 \text{ md})}{(1 \text{ cp})(0.3 \text{ ft})^2} \left(\frac{100 \text{ hours}}{6.9 \times 10^5} \right) \\ &= 4.6845 \times 10^{-6} \text{ psi}^{-1} . \end{aligned}$$

Consequently,

$$\bar{\phi} = \frac{4.6845 \times 10^{-6}}{c_t} = \frac{4.6845 \times 10^{-6}}{0.00003} = 0.1562 .$$

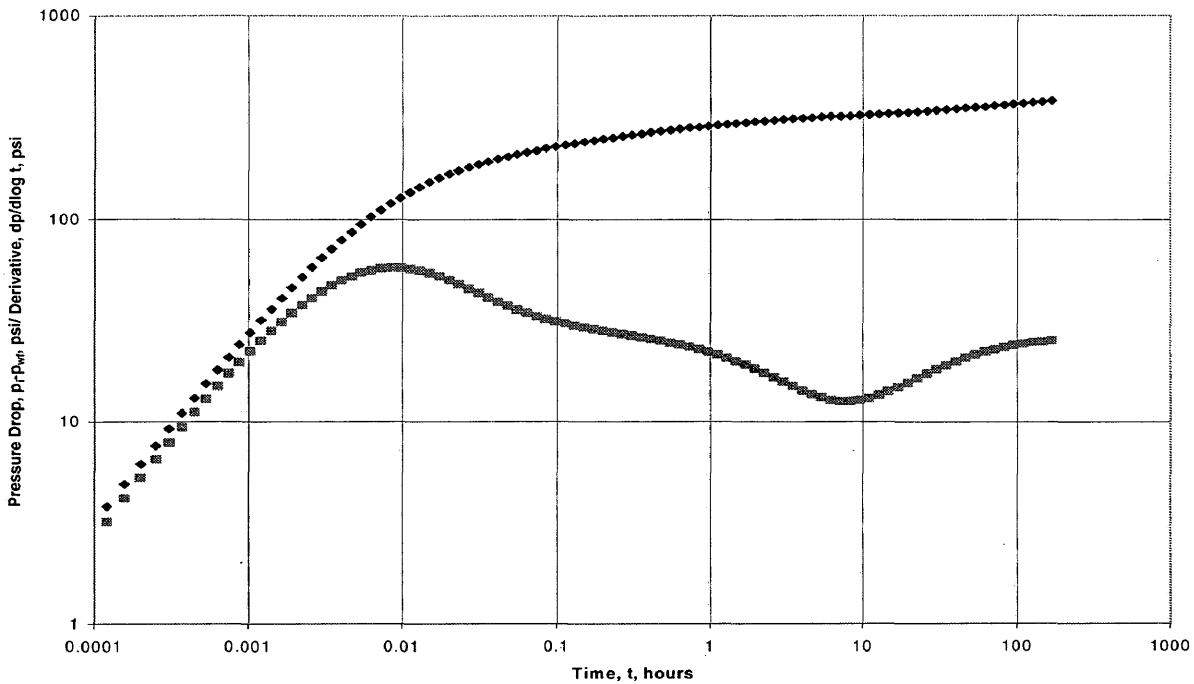


Fig. 5. 3 The diagnostic plot for Example 1

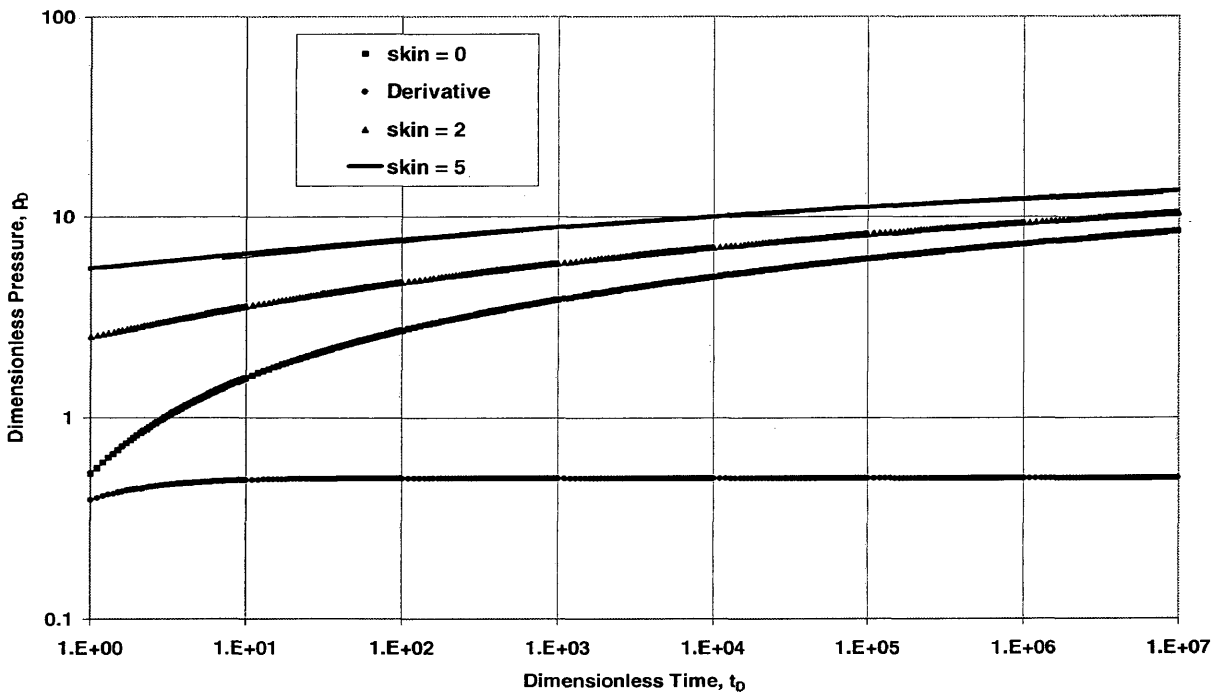


Fig. 5. 4 Homogeneous system type curve.

3) The value of κ can be estimated from production logging data. These data show the contribution of each layer to the total flow rate. Hence, κ is determined as the ratio of the higher flow rate (produced from the higher-permeability layer) to the total flow rate. Figure 5.5 shows the simulated flow rates of each layer that could be measured by the production-logging tool. Figure 5.5 indicates that layer 1 is the higher permeability layer with a flow rate of 730 stb/D and the total rate is 800 stb/D. Therefore,

$$\kappa = \frac{q_{\max}}{q_{\text{total}}} = \frac{730 \text{ stb/d}}{800 \text{ stb/d}} = 0.9125.$$

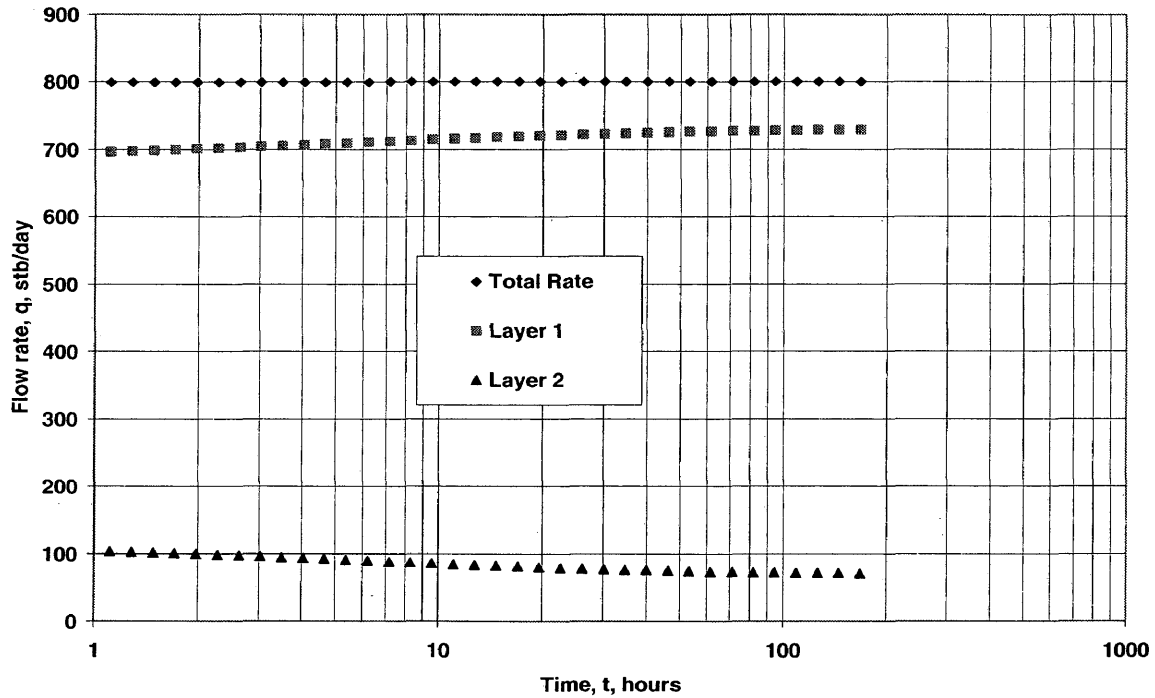


Fig. 5. 5 Simulated flow rates for Example 1

1) Estimation by using Eq. 4.36:

Using the estimates of $s = 0$, $\delta p_D = 0.78$, and $\kappa = 0.9125$ and solving Eq. 4.36 by the Newton-Raphson iteration method gives (the Newton-Raphson Method and the computational code are presented in Appendix D).

$$\omega = 0.0781.$$

Individual layer porosities, ϕ_1 and ϕ_2 , are computed as follows

$$\phi_1 = \phi_{HKZ} = \omega \frac{\bar{\phi} h_{total}}{h_{HKZ}}$$

$$\phi_2 = \phi_{LKZ} = (1 - \omega) \frac{\bar{\phi} h_{total}}{h_{LKZ}}$$

where,

ϕ_{HKZ} = the porosity of the high permeable zone.

ϕ_{LKZ} = the porosity of the low permeable zone.

Substituting the value of ω into the above equations yields

$$\phi_1 = \phi_{HKZ} = (0.0781) \frac{(0.1562)(200 \text{ ft})}{10 \text{ ft}} = 0.244 \quad (2.41 \% \text{ error}).$$

$$\phi_2 = \phi_{LKZ} = (1 - 0.0781) \frac{(0.1562)(200 \text{ ft})}{190 \text{ ft}} = 0.152 \quad (1.34 \% \text{ error}).$$

2) Estimation by using Eq. 4.40:

The RHS term and the constants a and b in Eq. 4.40 are calculated from Eqs. 4.41 – 4.43 as follows

$$\text{RHS} = 1194.$$

$$a' = 1.560968.$$

$$b' = -0.4449.$$

Hence, Eq. 4.40 yields

$$\omega = 0.067.$$

Consequently,

$$\phi_1 = \phi_{HKZ} = 0.21 \quad (16 \% \text{ error}).$$

and

$$\phi_2 = \phi_{LKZ} = 0.13 \quad (13.4 \% \text{ error}).$$

These results indicate that the solution, Eq. 4.40, yields results in close agreement with those obtained from the more rigorous equation given by Eq. 4.36.

3) Estimation by the Dual-Porosity Equation given by Eq. 3.1:

The empirical correlation given in Chapter 3 yields

$$\omega = e^{-2.303\left(\frac{\phi_1}{m}\right)} = e^{-2.303(0.677)} = 0.21.$$

Consequently, ϕ_1 and ϕ_2 are calculated as

$$\phi_1 = \phi_{HKZ} = 0.656 \quad (162 \% \text{ error}).$$

and

$$\phi_2 = \phi_{LKZ} = 0.13 \quad (13.4 \% \text{ error}).$$

As expected, this method does not yield satisfactory results.

4) Bourdet's Dual-Porosity Method²³:

Here the storativity ratio is estimated by using Bourdet's dual-porosity equation given by

$$\left(t_D \frac{\partial p_D}{\partial t_D}\right)_{\min} = \frac{1}{2} \left(1 + \omega^{\frac{1}{1-\omega}} - \omega^{\frac{\omega}{1-\omega}}\right)$$

where,

$$\left(t_D \frac{\partial p_D}{\partial t_D}\right)_{\min} = \frac{\bar{k} h_{total}}{141.2 q B \mu} \left(t \frac{\partial p}{\partial t}\right)_{\min}.$$

The term $\left(t \frac{\partial p}{\partial t}\right)_{\min}$ in the above expression is obtained as 12.6 psi from Fig. 5.3 when the pressure derivative reaches a minimum. Using this value yields

$$\left(t_D \frac{\partial p_D}{\partial t_D}\right)_{\min} = \frac{2205 \text{ md}\cdot\text{ft}}{141.2 (800 \text{ stb/d})(1 \text{ res bbl/stb})(1 \text{ cp})} [12.6 \text{ psi}]$$

$$= 0.246.$$

Using this value in Fig. 5.6 gives

$$\omega = 0.26.$$

Consequently, ϕ_1 and ϕ_2 are obtained as

$$\phi_1 = \phi_{HKZ} = 0.81 \quad (225 \% \text{ error}).$$

and

$$\phi_2 = \phi_{LKZ} = 0.12 \quad (18.8 \% \text{ error}).$$

These results indicate that Eq. 4.36 is more accurate than the other methods.

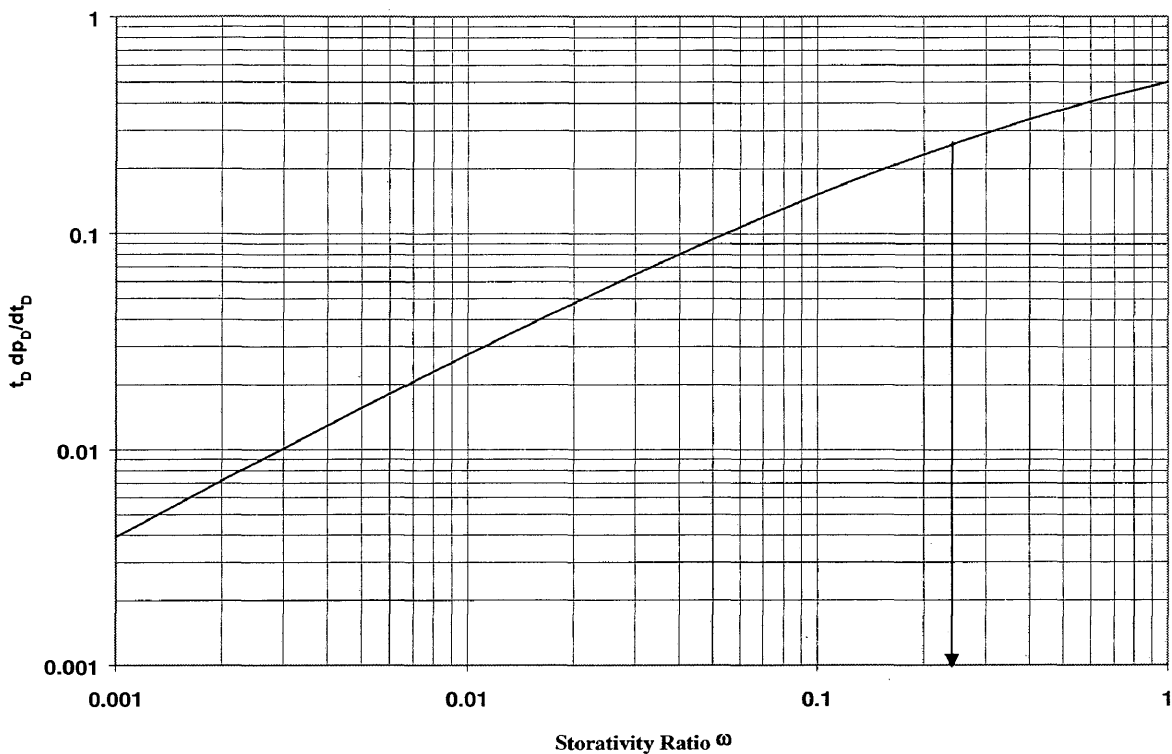


Fig. 5. 6 The plot of $(t dp/dt)_{min}$ as a function of ω for Bourdet's method.

Solution of Part B:

Equation 4.44 can be used to estimate κ provided that the storativity ratio is known from another source. The exact value of ω is

$$\omega = \frac{(\phi c_i h)_1}{(\phi c_i h)_1 + (\phi c_i h)_2} = \frac{(0.25)(0.00003)(10)}{(0.25)(0.00003)(10) + (0.15)(0.00003)(190)} = 0.08064.$$

Therefore, using $\delta p_D = 0.78$, $s = 0$, and $\omega = 0.08064$ in Eq. 4.44 and iterating by the Newton-Raphson method (Appendix D) yields

$$\kappa = 0.917.$$

Consequently, k_1 and k_2 can be calculated as follows

$$k_1 = k_{HKZ} = \kappa \frac{\bar{k} h_{total}}{h_{HKZ}}$$

$$k_2 = k_{LKZ} = (1 - \kappa) \frac{\bar{k} h_{total}}{h_{LKZ}},$$

where

k_{HKZ} = the permeability of the high permeable zone

k_{LKZ} = the permeability of the low permeable zone

Using the value of κ and total flow capacity, $\bar{k}h_{total}$, in the above equations gives

$$k_1 = k_{HKZ} = (0.917) \frac{(2205 \text{ md.ft})}{10 \text{ ft}} = 202 \text{ md.}$$

$$k_2 = k_{LKZ} = (1 - 0.5976) \frac{(3252 \text{ md.ft})}{190 \text{ ft}} = 0.963.$$

5.2 Example 2

A simulated case of pressure drawdown test followed by a buildup test is considered in this example. The relevant data are given in Table C-2 of Appendix C and the schematic of the four-layer system with cross flow is shown in Fig. 5.7. The production period is six months followed by 10 days of shut-in. Other data are given in Table 5.2.

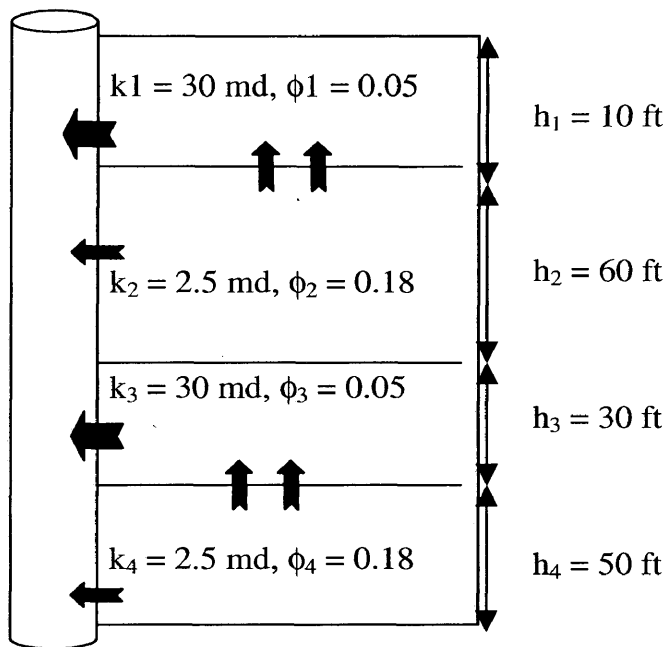


Fig. 5. 7 The schematic of the reservoir for Example 2

Table 5. 2 Well and reservoir data for Example 2

q	400 stb/day
p_i	4000 psi
μ	0.5 cp
B	1.2 rbbl/stb
c_t	0.00007 psi^{-1}
C_{wb}	0.001 stb/psi
$k_{z1,2,3,4}$	2 md
r_w	0.3 ft
r_e	3000 ft

Analyze the pressure buildup data to estimate the following:

- 1) The storativity ratio ω , ϕ_1 , and ϕ_2 .
- 2) The transmissivity ratio κ , and the radial permeability of each layer, k_1 and k_2 .

Solution of Part A:

The pressure buildup data are plotted on semi-log coordinates in Fig 5.8 and two parallel straight lines are drawn through the early-and late-times data. The slope (m) of the straight lines is 26 psi/cycle and δp is 16 psi.

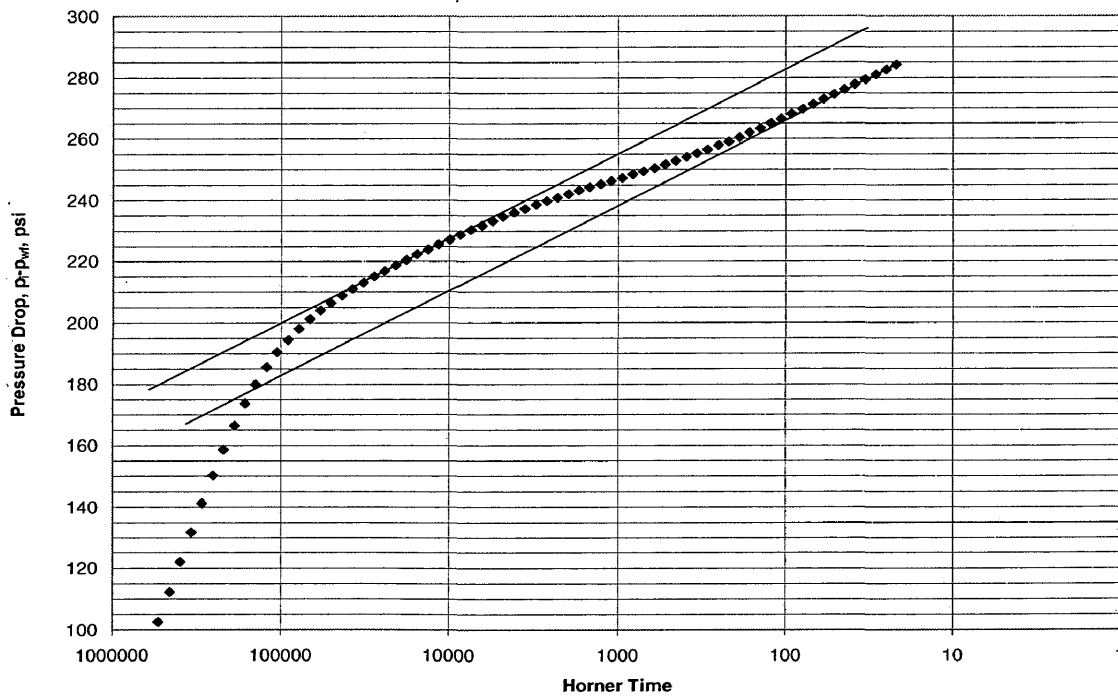


Fig. 5. 8 The semi-log plot for the buildup test of Example 2.

Consequently,

$$\bar{k}h_{\text{total}} = \frac{162.6 qB\mu}{m} = \frac{162.6 (400 \text{ stb/d})(1.2 \text{ res bbl/stb})(0.5 \text{ cp})}{26 \text{ psi/cycle}} = 1501 \text{ md}\cdot\text{ft}$$

hence,

$$\bar{k} = \frac{1501 \text{ md}\cdot\text{ft}}{h_{\text{total}}} = \frac{1501 \text{ md}\cdot\text{ft}}{150 \text{ ft}} = 10.0 \text{ md}$$

Also,

$$\delta p_D = 1.151 \frac{\delta p}{m} = 1.151 \frac{16 \text{ psi}}{26 \text{ psi/cycle}} = 0.708$$

Figure 5.9 is the diagnostic plot of the pressure data.

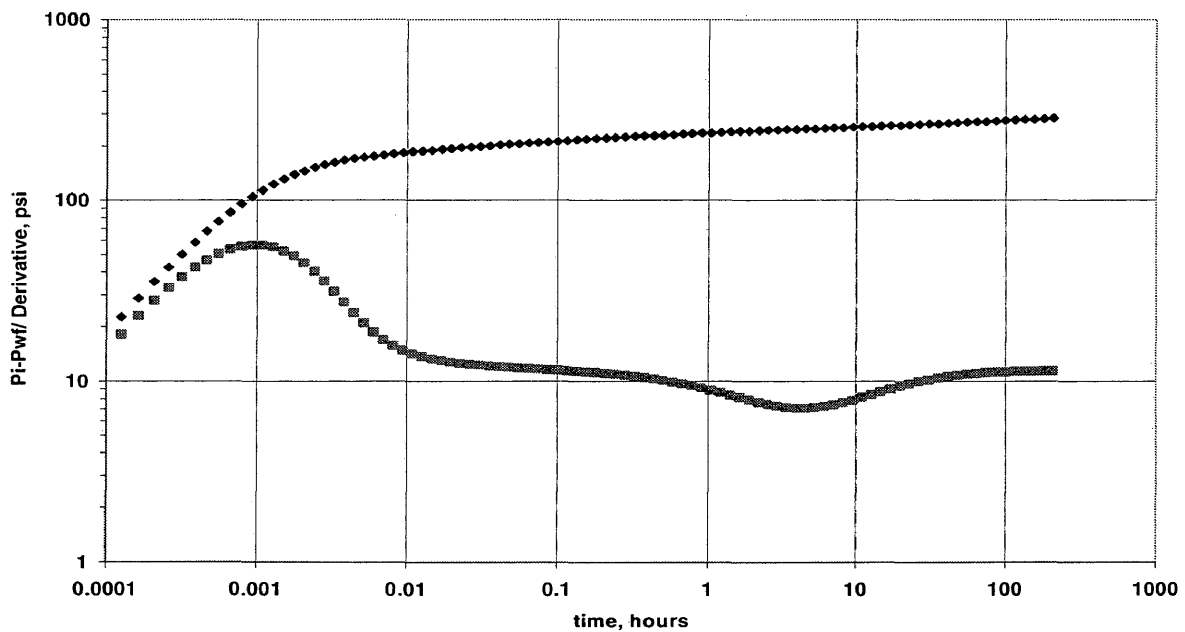


Fig. 5. 9 The diagnostic plot for the buildup test of Example 2

Therefore, using the homogeneous system type curve shown in Fig. 5.4 to match the late-time flow regime of Fig. 5.9 gives

$$s = 5.$$

The time match points are given by $t_{MP} = 100$ hrs and $t_{DMP} = 2.6 \times 10^5$. Therefore,

$$\begin{aligned} \bar{\phi} c_t &= \frac{0.000264 \bar{k}}{\mu r_w^2} \left(\frac{t}{t_D} \right)_{MP} \\ &= \frac{0.000264 (10 \text{ md})}{(0.5 \text{ cp})(0.3 \text{ ft})^2} \left(\frac{100 \text{ hours}}{5.9 \times 10^5} \right) \\ &= 9.94 \times 10^{-6} \text{ psi}^{-1}. \end{aligned}$$

and

$$\bar{\phi} = \frac{1.11 \times 10^{-5}}{c_t} = \frac{1.11 \times 10^{-5}}{0.00007} = 0.142.$$

The κ value is estimated from the production logging data. Figure 5.10 shows the simulated flow rates of each layer that would be obtained from production logging in practice. To distinguish between the high- and the low-permeability layers, Fig. 5.11 also presents the influx of each layer. Layers 1 and 3 are identified as the high-permeability layers.

Consequently,

$$\kappa = \frac{q_{\max}}{q_{\text{total}}} = \frac{(244.05 \text{ stb/d}) + (81.36 \text{ stb/d})}{400 \text{ stb/d}} = 0.813525.$$

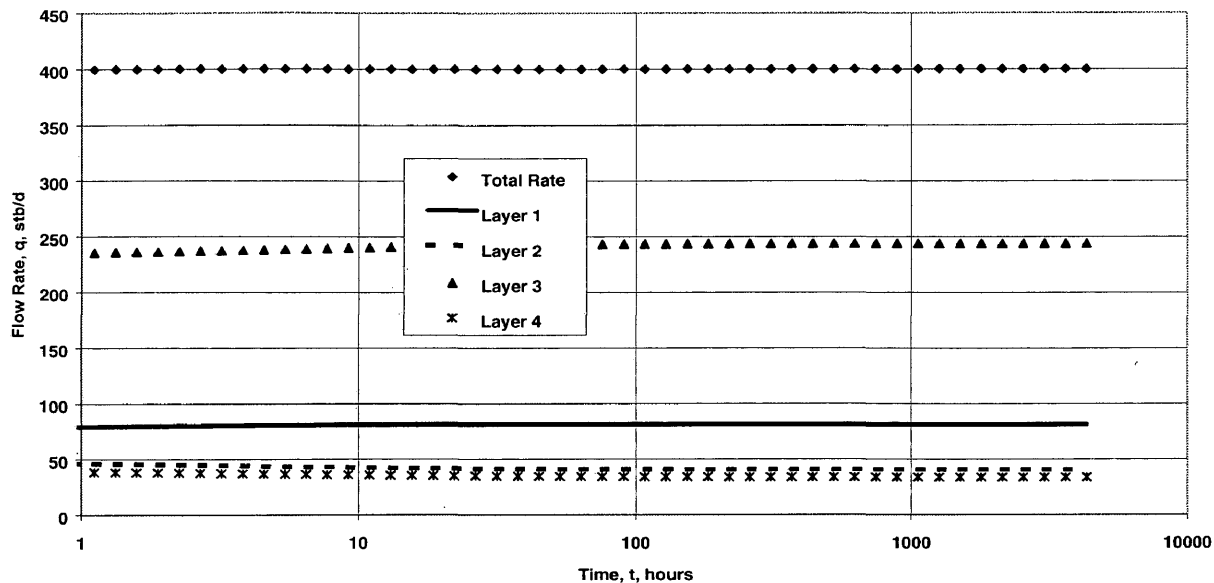


Fig. 5. 10 Simulated production logging results for Example 2.

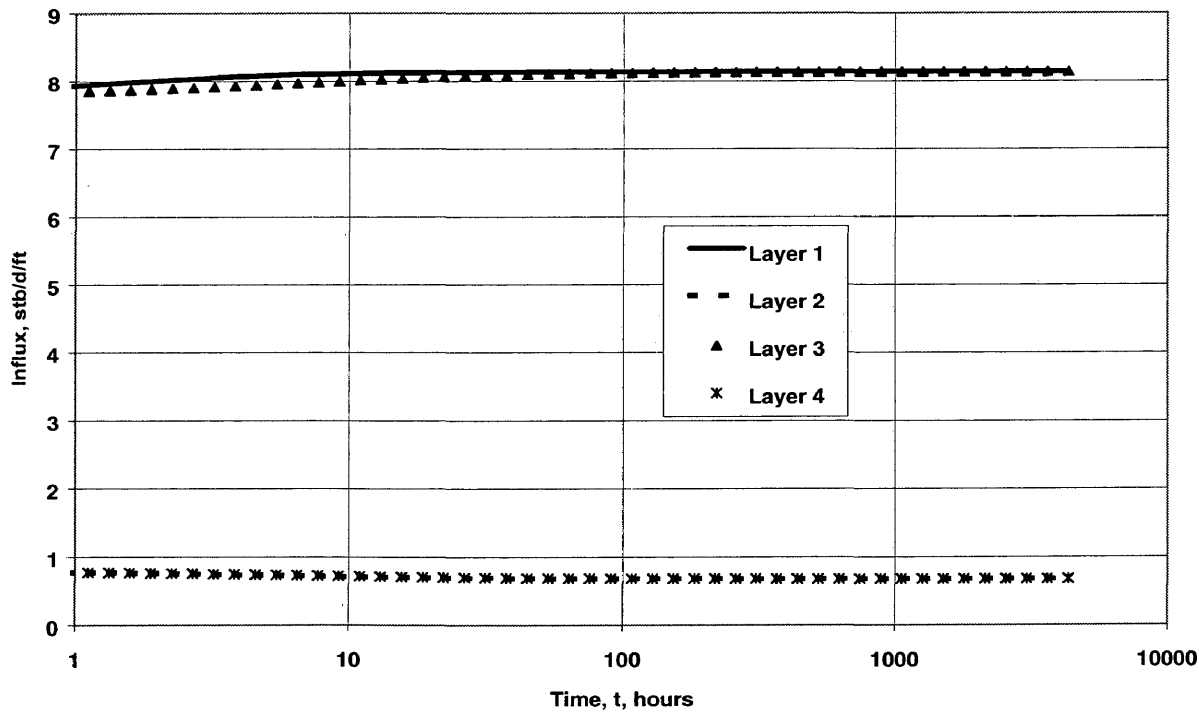


Fig. 5. 11 The influx of each layer for Example 2.

Using the Newton-Raphson iteration method for Eq. 4.36 gives

$$\omega = 0.082.$$

Thus, ϕ_1 and ϕ_2 are calculated as

$$\phi_1 = \phi_{HKZ} = (0.082) \frac{(0.142)(150 \text{ ft})}{40 \text{ ft}} = 0.044 \quad (12.7 \% \text{ error}).$$

$$\phi_2 = \phi_{LKZ} = (1 - 0.082) \frac{(0.142)(150 \text{ ft})}{110 \text{ ft}} = 0.178 \quad (1.2 \% \text{ error}).$$

Solution of Part B:

Equation. 4.44 can be used to estimate κ provided that the storativity ratio, ω , is obtained from another source . The exact value of ω is

$$\omega = \frac{(\phi c_i h)_1}{(\phi c_i h)_1 + (\phi c_i h)_2} = \frac{(0.05)(0.00007)(40)}{(0.05)(0.00007)(40) + (0.18)(0.00007)(110)} = 0.091743.$$

Therefore, substituting the values of δp_D , s , and ω into Eq. 4.41 and iterating by the Newton Raphson method yields

$$\kappa = 0.826.$$

Permeabilities, k_1 and k_2 , are calculated as follows

$$k_1 = k_{HKZ} = (0.826) \frac{(1501 \text{ md} \cdot \text{ft})}{40 \text{ ft}} = 31 \text{ md}.$$

$$k_2 = k_{LKZ} = (1 - 0.826) \frac{(1501 \text{ md} \cdot \text{ft})}{110 \text{ ft}} = 2.37 \text{ md}.$$

CHAPTER 6

SUMMARY AND CONCLUSIONS

A numerical model has been constructed to simulate well testing for single-phase radial flow in heterogeneous reservoirs. The model has been used to investigate the pressure responses of layered systems with cross flow.

Two methods have been developed to estimate ω and κ parameters characterizing such systems. The first method is an empirical correlation and does not yield satisfactory results. The second method is analytical and based on two new equations for estimating the storativity ratio (ω) and the transmissivity ratio (κ) of layered systems with cross flow. The analytical solutions have been derived based on the physical behavior of the layered system during the unsteady steady state flow conditions. The analytical solutions have been compared with the simulated cases for different conditions. The estimation of ω from different methods has also been compared. The specific conclusions drawn from this work are as follows:

1. The vertical separation (δp) between the semi-log straight lines on the pressure versus log-time plot of layered reservoir responses with cross flow is a function of the transmissivity ratio (κ) and storativity ratio (ω).
2. Increasing κ or decreasing ω increases δp .
3. The expressions given by Eq. 4.36 and Eq. 4.44 are sufficiently accurate for estimating the values of ω and κ from pressure transient analysis provided that, respectively, κ and ω are known from other sources.

REFERENCES

1. Warren, J.E. and Root, P.J.: "Behavior of Naturally Fractured Reservoirs", Society of Petroleum Engineers Journal (Sept. 1965) 245.
2. Pollard, P.: "Evaluation of Acid Treatments from Pressure Build-Up Analysis", Trans., AIME (1959) 216, 38-43.
3. Bourdet, D.: "Pressure Behavior of Layered Reservoirs With Cross Flow", Paper SPE 13268, presented at the SPE 1985 California Regional Meeting, Held in Bakersfield, California (March 1985).
4. Woods, E.G.: "Pulse-Test Response of a Two -Zone Reservoir", Paper SPE 2570, Annual Fall Meeting, held in Denver, Colorado (March 17, 1970).
5. Olarewaju, J.S. and Lee, W.J.: "Rate Performance of a Layered Reservoir With Unsteady-State Interlayer Crossflow", Paper SPE 18544, presented at the 1988 SPE Eastern Regional Meeting held in Charleston, WV, Nov. 1-4.
6. Kazemi, H.: Personal communication; Petroleum Engineering Department, Colorado School of Mines, (2002).
7. Claridge, Elmond L.: "CO₂ Flooding Strategy in a Communicating Layered Reservoir", Paper SPE 10289, presented in the 58th Annual Fall Technical Conference and Exhibition of the Society of Petroleum Engineers of AIME, San Antonio, Texas, (Oct. 1981).
8. Vela, S., Peaceman, D.W. and Sandvik, E.I.: "Evaluation of Polymer Flooding in a Layered Reservoir With Cross Flow, Retention, and Degradation", Paper

- SPE 5102, presented at the SPE-AIME 49th Annual Fall Meeting, held in Houston, (Oct. 1974).
9. Watson, A.T. and Lee, W.J.: "A New Algorithm for Automatic History Matching Production Data", Paper SPE 15228, presented at the SPE Unconventional Gas Technology Symposium, Louisville, KY, (May 1986).
 10. Hollabaugh, G.R. and Slotboom, R.A.: "A Vertical Permeability Study", Society of Petroleum Engineers Journal, (June 1972), 199-205
 11. Ramey, H.J. JR. and Robert, A.: "An Investigation of Wellbore Storage and Skin Effect Unsteady Liquid Flow: II. Finite Difference Treatment", Society of Petroleum Engineers Journal, (Sept. 1970), 291-96.
 12. Hawkins, M.F. Jr.: "A Note on the Skin Effect", Trans., AIME (1956), 207, 356-357.
 13. Phipps, S.C., Khalil, J.N. and MacCord, D.R.: "A Method for Determining the Exponent Value in a Forchheimer-Type Flow Equation", Paper SPE 5325, JPT Forum, SPE-AIME, Dallas, Texas (July 1975).
 14. Civan, F. and Ronald, E.: "Determination of non-Darcy Flow Parameters Using a Differential Formulation of the Forchheimer", Paper SPE 35621, University of Oklahoma, SPE Gas Technology Symposium, Calgary, Alberta, Canada (April 28th – May 1st, 1996) 415-429.
 15. Wijesinghe, A.M. and Culham, W.E.: "Single-Well Pressure Testing Solution for Naturally Fractured Reservoirs with Arbitrary Fracture Connectivity", Paper SPE 13055 presented at the 59th Annual Fall Technical Conference and Exhibition of SPE of AIME, Houston (September 16th – 19th, 1984).

16. Schaprey, R.A.: "Approximation Methods of Transform Inversion for Viscoelastic Stress analysis", Proc., Fourth U.S. National Congress of Applied Mechanics (1961) 1075-85.
17. Najurieta, H. L.: "A Theory for Transient Analysis in Naturally Fractured Reservoirs," Journal of Petroleum Technology (July 1980) 1241-50.
18. Russell, D.G. and Prats, M.: "Performance of Layered Reservoirs with Crossflow –Single-Compressible-Fluid Case", Society of Petroleum Engineers Journal (March 1962), 53-67.
19. Katz, M.L. and Tek, M.R.: "A Theoretical Study of Pressure Distribution and Fluid Flux in Bounded Stratified Porous System with Crossflow", Soc. Pet. Eng. Journal (March 1962), 68-82.
20. Pendegrass, J.D. and Berry, V.J. Jr.: "Pressure Transient Performance of a Multilayered Reservoir with Crossflow", Society of Petroleum Engineers Journal (December 1962), 347-354.
21. Prijambodo, R., Raghavan, R. and Reynolds, A.C.: "Well Test Analysis for Wells Producing Layered Reservoirs with Crossflow", Paper SPE 10262, presented at the SPE, ATCE, San Antonio, Texas, (October 1981).
22. Olarewaju, J.S. and Lee, W.J.: "Pressure Behavior of Layered and Dual-Porosity Reservoirs in the Presence of Wellbore Effects", Paper SPE 17302, presented at the 1988 SPE Permian Basin Oil and Gas Recovery Conference held in Midland, Texas, March 10-11.
23. Bourdet, D., Whittle, T. M., Douglas, A.A. and Pirard, Y.M.: "A New Set of Type Curves Simplifies Well Test Analysis", World Oil (May 1983) 196, No. 6, 95-106.

LIST OF SYMBOLS

B	= Formation volume factor of fluid, rbbl/ stb
c_t	= Total system compressibility, psi^{-1}
C_{wb}	= Wellbore storage constant, stb/psi
C_D	= Dimensionless wellbore storage constant
d_j	= Depth of layer j, ft
F_A, F_B	= Flow coefficients for the reservoir-well system
h_{total}	= Net formation thickness, ft
h_j	= Thickness of layer j, ft
h_{HKZ}	= Thickness of the high permeability zone, ft
h_{LKZ}	= Thickness of the low permeability zone, ft
k	= Permeability, md
$k_v = k_z$	= Vertical permeability, md
\bar{k}	= Average permeability, md
k_{HKZ}	= Permeability of the high permeability zone, md
k_{LKZ}	= Permeability of the low permeability zone, md
K	= Modified Bessel Function
m	= Slope of the pressure transient response in semi-log plot
n	= Time step
n	= Velocity exponent for non-Darcy flow defined by Eq. 2.39
p	= Pressure, psi
p_{wf}	= Flow pressure of the wellbore, psi
p_i	= Initial pressure
p_D	= Dimensionless pressure
δp	= Vertical separation between the two parallel straight lines in semi-log plot for dual porosity/permeability systems
$\hat{\delta p}_D$	= Dimensionless pressure of vertical separation
q	= Production rate, scf/day

r	= Radial distance, ft
r_w	= Wellbore radius, ft
r_e	= Reservoir radius, ft
s	= Skin factor
s_a	= Apparent skin factor
t	= Time, hour
Δt	= Time increment, hour
t_{cum}	= Cumulative time, hour
t_D	= Dimensionless time
T	= Transmissibility, scf/psi-day
V_R	= Grid block volume, scf
V_r	= Velocity in radial flow regime, scf/sec
WI	= Wellbore Index, scf/psi
z	= Laplace variable
Δz	= Grid block thickness, ft
α	= Non-Darcy coefficient defined by Eq. 2.43
β	= $4/e^\gamma$
β'	= Non-Darcy coefficient defined by Eq. 2.41
κ	= Transmissivity ratio defined by Eq. 1.5
λ	= Interporosity flow parameter defined by Eqs. 1.1, 1.3 and 4.2
ϕ	= Local porosity
ϕ_g	= Global porosity
$\bar{\phi}$	= Average porosity
ϕ_{HKZ}	= Porosity of the high permeability zone
ϕ_{LKZ}	= Porosity of the Low permeability zone
ω	= Storativity ratio defined by Eqs. 1.2 and 1.4
ρ	= Fluid density, lbf/ cu-ft
σ	= Shape factor, ft ⁻²
γ	= Euler's Constants = 0.5772

γ_f = Specific gravity of fluid
 Δ = Finite difference operator

APPENDIX A

NUMERICAL MODEL (FORTRAN 90) FOR RADIAL TRANSIENT FLOW

```

PROGRAM Welltesting_simulator
! Last Update: 11.10.02
!-----
! This program is two dimensional simulation of welltesting for single phase
! flow of multi-layered reservoir with and without cross flow. It generates
! data of pressure versus time for a draw down followed by a buildup tests.
! The Variables used for the wellbore and reservoir properties are:
!
! I           : Number of matrix in the horizontal direction (X)
! K           : Number of matrix in the vertical direction (Z)
! DZ(K)      : Hight thickness of matrices, ft.
! DEPTH(K)   : Top depth of individual layer, ft
! PRN(K)     : Pressure at the wellbore, psia
! SKIN(K)    : Near wellbore damage, dimensionless
! PHI(I,K)   : Connested pore spaces of the matrix, fraction
! KR(I,K)    : Horizontal permeablilty, md
! KZ(I,K)    : Vertical permeability, md
! MU         : Viscosity or resistivity of the fluid to flow, cp
! FVF        : Formation Volume Factor, Res bbl/stb.
! RHU        : Fluid density, lb/cu.ft
! CT         : Total rock and fluid thermal compressibility,1/psia
! CW         : Wellbore storage coefficinet, stb/psia
! Q          : Total rate, SCF/day
! RW         : Wellbore Radius, ft

```

```

! RE                : Radius from well to the resevoir boundary, ft
! DT                : Delta time for each time step, hours
! TIMEP            : Production period of the well before shutin, hours
! TIMEB            : Shutin time, hours
!
! Input: I, K, DZ, D, SKIN, PHI, KR, KZ, MU, FVF, RHU, CT, CW, PR, RATE, RW
!   DT, TIMEP, TIMEB RE
! Output file: Pressure versus time (PRESSURE_TIME.DATA).
!-----

```

```

IMPLICIT NONE

```

```

CHARACTER(3) :: ENTER

```

```

INTEGER, PARAMETER :: DP = SELECTED_REAL_KIND(14,50)
INTEGER, PARAMETER :: DP2 = SELECTED_INT_KIND(9)
REAL (KIND = DP), DIMENSION(:), ALLOCATABLE :: DZ, DEPTH, PR, PRN,
SKIN, WI, R, X, LRATE
REAL (KIND = DP), DIMENSION(:), ALLOCATABLE :: RI0, RI, RI1, DRI0, DRI1,
KS, RS, TIMEP, TIMEB
REAL (KIND = DP), DIMENSION(:,,:), ALLOCATABLE :: PHI, KR, KZ, G, C, D, E,
F, H, A, KZAVG, KRAVG
REAL (KIND = DP), DIMENSION(:,,:), ALLOCATABLE :: KR_NONDARCY

INTEGER (KIND = DP2) :: I, II, III, IMAX, K, KMAX, M, N, W, J
INTEGER (KIND = DP2) :: SELECT, NUMBER_OF_GRIDS, ALLOCATESTATUS
REAL (KIND = DP) :: PHI1, KR1, KZ1, PR1, DEPTH1, MU, FVF, RHU, CT, CW, DT

```

```

REAL (KIND = DP) :: DT1, RW, RE, DU, R1, DZ1, SKIN1, Q, WISUM, L, L1, WI1
REAL (KIND = DP) :: GW, PI = 3.1415926535898_DP, CF = 0.006328_DP ! cu.ft/day
REAL (KIND = DP) :: KS1, RS1, SKIN_FACTOR_FROM_PERMEABILITY
REAL (KIND = DP) :: RS_PRIME, RGRID, TOTAL_LENGTH, ALFA, BETA, VR,
TAWP, TAWB
REAL (KIND = DP) :: DRAWDOWN, BUILDUP

```

```
!-----
```

```
!
```

```
!           INPUT DATA
```

```
!
```

```
!-----
```

```
PRINT *, "Enter the (Imax) and (Kmax) of the system"
```

```
READ *, IMAX, KMAX
```

```
M = IMAX * KMAX
```

```
! PRINT *, "Enter the well and reservoir properties"
```

```
! READ *, MU, FVF, RHU, CT, DT, RE, RW, PR1
```

```
MU = 1.0_DP
```

```
FVF = 1.0_DP
```

```
RHU = 0.0_DP
```

```
CT = 0.00003_DP
```

```
CW = 0.001_DP
```

```
DT1 = .0001_DP
```

```
RE = 5000.0_DP
```

```
RW = 0.3_DP
```

```
PR1 = 2000.0_DP
```

```
Q = 4491.68_DP
```

```

ALLOCATE(RI0(IMAX), RI(0:IMAX), RI1(IMAX), DRI0(0:IMAX), DRI1(IMAX))
ALLOCATE(DZ(KMAX), WI(KMAX), DEPTH(0:KMAX+1), PR(KMAX),
SKIN(KMAX) &
& , KS(KMAX), RS(KMAX), TIMEP(100), TIMEB(100), STAT =
ALLOCATESTATUS)
IF (ALLOCATESTATUS /= 0) STOP "*** NOT ENOUGH MEMORY ***"

```

```

ALLOCATE(PHI(IMAX,KMAX), KR(IMAX,KMAX), KZ(IMAX,KMAX),
G(IMAX,KMAX), C(IMAX,KMAX), &
& D(IMAX,KMAX), E(IMAX,KMAX), F(IMAX,KMAX), H(IMAX,KMAX),
A(M+2,M+1), R(M+1), &
& X(M+1), PRN(M+1), KZAVG(IMAX,0:KMAX), KRAVG(0:IMAX,KMAX),
KR_NONDARCY(0:IMAX,KMAX) &
& , STAT = ALLOCATESTATUS)
IF (ALLOCATESTATUS /= 0) STOP "*** NOT ENOUGH MEMORY ***"

```

```

! -----
!
!           Input data for Reservoir _ Description
!
! -----

```

```
PRINT '(/)
```

```
PRINT *, "Enter the (Thickness) of each layer"
```

```
DO K = 1, KMAX
```

```
    READ *, DZ1
```

```
    DZ(K) = DZ1
```

```
END DO
```

```
PRINT '(/)
```

```
PRINT *, "(1) PHYSICAL SKIN [S] (2) ALTERED PERMEABILITY [KS]"
```

```
200 READ *, SELECT
```

```
SKIN_FACTOR_FROM_PERMEABILITY = 0.0
```

```
IF ( SELECT == 2 ) THEN
```

```
    DO K = 1, KMAX
```

```
        PRINT '( /, 1X, A, I2, A)', "ENTER [KS] AND [RS] OF LAYER", K, ",  
RESPECTIVELY"
```

```
            READ *, KS1, RS1
```

```
            KS(K) = KS1
```

```
            RS(K) = RS1
```

```
    END DO
```

```
PRINT '(/)
```

```
SKIN(1:KMAX) = 0.0_DP
```

```
SKIN_FACTOR_FROM_PERMEABILITY = 1 ! a remark for skin option
```

```
ELSE IF ( SELECT == 1 ) THEN
```

```
PRINT '(/)
```

```
PRINT *, "Enter the (skin) of each layer"
```

```
DO K = 1, KMAX
```

```
    READ *, SKIN1
```

```
    SKIN(K) = SKIN1
```

```
END DO
```

```
PRINT '(/)
```

```
ELSE
```

```
GOTO 200
```

```
END IF
```

```
PRINT *, " Is the reservoir homogenous? (Y/N)"
```

```
READ *, ENTER
```

```
IF ( ENTER == "Y" .OR. ENTER == "y" ) THEN
```

```
PRINT '(/)
```

```
PRINT *, "Enter (PHI) of each layer"
```

```
DO K = 1, KMAX
```

```
    READ *, PHI1
```

```
    DO I = 1, IMAX
```

```
        PHI(I,K) = PHI1
```

```
    END DO
```

```
END DO
```

```
PRINT '(/)
```

```
PRINT *, "Enter (Kr) of each layers"
```

```
DO K = 1, KMAX
```

```
    READ *, KR1
```

```
    DO I = 1, IMAX
```

```
        KR(I,K) = KR1
```

```
    END DO
```

```
END DO
```

```
PRINT '(/)
```

```
PRINT *, "Enter (Kz) of each layers"
```

```
DO K = 1, KMAX
```

```
    READ *, KZ1
```

```
    DO I = 1, IMAX
```

```
        KZ(I,K) = KZ1
```

```
    END DO
```

```
END DO
```

```
ELSE
```

```
DO K = 1, KMAX
```

```
    DO I = 1, IMAX
```

```
        PRINT *, "Enter PHI, Kr, Kz of Matrix (", I, ", ", K, ")"
```

```
        READ *, PHI1, KR1, KZ1
```

```
        PHI(I,K) = PHI1
```

```
        KR(I,K) = KR1
```

```
        KZ(I,K) = KZ1
```

```
    END DO
```

```
END DO
```

```
ENDIF
```

```
!-----
```

```
!
```

```
!           Define Periods of Production and Shutin
```

```
!
```

```
!-----
```

```
PRINT '(/)
```

```
PRINT*, "Enter the duration (hours) of the production and shut-in periods, respectively"
```

```
READ *, DRAWDOWN, BUILDUP
```

```
TAWP = DBLE(LOG(DRAWDOWN/0.0001_DP))/100.0_DP
```

```
TAWB = DBLE(LOG(BUILDUP/ 0.0001_DP))/100.0_DP
```

```
DO I = 1, 100
```

```
TIMEP(I) = 0.0001_DP * EXP(REAL(I) * TAWP)
```

```
TIMEB(I) = 0.0001_DP * EXP(REAL(I) * TAWB)
```

```
END DO
```

```
!-----
```

```
!
```

```

!           Calculation of Node Radiuses
!
! -----

DU = DBLE (LOG(RE/RW)) / REAL(IMAX)
R1 = RW * DBLE (EXP(DU/2.0_DP))

DO I = 1, IMAX

    RI0(I) = RW * DBLE (EXP((REAL(I) - 1.0_DP) * DU))
    RI(I) = R1 * DBLE (EXP((REAL(I) - 1.0_DP) * DU))
    RI1(I) = RW * DBLE (EXP(REAL(I) * DU))
END DO

RI0(IMAX) = RW * DBLE (EXP((REAL(IMAX) - 1) * DU))

RI(0) = RW

DO I = 1, IMAX
    DRI0(I) = RI(I) - RI(I-1)
END DO

DO I = 1, IMAX-1
    DRI1(I) = RI(I+1) - RI(I)
END DO

! -----
!
!           Establishing (Krs) in the Grid System

```

```

!
!-----

IF ( SKIN_FACTOR_FROM_PERMEABILITY == 1) THEN

DO K = 1, KMAX

TOTAL_LENGTH = 0.0_DP

RS_LOOP: DO I= 1, IMAX

                TOTAL_LENGTH = TOTAL_LENGTH + RI1(I) -RI0(I)
                NUMBER_OF_GRIDS = I
                IF (RS(K) .LT. TOTAL_LENGTH) EXIT RS_LOOP

        END DO RS_LOOP

                KR(1:NUMBER_OF_GRIDS-1,K) = KS(K)
                RGRID = RI1(NUMBER_OF_GRIDS) -RI0(NUMBER_OF_GRIDS)
                RS_PRIME = RS(K) -(TOTAL_LENGTH -RGRID)
                KR(NUMBER_OF_GRIDS,K) = RGRID/( RS_PRIME / KS(K) +
                (RGRID - RS_PRIME) / KR(NUMBER_OF_GRIDS,K) )

        END DO

END IF

!-----
!
!           Harmonic Averaging for (Kr) and (Kz)
!
!-----

```

```
DO K = 1, KMAX-1
```

```
    DO I = 1, IMAX
```

```
        KZAVG(I,K) = 2.0 * ( DZ(K) / 2.0 + DZ(K+1) / 2.0 ) / ( DZ(K) / KZ(I,K) +
DZ(K+1) / KZ(I,K+1) )
```

```
        IF (KZ(I,K) == 0.0_DP .AND. KZ(I,K+1) == 0.0_DP ) THEN
```

```
            KZAVG(I,K) = 0.0_DP
```

```
        END IF
```

```
    END DO
```

```
END DO
```

```
KZAVG(:,0) = 0.0_DP
```

```
KZAVG(:,KMAX) = 0.0_DP
```

```
DO K = 1, KMAX
```

```
    DO I = 1, IMAX-1
```

```
        KRAVG(I,K) = KR(I,K) * KR(I+1,K) * (RI(I+1) -RI(I)) / (KR(I,K) * ( RI(I+1) -
RI(I) ) + KR(I+1,K) * ( RI(I) -RI(I) ))
```

```
        IF (KR(I,K) == 0.0_DP .AND. KR(I+1,K) == 0.0_DP ) THEN
```

```
            KRAVG(I,K) = 0.0_DP
```

```
        END IF
```

```
END DO
```

```
END DO
```

```
KRAVG(0,:) = 0.0_DP
```

```
KRAVG(IMAX,:) = 0.0_DP
```

```
KR_NONDARCY(:,:) = KRAVG(:,:)
```

```
! -----
```

```
!
```

```
!           Calculation of WI and PR of each layer
```

```
!
```

```
! -----
```

```
WISUM = 0
```

```
DEPTH1 = 0.0_DP
```

```
DEPTH (0) = DEPTH1
```

```
DO K = 1, KMAX
```

```
    WI(K) = 2.0_DP * PI * CF * KRAVG(1,K) * DZ(K)/(MU * ((R1 -RW)/RW +  
SKIN(K)))
```

```
    WISUM = WISUM + WI(K)
```

```
END DO
```

```
DO K = 1, KMAX
```

```
    DEPTH(K) = DEPTH1
```

```
    DEPTH1 = DEPTH(K) + DZ (K)/2.0_DP + DZ(K+1)/2.0_DP
```

```
END DO
```

```
DEPTH(KMAX+1) = DEPTH(KMAX)
```

```
GW = RHU/144.0_DP
```

```
DO K = 1, KMAX
```

```
    PR(K) = PR1
```

```
    PR1 = PR(K) + GW * (DEPTH(K+1) -DEPTH(K))
```

```
END DO
```

```
!-----
```

```
!
```

```
!           Allocating Initial Pressures for the Pressure array PRN(x)
```

```
!
```

```
!-----
```

```
N = 0
```

```
DO J = IMAX, M, IMAX
```

```
    III = (J -IMAX + 1)
```

```
    N = N + 1
```

```
    PRN(III:J) = PR(N)
```

END DO

PRN(M+1) = PR(1)

!-----START TIME LOOP -----

DO II = 1, 199

DT = TIMEP(II+1) -TIMEP(II)

IF (II >= 100) THEN

Q = 0

DT = TIMEB(II-99+1) -TIMEB(II-99)

END IF

PRINT *, II

!-----

!

!

Calculation of Pressure Coefficients

!
!-----

DO K = 1, KMAX

DO I = 1, IMAX

$G(I,K) = PHI(I,K) * CT * PI * (RI1(I)**2.0 - RI0(I)**2.0) * DZ(K) / (DT / 24.0_DP)$

$C(I,K) = CF * (KZAVG(I,K-1)/MU) * PI * (RI1(I)**2.0 - RI0(I)**2.0) / (DZ(K)/2 + DZ(K-1)/2)$

$H(I,K) = CF * (KZAVG(I,K)/MU) * PI * (RI1(I)**2.0 - RI0(I)**2.0) / (DZ(K)/2.0 + DZ(K+1)/2)$

$D(I,K) = CF * (KR_NONDARCY(I-1,K)/MU) * 2.0_DP * PI * RI0(I) * DZ(K) / DRI0(I)$

$F(I,K) = CF * (KR_NONDARCY(I,K)/MU) * 2.0_DP * PI * RI1(I) * DZ(K) / DRI1(I)$

$F(IMAX,K) = 0.0_DP$

$C(I,1) = 0.0_DP$

$D(1,K) = 0.0_DP$

$H(I,KMAX) = 0.0_DP$

$E(I,K) = -(G(I,K) + C(I,K) + D(I,K) + F(I,K) + H(I,K))$

$E(1,K) = -(G(1,K) + C(1,K) + D(1,K) + F(1,K) + H(1,K) + WI(K))$

END DO

END DO

```
!-----
!  
!           Allocating values for Array R(M)  
!  
!-----
```

N = 0

DO K = 1, KMAX

DO I = 1, IMAX

N = N + 1

$R(N) = H(I,K) * GW * (DEPTH(K+1) - DEPTH(K)) - C(I,K) * GW * \&$
 $\& (DEPTH(K) - DEPTH(K-1)) - G(I,K) * PRN(N)$

END DO

END DO

L = 0

WI1 = 0

DO K = KMAX, 2, -1

WI1 = WI1 + WI(K)

L1 = WI1 * GW * (DEPTH(K) - DEPTH(K-1))

L = L + L1

```
END DO
```

```
R(M+1) = -(Q * FVF) + 5.6146_DP * CW / (DT / 24.0_DP) * PRN(M+1) -L
```

```
K = 1
```

```
L = 0
```

```
DO N = IMAX+1, M, IMAX
```

```
    K = K+1
```

```
    L = L + (DEPTH(K) -DEPTH(K-1))
```

```
    R(N) = R(N) -WI(K) * GW * L
```

```
END DO
```

```
!-----  
!  
!           Creating Array (M x M)  
!  
!-----
```

```
N = 0
```

```
C_LOOP: DO K = 2, KMAX
```

```
        DO I = 1, IMAX
```

```
            N = N + 1
```

A(N,N+IMAX) = C(I,K)

END DO

END DO C_LOOP

N = 0

D_LOOP: DO K = 1, KMAX

DO I = 1, IMAX

N = N + 1

A(N,N+1) = D(I,K)

IF ((K .EQ. 1) .AND. (I .EQ. 1)) THEN

A(N,N+1) = D(2,K)

N = 0

END IF

END DO

END DO D_LOOP

N = 0

```
E_LOOP: DO K = 1, KMAX
```

```
    DO I = 1, IMAX
```

```
        N = N + 1
```

```
        A(N,N) = E(I,K)
```

```
    END DO
```

```
END DO E_LOOP
```

```
N = 0
```

```
F_LOOP: DO K = 1, KMAX
```

```
    DO I = 1, IMAX
```

```
        N = N + 1
```

```
        IF ( N .EQ. M ) EXIT F_LOOP
```

```
        A(N+1,N) = F(I,K)
```

```
    END DO
```

```
END DO F_LOOP
```

N = 0

H_LOOP: DO K = 1, KMAX

DO I = 1, IMAX

N = N + 1

IF (N + IMAX > M) EXIT H_LOOP

A(N+IMAX,N) = H(I,K)

END DO

END DO H_LOOP

N = 1

DO I = 1, M-IMAX+1, IMAX

A(I,M+1) = -WI(N)

A(M+1,I) = WI(N)

N = N + 1

END DO

A(M+1,M+1) = WISUM + 5.6146_DP * CW / (DT / 24.0_DP)

$A(M+2,1:M+1) = R(1:M+1)$

$N = M + 1$

OPEN (UNIT = 1, FILE = "Pressure_Time.DATA", STATUS = "UNKNOWN")

CALL GAUSSIAN_ELIMINATION (N, A, X)

DO J = 1, M+1

PRN(J) = X(J)

END DO

WRITE (1, 20) DT, PRN(M+1)

20 FORMAT (1X, 2(F30.14, 1X))

$A(1:M+2,1:M+1) = 0.0_DP$

$R(1:M+1) = 0.0_DP$

!-----

!

```

!           Non-Darcy Flow Effect
!
!-----

ALFA = 0.0_DP

N = 0

DO K = 1, KMAX

    DO I = 1, IMAX-1

        N = N + 1

        IF (KRAVG(I,K) == 0.0_DP) GOTO 120

        BETA = 6.15E10 * KRAVG(I,K) ** (-1.55)

        VR = -CF * KRAVG(I,K)/MU * ( PRN(N+1) -PRN(N) ) / DRI1(I) / (1 +
ALFA)

        ALFA = 1.8295E-16 * (BETA * RHU * KRAVG(I,K)/MU) *
(ABS(VR))

120  KR_NONDARCY(I,K) = KRAVG(I,K) / (1 + ALFA)

        ALFA = 0.0_DP
    END DO

```

```
N = N + 1
```

```
END DO
```

```
KR_NONDARCY(0,:) = 0.0
```

```
KR_NONDARCY(IMAX,:) = 0.0
```

```
END DO
```

```
CONTAINS
```

```
! -----  
!  
!           Gaussian_Elimination Subroutine  
!  
! -----
```

```
SUBROUTINE GAUSSIAN_ELIMINATION (N, A, X)
```

```
!   DEFINE INPUT VARIABLES
```

```
IMPLICIT NONE
```

```
INTEGER, PARAMETER :: DP = SELECTED_REAL_KIND(14,50)
```

```
INTEGER, PARAMETER :: DP2 = SELECTED_INT_KIND(9)
```

```
INTEGER (KIND = DP2) :: N
```

```
REAL (KIND = DP), DIMENSION (N+1, N):: A
```

```
REAL (KIND = DP), DIMENSION (N):: X
```

```
! DEFINE LOCAL VARIABLES
```

```
INTEGER (KIND = DP2) :: J,K,P,I
```

```
REAL(KIND = DP), DIMENSION (N+1, N):: M
```

```
REAL (KIND = DP):: SUM1
```

```
REAL (KIND = DP), DIMENSION (N+1):: TEMP1
```

```
REAL (KIND = DP), DIMENSION (N+1):: TEMP2
```

```
! DETERMINE IF A UNIQUE SOLUTION EXISTS AND START PARTIAL  
PIVOTING
```

```
DO J=1,N-1
```

```
  DO K=J,N
```

```
    IF (A(J,K) .NE. 0) THEN
```

```
      GO TO 100
```

```
    END IF
```

```
  END DO
```

```
  PRINT *, "NO UNIQUE SOLUTION EXISTS TO THIS SYSTEM."
```

```
  STOP
```

```
! EXCHANGE ROWS J AND K
```

```
100  TEMP1 = A(:,K)
```

```
    TEMP2 = A(:,J)
```

```
    A(:,J) = TEMP1
```

$A(:,K) = \text{TEMP2}$

! CALCULATE MULTIPLIER AND PERFORM PIVOTTING

DO K=J+1,N

$M(J,K) = A(J,K)/A(J,J)$

 DO P=J,N+1

$A(P,K) = A(P,K) - M(J,K)*A(P,J)$

 END DO

END DO

END DO

IF (A(N,N) .EQ. 0) THEN

 PRINT *, "NO UNIQUE SOLUTION TO THIS SYSTEM EXISTS."

 STOP

END IF

$X(N) = A(N+1,N)/A(N,N)$

DO I=N-1,1,-1

 SUM1 = 0

 DO K=I+1,N

 SUM1 = SUM1 + A(K,I)*X(K)

 END DO

$X(I) = 1/(A(I,I)) * (A(N+1,I) - \text{SUM1})$

END DO

RETURN

END SUBROUTINE

END PROGRAM

APPENDIX B

THE ANALYTICAL SOLUTION FOR THE STORATIVITY RATIO DUAL-POROSITY SYSTEM

B.1 Analytical Solution for Homogeneous System

The differential equation for radial flow in an infinite the homogeneous reservoir is given by

$$\frac{1}{r_D} \frac{\partial}{\partial r_D} \left(r_D \frac{\partial p_D}{\partial r_D} \right) = \frac{\partial p}{\partial t} \quad (\text{B.1})$$

with the following conditions:

$$p_D(r_D, t_D = 0) = 0, \quad (\text{B.2})$$

$$p_D(r_D \rightarrow \infty, t_D) = 0, \quad (\text{B.3})$$

$$C_D \frac{\partial p_{wD}}{\partial t_D} - \left(r_D \frac{\partial p_D}{\partial r_D} \right)_{r_D=1} = 1, \quad (\text{B.4})$$

and

$$p_{wD} = p_D(r_D = 1) - \left(r_D \frac{\partial p_D}{\partial r_D} \right)_{r_D=1} s \quad (\text{B.5})$$

Application of the Laplace transformation to the above gives

$$\bar{p}_{wD} = 1/z \left(C_D z + \frac{1}{s + K_1^o(\sqrt{z})} \right) \quad (\text{B.6})$$

where,

$$K_1^o(\sqrt{z}) = \frac{K_o(\sqrt{z})}{\sqrt{z} K_1(\sqrt{z})}$$

Ignoring the wellbore storage, Eq. B.6 becomes

$$\bar{p}_{wD} = 1/z \left(1 / \left(s + \frac{K_o(\sqrt{z})}{\sqrt{z} K_1(\sqrt{z})} \right) \right) \quad (\text{B.7})$$

For late time approximation ($z \rightarrow 0$), $\sqrt{z} K_1(\sqrt{z}) \approx 1$ and $K_0(x) = -\ln\left(\frac{e^\gamma}{2} \sqrt{x}\right)$ and consequently

$$\bar{p}_{wD} = -\frac{1}{z} \left[\ln(\sqrt{z}/2) - 0.5772 + s \right] \quad (\text{B.8})$$

Using Schapery Approximations¹⁶ with Najurieta's Modification¹⁷, Eq. B.8 yields

$$p_{wD} = 0.5 \ln t_D + 0.4045 + s \quad (\text{B.9})$$

B.2 Analytical Solution for Commingled System

The solution of Eq. 4.1 in the Laplace domain is given by

$$\bar{p}_D = \frac{1}{z \left[z C_D + \frac{1-\kappa}{s_2 + K_1^o \left(\sqrt{\frac{1-\omega}{1-\kappa}} z \right)} + \frac{\kappa}{s_1 + K_1^o \left(\sqrt{\frac{\omega}{\kappa}} z \right)} \right]} \quad (\text{B.10})$$

For details on the derivation of this Eq. B.10, see reference 3.

For late time approximation $x \rightarrow 0$, $(x) K_1(x) = 1$, Consequently, Eq. B.10 becomes

$$\bar{p}_D = \frac{1}{z \left[z C_D + \frac{1-\kappa}{s_2 + K_o \left(\sqrt{\frac{1-\omega}{1-\kappa}} z \right)} + \frac{\kappa}{s_1 + K_o \left(\sqrt{\frac{\omega}{\kappa}} z \right)} \right]} \quad (\text{B.11})$$

• Neglecting the skin and wellbore storage effects and rewritten Eq. B.11 as follows

$$\bar{p}_D = \frac{1}{z \left[\frac{(1-\kappa) \left[K_o \left(\sqrt{\frac{\omega}{\kappa}} z \right) \right] + (\kappa) \left[K_o \left(\sqrt{\frac{1-\omega}{1-\kappa}} z \right) \right]}{\left[K_o \left(\sqrt{\frac{1-\omega}{1-\kappa}} z \right) \right] \left[K_o \left(\sqrt{\frac{\omega}{\kappa}} z \right) \right]} \right]} \quad (\text{B.12})$$

or,

$$\bar{p}_D = \frac{\left[K_o \left(\sqrt{\frac{1-\omega}{1-\kappa}} z \right) \right] \left[K_o \left(\sqrt{\frac{\omega}{\kappa}} z \right) \right]}{z \left[(1-\kappa) \left[K_o \left(\sqrt{\frac{\omega}{\kappa}} z \right) \right] + (\kappa) \left[K_o \left(\sqrt{\frac{1-\omega}{1-\kappa}} z \right) \right] \right]} \quad (\text{B.13})$$

Rearranging Eq. B.13 for approximation purposes into the following form

$$\bar{p}_D = \frac{\left[K_o \left(\sqrt{\frac{\omega}{\kappa}} z \right) \right]}{z \left[(1-\kappa) \left[\frac{K_o \left(\sqrt{\frac{\omega}{\kappa}} z \right)}{\left[K_o \left(\sqrt{\frac{1-\omega}{1-\kappa}} z \right) \right]} \right] + (\kappa) \right]} \quad (\text{B.14})$$

or

$$\bar{p}_D = \frac{\left[K_o \left(\sqrt{\frac{\omega}{\kappa}} z \right) \right]}{z \kappa \left[\frac{(1-\kappa)}{\kappa} \frac{\left[K_o \left(\sqrt{\frac{\omega}{\kappa}} z \right) \right]}{\left[K_o \left(\sqrt{\frac{1-\omega}{1-\kappa}} z \right) \right]} + 1 \right]} \quad (\text{B.15})$$

Using the Binomial expansion for the domination of the bracket term of Eq. B.15; that is,

$$(1+x)^{-1} = 1-x+x^2-x^3 \dots\dots$$

and using the first term of the expanded function, Eq. B.15 becomes

$$\bar{p}_D = \frac{\left[K_o \left(\sqrt{\frac{\omega}{\kappa}} z \right) \right]}{z \kappa} \left[1 - \frac{(1-\kappa)}{\kappa} \frac{\left[K_o \left(\sqrt{\frac{\omega}{\kappa}} z \right) \right]}{\left[K_o \left(\sqrt{\frac{1-\omega}{1-\kappa}} z \right) \right]} \right] \quad (\text{B.16})$$

For The dual-porosity system, $\kappa = 1$. Thus, Eq. B.16 becomes

$$\bar{p}_D = \frac{\left[K_o \left(\sqrt{\omega z} \right) \right]}{z} \quad (\text{B.17})$$

Substituting for the approximation of $K_0(x) = -\ln\left(\frac{e^x}{2}\sqrt{x}\right)$ into Eq. B.17, gives

$$\bar{p}_{wD} = \frac{1}{z} \left[-\ln\left(\sqrt{\omega z}/2\right) - 0.5772 \right] \quad (\text{B.18})$$

Using Eq. B.8 with $s = 0$, and subtracting from Eq. B.18 yields

$$\begin{aligned} (\bar{p}_{wD})_{com} - (\bar{p}_{wD})_{Hom} &= \frac{1}{z} \left[-\ln(\sqrt{\omega z}/2) - 0.5772 + \ln(\sqrt{z}/2) + 0.5772 \right] \\ &= -\frac{1}{2z} \ln(\omega) \end{aligned} \tag{B.19}$$

Thus,

$$\delta p_D = (p_{wD})_{com} - (p_{wD})_{Hom} = \ln(\omega)^{1/2} \tag{B.20}$$

Therefore,

$$\omega = e^{-2\delta p_D} \tag{B.21}$$

APPENDIX C

PRESSURE VERSUS TIME DATA FOR EXAMPLE APPLICATIONS

Table C-1: The pressure data of Example 1

Time(hours)	BHP(psi)
1.7788E-05	1999.418
3.83177E-05	1998.757
6.20114E-05	1998.005
8.9357E-05	1997.15
0.000120917	1996.177
0.000157342	1995.072
0.00019938	1993.818
0.000247898	1992.396
0.000303893	1990.787
0.000368519	1988.97
0.000443105	1986.92
0.000529187	1984.614
0.000628537	1982.027
0.000743198	1979.132
0.000875532	1975.903
0.001028262	1972.314
0.001204532	1968.341
0.001407969	1963.961
0.001642761	1959.157
0.001913741	1953.914
0.002226486	1948.226
0.002587432	1942.093
0.00300401	1935.525
0.003484793	1928.544
0.004039677	1921.181
0.004680083	1913.481
0.005419192	1905.5
0.006272217	1897.305
0.007256714	1888.971
0.008392948	1880.578
0.009704304	1872.209
0.011217775	1863.944
0.012964509	1855.856
0.014980461	1848.007
0.017307122	1840.446
0.019992382	1833.208
0.023091509	1826.309
0.02666829	1819.752
0.030796346	1813.527
0.035560641	1807.614
0.041059236	1801.986
0.047405305	1796.615
0.054729467	1791.471
0.063182469	1786.524
0.072938296	1781.75
0.084197747	1777.126
0.097192567	1772.632
0.112190223	1768.253
0.129499401	1763.975
0.149476369	1759.789

Time(hours)	BHP(psi)
0.172532299	1755.687
0.19914174	1751.663
0.229852378	1747.712
0.265296313	1743.831
0.306203067	1740.02
0.353414602	1736.279
0.407902644	1732.607
0.470788692	1729.007
0.543367093	1725.483
0.627131687	1722.038
0.723806553	1718.676
0.835381496	1715.403
0.964153	1712.225
1.112771495	1709.146
1.284295912	1706.174
1.482256641	1703.314
1.710728196	1700.57
1.974413077	1697.947
2.278738562	1695.445
2.62996841	1693.064
3.035331787	1690.801
3.503172057	1688.651
4.043118512	1686.601
4.666284565	1684.64
5.38549649	1682.748
6.21555742	1680.907
7.17355203	1679.094
8.279198181	1677.283
9.555252762	1675.451
11.02798008	1673.575
12.72769246	1671.632
14.68937411	1669.606
16.95340122	1667.479
19.56637297	1665.241
22.5820707	1662.884
26.06256479	1660.401
30.07949229	1657.792
34.71553135	1655.055
40.06610294	1652.195
46.24133485	1649.216
53.36832839	1646.125
61.59377443	1642.931
71.08697269	1639.645
82.04331628	1636.276
94.68831344	1632.837
109.282229	1629.338
126.1254413	1625.79
145.5646246	1622.203
167.9998846	1618.585

Table C-2: The pressure data of Example 2

Time(hours)	BHP(psi)	Time(hours)	BHP(psi)	Time(hours)	BHP(psi)	Time(hours)	BHP(psi)
2.29163E-05	3999.543	0.934105915	3765.191	4319.99992	3680.547	4320.240485	3900.278
5.02374E-05	3999.001	1.113678656	3763.598	4319.999945	3681.034	4320.278579	3902.011
8.28101E-05	3998.357	1.327768097	3762.068	4319.999973	3681.596	4320.322701	3903.7
0.000121644	3997.594	1.58300889	3760.601	4320.000006	3682.244	4320.373805	3905.346
0.000167942	3996.69	1.887310972	3759.193	4320.000045	3682.99	4320.432997	3906.949
0.000223139	3995.621	2.250104692	3757.837	4320.000089	3683.85	4320.501556	3908.511
0.000288946	3994.356	2.682633062	3756.526	4320.00014	3684.838	4320.580964	3910.031
0.000367402	3992.864	3.198300176	3755.249	4320.000199	3685.974	4320.672938	3911.508
0.000460939	3991.106	3.813086606	3753.992	4320.000268	3687.279	4320.779467	3912.941
0.000572455	3989.04	4.546044642	3752.742	4320.000348	3688.774	4320.902855	3914.33
0.000705406	3986.617	5.419888722	3751.483	4320.00044	3690.486	4321.045768	3915.673
0.000863913	3983.784	6.461699355	3750.201	4320.000547	3692.443	4321.211298	3916.972
0.001052887	3980.482	7.70376235	3748.882	4320.000671	3694.675	4321.403022	3918.226
0.001278184	3976.648	9.184569357	3747.514	4320.000814	3697.215	4321.625087	3919.437
0.001546788	3972.22	10.95001072	3746.09	4320.00098	3700.099	4321.882293	3920.607
0.001867021	3967.13	13.05479764	3744.605	4320.001172	3703.365	4322.180202	3921.739
0.002248808	3961.317	15.56415765	3743.055	4320.001395	3707.05	4322.525256	3922.839
0.00270398	3954.728	18.55585606	3741.441	4320.001653	3711.193	4322.924913	3923.912
0.003246644	3947.32	22.12260588	3739.766	4320.001952	3715.831	4323.387816	3924.966
0.003893616	3939.076	26.37494102	3738.032	4320.002298	3720.998	4323.923974	3926.008
0.004664946	3930.003	31.44464175	3736.246	4320.002699	3726.724	4324.544978	3927.048
0.005584539	3920.147	37.48881856	3734.414	4320.003163	3733.03	4325.264255	3928.094
0.006680891	3909.601	44.69478106	3732.541	4320.003701	3739.925	4326.097358	3929.155
0.007987979	3898.504	53.2858427	3730.635	4320.004324	3747.407	4327.062299	3930.239
0.009546311	3887.05	63.52824129	3728.7	4320.005045	3755.452	4328.179941	3931.353
0.011404178	3875.474	75.73938972	3726.743	4320.005881	3764.017	4329.47445	3932.503
0.013619156	3864.047	90.29771262	3724.768	4320.006849	3773.036	4330.973814	3933.694
0.016259888	3853.049	107.6543738	3722.779	4320.00797	3782.415	4332.710451	3934.927
0.01940821	3842.743	128.3472578	3720.78	4320.009268	3792.036	4334.72191	3936.205
0.023161689	3833.344	153.0176389	3718.774	4320.010772	3801.758	4337.051682	3937.527
0.027636646	3824.997	182.4300548	3716.762	4320.012514	3811.422	4339.750139	3938.892
0.032971759	3817.758	217.4959988	3714.746	4320.014531	3820.863	4342.875626	3940.298
0.039332365	3811.592	259.3021679	3712.728	4320.016868	3829.914	4346.495719	3941.742
0.046915579	3806.392	309.1441391	3710.707	4320.019575	3838.425	4350.688689	3943.221
0.055956407	3802.007	368.5665198	3708.686	4320.022709	3846.275	4355.545196	3944.731
0.066735023	3798.265	439.4108151	3706.663	4320.02634	3853.378	4361.170241	3946.267
0.079585459	3795.006	523.8724964	3704.64	4320.030546	3859.694	4367.685448	3947.826
0.09490595	3792.096	624.5690391	3702.617	4320.035417	3865.231	4375.231682	3949.404
0.11317128	3789.436	744.6210385	3700.593	4320.041059	3870.035	4383.972104	3950.996
0.134947493	3786.953	887.7489172	3698.569	4320.047594	3874.187	4394.095693	3952.6
0.160909436	3784.602	1058.388222	3696.545	4320.055163	3877.784	4405.821335	3954.21
0.191861673	3782.352	1261.82708	3694.52	4320.063929	3880.93	4419.402553	3955.825
0.228763416	3780.187	1504.370081	3692.494	4320.074083	3883.723	4435.132993	3957.441
0.272758252	3778.094	1793.533656	3690.463	4320.085844	3886.247	4453.352765	3959.055
0.325209588	3776.067	2138.27901	3688.423	4320.099466	3888.569	4474.455808	3960.664
0.387742893	3774.102	2549.289834	3686.361	4320.115244	3890.74	4498.898396	3962.267
0.462296082	3772.197	3039.303393	3684.256	4320.133518	3892.797	4527.20901	3963.86
0.551179564	3770.353	3623.505251	3682.073	4320.154684	3894.765	4559.99765	3965.442
0.657147847	3768.57	4319.999881	3679.759	4320.1792	3896.661		
0.783484899	3766.849	4319.999899	3680.125	4320.207596	3898.496		

APPENDIX D

COMPUTER PROGRAM FOR THE NEWTON RAPHSON METHOD

D.1 Newton Raphson Method for Storativity Ratio (FORTRAN 90)

```
PROGRAM NEWTON_RAPHSON
```

```
!-----
```

```
!
```

```
! This program is Code for Equation 4.36 to estimate storativity ratio.
```

```
!
```

```
!-----
```

```
INTEGER, PARAMETER :: D=SELECTED_REAL_KIND(14)
```

```
REAL(KIND = D)    :: A, B, F, DP, BETA, S, DIFF
```

```
REAL(KIND = D)    :: WLP1,WL, K, F1, F2, DF1
```

```
INTEGER :: COUNT
```

```
PRINT *, " ENTER KAPPA, dPD AND SKIN RESPECTIVELY"
```

```
PRINT '(/)
```

```
READ *, K, DP, S
```

```
WL = 0.001 ! First Estimate of omega.
```

BETA= 4.0_D/DBLE(EXP(.5772_D))

BETA= SQRT(BETA)

A = 2*(K*S+K*LOG(BETA)+K*DP-S+2.5*K-2.5-LOG((BETA)*(SQRT(K))))

B = 2*((1-K)*DP+(1-K)*LOG(BETA)-2.5*K-K*S-LOG(BETA*(SQRT(1-K))))

F = 10*DP+4*DP*S+4*DP*LOG(BETA)

F2 = (1-K)**(A) * K**(B+LOG(1-K)) * DBLE(EXP(F))

COUNT = 0

100 F1 = (1-WL)**(LOG(WL)+A) * WL**B

DF1 = (1/WL*LOG(1-WL)-1/(1-WL)*(LOG(WL)+A)+B/WL)*((1-WL)**(LOG(WL)+A)*WL**B)

WLP1 = WL -(F1-F2)/DF1

DIFF = WLP1-WL

COUNT = COUNT + 1

IF (ABS(DIFF) < 1E-5) THEN

GOTO 200

ELSE

WL = ABS(WLP1)

GOTO 100

200 END IF

PRINT '(/)

PRINT *, " Omega epsilon No Iterations"

PRINT '(/)

PRINT *, WL, DIFF, COUNT

PRINT '(/)

END

D.2 Newton Raphson Method for Transmissivity Ratio (FORTRAN 90)

```
PROGRAM NEWTON_RAPHSON
```

```
!-----
```

```
!
```

```
!This program is Code for Equation 4.44 to estimate kappa.
```

```
!
```

```
!
```

```
! Note: If you got this message (Domain Error), Then
```

```
!
```

```
! change the first estimate of kappa value as 0.5,0.6,
```

```
! 0.7, 0.8 or 0.9.
```

```
!-----
```

```
INTEGER, PARAMETER :: DPN=SELECTED_REAL_KIND(14)
```

```
REAL(KIND = DPN)      :: A, B, F, G, DP, BETA, S, DIFF
```

```
REAL(KIND = DPN)      :: W, KP1,K, F1, F2, DF1
```

```
INTEGER :: COUNT
```

```
PRINT *, " ENTER OMEGA, dPD AND SKIN RESPEBETATIVELY"
```

```
PRINT '(/)
```

```
READ *, W, DP, S
```

K= 0.95_DPN ! First estimate of kappa

BETA= 4.0_DPN/EXP(.5772_DPN)

A = 5.0_DPN-LOG(W/BETA)+2.0_DPN*S

B = -5.0_DPN-2*DP-LOG(BETA)-2*S

C = -LOG(1-W)-2*DP

F = (5.0_DPN+2.0_DPN*DP+LOG(BETA)+2.0_DPN*S)*(LOG(1-W)-LOG(W))

G = 10.0_DPN*DP+5.0_DPN*LOG(BETA)+(5.0+2*S-log(W/BETA))*LOG((1-W)/BETA)&

& -(2*DP+LOG(BETA))*LOG(W/BETA)+4*DP*S+2*S*LOG(BETA)

F2 = EXP(G)

COUNT = 0

100 F1 = (1-K)**(LOG(K)+A+B*K) * K**(C-B*K)*EXP(F*K)

DF1 = ((1/K+B)*LOG(1-K)-1/(1-K)*(LOG(K)+A+B*K))*(1-K)**(LOG(K)+A+B*K)*K**(C-B*K) * EXP(F*K)&

& + (-B*LOG(K)+1/K*(C-B*K))*K**(C-B*K)*(1-K)**(LOG(K)+A+B*K)*EXP(F*K)&

& + K**(C-B*K)*(1-K)**(LOG(K)+A+B*K)* EXP(F*K)*F

$KP1 = K - (F1 - F2) / DF1$

$DIFF = KP1 - K$

$COUNT = COUNT + 1$

IF (ABS(DIFF) < 1E-5) THEN

GOTO 200

ELSE

$K = ABS(KP1)$

GOTO 100

200 END IF

PRINT '(/)

PRINT *, " kappa epsilon No Iterations"

PRINT '(/)

PRINT *, K, DIFF, COUNT

END